

Elucidating the Role of Mechanics in Neural Plate Convergent Extension

by

Deepthi Sudha Vijayraghavan

B.S. in Bioengineering, University of California San Diego

Submitted to the Graduate Faculty of

Swanson School of Engineering in partial fulfillment

of the requirements for the degree of

Doctor of Philosophy

University of Pittsburgh

2017

UNIVERSITY OF PITTSBURGH
SWANSON SCHOOL OF ENGINEERING

This dissertation was presented

by

Deepthi Sudha Vijayraghavan

It was defended on

September 15, 2017

and approved by

Ipsita Banerjee, PhD, Associate Professor, Departments of Chemical and Petroleum
Engineering, and Bioengineering

Jeffrey Hildebrand, PhD, Associate Professor, Department of Biological Science

Partha Roy, PhD, Associate Professor, Departments of Bioengineering, Cell Biology, and
Pathology

Dissertation Director: Lance Davidson, PhD, Professor, Professor, Departments of
Bioengineering, Developmental Biology, and Computational and Systems Biology

Copyright © by Deepthi Sudha Vijayraghavan

2017

ELUCIDATING THE ROLE OF MECHANICS IN NEURAL PLATE CONVERGENT EXTENSION

Deepthi Vijayraghavan, Ph.D.

University of Pittsburgh, 2017

Neural tube formation is crucial for the proper development of the brain and spinal cord and its failure results in congenital disorders known as neural tube defects (NTDs). Several known genetic mutations are associated with NTDs but the physical mechanisms by which they affect neural tube morphogenesis remain unclear. The neural tube begins as an epithelial sheet on the embryo surface called the neural plate that undergoes a series of shape changes to form an elongated tubular structure, internalized within the embryo. Integrated behaviors of embryonic cells orchestrate these tissue-level deformations. Our study aimed to identify the cell behaviors accompanying early neural plate shaping in *Xenopus laevis* embryos when the tissue elongates in the anterior-posterior axis while narrowing in a perpendicular mediolateral axis. Through observation and quantification of local cell and tissue mechanical strains, we identified the emergence of distinctive spatiotemporal patterns of cell behavior. Cells undergo oriented rearrangements within the medial neural plate whereas at its lateral edges, cells assume an elongated morphology.

Among the mutations associated with human NTDs, planar cell polarity (PCP) pathway mutations are known to inhibit plate narrowing and elongation and prevent cell rearrangements in vertebrate models of human development. As a cell's local tissue mechanical environment can influence its behaviors, we sought to determine whether the lack of rearrangement in PCP-compromised embryos might be due to the lack of tissue deformation. We tested how wild type

and PCP-compromised plate cells behave in altered tissue strain environments. We find that medial plate cell rearrangement is an intrinsic program independent of tissue extension; however, lateral cell elongation is likely strain dependent. PCP compromised cells in a narrowing and extending tissue assume an elongated morphology compared to wild type cells, becoming stretched in the direction of tissue elongation. These distinctive behaviors under similar mechanical conditions suggest that the PCP pathway mediates a cell's response to its mechanical microenvironment, guiding morphology during plate shaping. This dissertation exposes a role for tissue mechanics in the PCP-mutant phenotype and provides a framework to test the interplay between tissue mechanics and planar patterning in guiding cell behaviors during neural tube morphogenesis.

TABLE OF CONTENTS

PREFACE.....	XIV
1.0 INTRODUCTION.....	1
1.1 EPITHELIAL CONVERGENT EXTENSION	2
1.1.1 Apical vs. Basal Cell Behaviors During Convergent Extension	4
1.1.2 Planar Polarized Behaviors.....	7
1.1.3 Mechanics: a polarizing subject.	10
1.2 CONVERGENT EXTENSION DURING NEURAL PLATE SHAPING ...	11
1.3 GOALS AND SPECIFIC AIMS.....	11
1.4 SIGNIFICANCE.....	12
2.0 MECHANICS OF NEURULATION: FROM CLASSICAL TO CURRENT PERSPECTIVES ON THE PHYSICAL MECHANICS THAT SHAPE, FOLD, AND FORM THE NEURAL TUBE.....	15
2.1 A BRIEF HISTORY OF NEURAL TUBE MORPHOGENESIS.....	16
2.2 QUALITATIVE DESCRIPTION OF PHENOMENA AND EMPIRICAL EVIDENCE	19
2.3 QUALITATIVE EXPERIMENTS WHERE COMPONENTS ARE REMOVED OR ALTERED.	25
2.4 INTEGRATING QUANTITATIVE DESCRIPTION OF KINEMATICS AND MORPHOMETRICS WITH MOLECULAR ANALYSIS.....	26
2.5 MEASUREMENT OF FORCES AND MATERIAL PROPERTIES	33
2.5.1 Measurement of Material Properties	36

2.5.2	Measurement of Force Production and Stresses within the neural plate.....	37
2.5.3	Estimating the mechanical status of contractile epithelia using microdissection via microsurgery or laser ablation.....	38
2.6	SIMULATING NEURAL TUBE FORMATION.....	40
2.6.1	Physical Analog Models of Neurulation.....	40
2.6.2	Computational Models of Neurulation	43
2.7	MECHANICS AS COMPONENT IN THE SIGNALING NETWORKS OF NEURULATION.....	45
2.8	BIOMECHANICS OF NEURULATION, NEURAL TUBE DEFECTS, AND ROBUST DEVELOPMENT.....	46
3.0	NEUROEPITHELIUM CELL BEHAVIORS DURING <i>XENOPUS</i> NEURAL PLATE SHAPING	48
3.1	INTRODUCTION	48
3.2	RESULTS.....	51
3.2.1	Regional patterns of cell shape across dorsal ectoderm and neural ectoderm during plate shaping	51
3.2.2	Distinctive patterns of 4-cell and higher order multicellular rosettes during neurulation.....	58
3.2.3	Neuroepithelial cells undergo directed rearrangements and apical junctional remodeling.....	61
3.2.4	Basal first mechanism of rearrangement.....	64
3.3	DISCUSSION.....	67
3.3.1	Regional difference in cell shape strains.....	67
3.3.2	Cell rearrangement as a conserved behavior in converging and extending tissues.....	68
3.3.3	Limitations.....	70
3.4	EXPERIMENTAL PROCEDURES	71
3.4.1	Embryo Handling, Histology, Immunostaining and Imaging	71

3.4.2	Microinjection	72
3.4.3	Image Processing and Segmentation.....	72
3.4.4	Tissue Tectonics strain analysis.....	74
3.4.5	Apical Basal Vertex Analysis	76
3.4.6	Statistical analysis	76
4.0	STRAIN-DEPENDENT AND INTRINSIC CELL BEHAVIORS WITHIN THE NEURAL PLATE	77
4.1	INTRODUCTION	77
4.2	RESULTS	79
4.2.1	Embedding dorsal isolates in agarose gels alters tissue strain.....	79
4.2.2	Cell rearrangements persist in gel confined tissues	87
4.2.3	Gel confined tissues exhibit increased cell division.....	90
4.2.4	Convergent extension and cell rearrangement is intrinsic to the superficial layer of the neuroepithelium	91
4.3	DISCUSSION.....	98
4.3.1	Strain dependent cell morphologies of the lateral neural plate.....	98
4.3.2	Cell rearrangement and tissue CE is intrinsic to the neuroepithelium..	99
4.3.3	Limitations.....	100
4.4	EXPERIMENTAL PROCEDURES	101
4.4.1	Embryo Handling, Immunofluorescence and Microinjection	101
4.4.2	Gel Confinement assay	101
4.4.3	Tissue grafting.....	102
4.4.4	Image Processing.....	102
4.4.5	Statistical analysis	103
5.0	PLANAR CELL POLARITY AND NEUROEPITHELIAL CELL BEHAVIORS.....	104

5.1	RESULTS	105
5.1.1	Vangl-2 Overexpression disrupts CE and alters cell morphology	105
5.1.2	Vangl-2 Overexpression causes cell AP elongation.....	110
5.2	DISCUSSION.....	117
5.2.1	Limitations.....	118
5.3	EXPERIEMENTAL PROCEDURES	118
5.3.1	Embryo Handling, Immunofluorescence and Microinjection	118
5.3.2	Image Processing.....	120
5.3.3	Statistical analysis	120
6.0	CONCLUSIONS	121
6.1	SUMMARY OF FINDINGS.....	121
6.2	SIGNIFICANCE OF FINDINGS.....	124
6.3	FUTURE DIRECTIONS.....	125
6.3.1	What controls the spatial differences in cell behaviors? Why do lateral cells undergo strain dependent elongation while medial cells remain more isodiametric?.....	126
6.3.2	How does planar cell polarity maintain neuroepithelial cell morphology?.....	127
6.3.3	What is the function of basal protrusions? Are they necessary and sufficient to drive cell intercalations?	127
APPENDIX A		129
BIBLIOGRAPHY.....		139

LIST OF TABLES

Table 1 Useful image analysis software to measure cell and tissue morphological changes. 31

LIST OF FIGURES

Figure 1. Cell behaviors that accompany tissue deformation	3
Figure 2. Schematic of apical-basal epithelial organization	5
Figure 3. Junction remodeling and cell rearrangement.....	6
Figure 4. Planar tissue polarity can arise through polarized protein localization.....	9
Figure 5. Concurrent mechanical processes shape the neural tube in <i>Xenopus laevis</i>	24
Figure 6. Formal definitions of mechanical terminology.	35
Figure 7. Simulating the mechanics of neurulation with physical analogs and computational models.....	42
Figure 8. Spatiotemporal changes in cell shape during plate shaping.	53
Figure 9. Morphometric measurements of cells at different stages reveal distinct patterns of cell shape.	54
Figure 10. Tissue tectonic approach to quantify cell and tissue strains.....	57
Figure 11. High order vertices, indicative of rearrangement, increase medially with stage.....	60
Figure 12. Neuroepithelial cells undergo oriented rearrangements.	63
Figure 13. Basolateral rearrangement precedes apical junction remodeling.	66
Figure 14. Image Processing Workflow	73
Figure 15. Confinement alters tissue strain patterns and cell morphology.....	80
Figure 16. Strain patterns of gel-confined tissues.....	82
Figure 17. Gel confinement alters cell and tissue strain patterns in the lateral neural plate.....	86
Figure 18. Orientation of rearrangements preserved in gel-confined tissues.	89
Figure 19. Cell Division Increases in gel confined tissues.	91

Figure 20. Neuroepithelial cells grafts show altered cell morphology compared to host tissue cells.....	94
Figure 21. Grafted neuroepithelia converge and extend.....	97
Figure 22. Vangl2 overexpression inhibits neural plate convergent extension.	107
Figure 23. Global Vangl2 overexpression within the neural plate alters cell morphology.	109
Figure 24. Elongation of Vangl2 overexpressing cells increases at later stages.	112
Figure 25. Strain patterns in mosaic Vangl2-Overexpression tissues.....	114
Figure 26. Gel confinement reduces Vangl2-overexpressing cell elongation	116
Figure 27. Framework to investigate mechanical and molecular controls of cell behaviors.....	123

PREFACE

First, I would like to thank the members of this dissertation committee for their guidance and helpful discussion as my thesis took shape. A special thank you to Dr. Lance Davidson for allowing me to join his lab and to explore the fascinating world of developmental biomechanics. His patience, support and mentorship through this process have made a lasting impact and I will cherish my time spent in the MechMorpho Lab forever. My graduate experience would not have been the same without my amazing labmates who provided sound research advice and stimulating discussions about science, life and the world at large.

I'd like to thank the Pitt Bioengineering Department and Swanson School of Engineering for both the academic support and giving me many extracurricular leadership and teaching opportunities that have helped define me over the last 6 years.

A huge thanks to my awesome friends who made it so easy to call Pittsburgh my new home and whose support through the inevitable highs and lows of school was invaluable. I think I had way too much fun in grad school thanks to them.

Finally, this work is dedicated to my wonderful family who has been so dedicated to me. To my parents, Vijay and Preethi and my siblings, Karun and Meghana, as well as my grandparents, uncles, aunts and cousins. I am infinitely grateful for your support. I love you all very much.

1.0 INTRODUCTION

Epithelial tissues are found throughout the body and provide structure to organs, maintain barriers that protect tissues, and compartmentalize different chemical and physical environments. During embryogenesis, structural precursors to a variety of organs, from the brain to the kidney, are derived from epithelial tissues. Epithelia are comprised of connected cells that form cohesive sheets. Because of their connectivity, epithelial cells require unique ways of coordinating their behaviors during morphogenesis to bend, elongate, fold and fuse tissues. Through these movements, epithelia can deform into different shapes and structures including cavities, tubes, and ridges. At the cellular level, epithelial cells must be able to remodel to facilitate these tissue deformations. Cells can constrict, heighten, rearrange, divide, apoptose, and extrude in the face of a changing tissue landscapes. These cell behaviors can actively promote tissue deformation by generating coordinated forces that act within the tissue or alternatively can be passive responses guided by tensions within tissues. Understanding the mechanisms behind epithelial cell behaviors and their relationship to tissue deformation is essential to understand how nature engineers tissues during embryonic development.

1.1 EPITHELIAL CONVERGENT EXTENSION

While there are a number of deformations epithelial tissues can undergo, convergent extension (CE) is a particularly versatile tissue movement that occurs in a many contexts of morphogenesis including vertebrate body axis elongation, *Drosophila* germband elongation, kidney tubule, cochlear and neural tube morphogenesis (Keller, Shih et al. 1992, Irvine and Wieschaus 1994) (Chacon-Heszele, Ren et al. 2012, Lienkamp, Liu et al. 2012). During convergent extension, tissues undergo an anisotropic deformation in which they narrow in one direction, while elongating in a perpendicular axis. Conceivably, there are many cellular mechanisms that could drive or accommodate CE. For example, as the tissue lengthens and narrows, the shapes of cells within the tissue may also lengthen and narrow (Fig 1). Cells may undergo divisions in which daughter cells separate in an oriented manner parallel to the axis of tissue elongation. Alternatively, cells may preserve their shapes, but coordinate their behaviors with neighboring cells to undergo rearrangements that turn wide arrays of cells into long narrow array of cells.

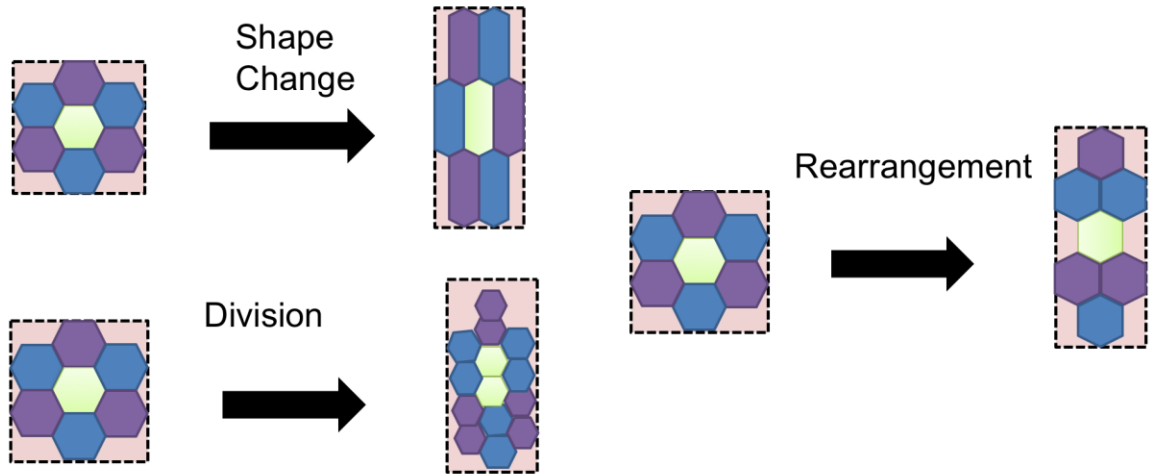


Figure 1. Cell behaviors that accompany tissue deformation

Many cellular mechanisms can accommodate or generate tissue convergent extension. For example, cells may change shape and stretch in the direction of tissue elongation while narrowing in the direction of tissue convergence. They may rearrange and exchange neighbors to form a narrow array of cells. Alternatively, they may undergo oriented divisions allowing them to move material from one direction to another.

Anisotropic deformations of epithelia, such as convergent extension, are the result of polarized stresses or anisotropic material properties within the tissue (Heisenberg and Bellaiche 2013). Anisotropic mechanics may be derived from the polarized architecture of epithelial tissues. Polarity is a defining feature of epithelia and occurs both in the depth of the tissue, apicobasal polarity, as well as in the plane of the sheet, planar tissue polarity. Polarity can organize the localization of specific cell behaviors that may generate anisotropic forces or modulate material properties.

1.1.1 Apical vs. Basal Cell Behaviors During Convergent Extension

Epithelial cell architecture compartmentalizes into an apical domain and a basolateral domain that confer polarity through the depth of the cell. Distinct cell behaviors and subcellular structures can reside within these compartments.

Within the apical domain, junctional complexes provide external mechanical linkages to neighboring cells that can facilitate collective behaviors needed for tissue deformation (Baum and Georgiou 2011). The apical junction complexes are internally connected to the cytoskeletal network within the cell that can generate forces to drive polarized behaviors at the apical surface (Arnold, Stephenson et al. 2017). For example, an actin cortex spans the medial apical surface and attaches to junctional actin (Fig 2). Pulsatile contraction of this cortex facilitates cell shape changes, such as apical constriction that can result in tissue deformation like bending or invagination (Martin and Goldstein 2014). Contractility is also thought to facilitate apical junctional remodeling that accompanies cell rearrangement in many converging and extending epithelia (Bertet, Sulak et al. 2004, Blankenship, Backovic et al. 2006, Chacon-Heszele, Ren et

al. 2012, Lienkamp, Liu et al. 2012, Nishimura, Honda et al. 2012, Williams, Yen et al. 2014). During this process, cell-cell boundaries contract and bring together four or more cells into a single vertex (Bertet, Sulak et al. 2004, Blankenship, Backovic et al. 2006). These vertices form transiently and eventually resolve into new junctions that form between cells that were previously not neighbors (Fig 3).

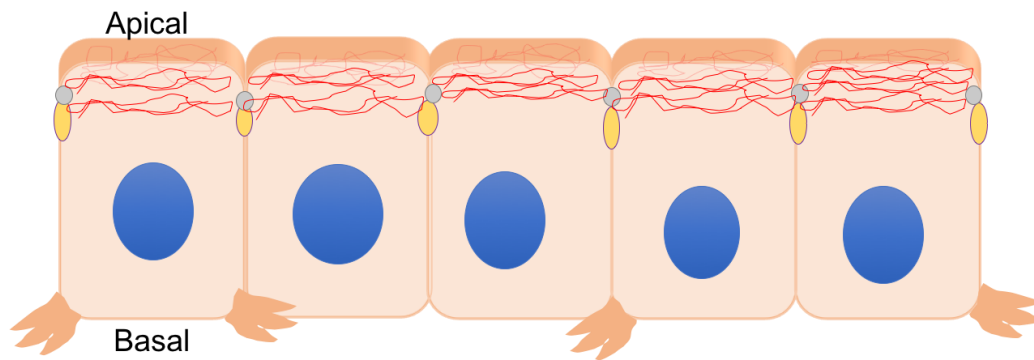
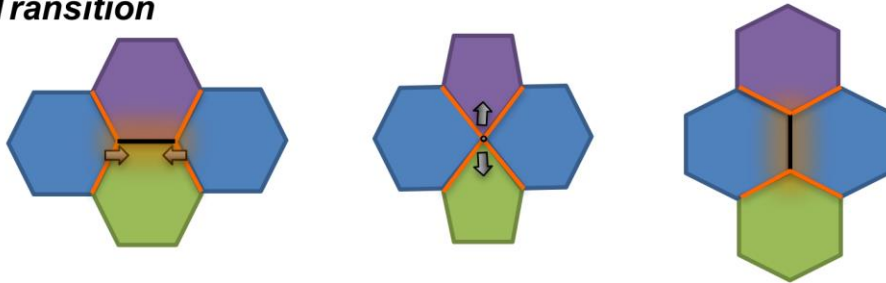


Figure 2. Schematic of apical-basal epithelial organization

Epithelial cells have different subcellular structures located in their apical and basolateral domains. Apically, junctional protein complexes (grey and yellow ovals) connect adjacent cells. These junctional protein are linked into the apical actin network (red lines). Basally, lamellipodia-like protrusions sometimes form.

T1 Transition



Rosette Transition

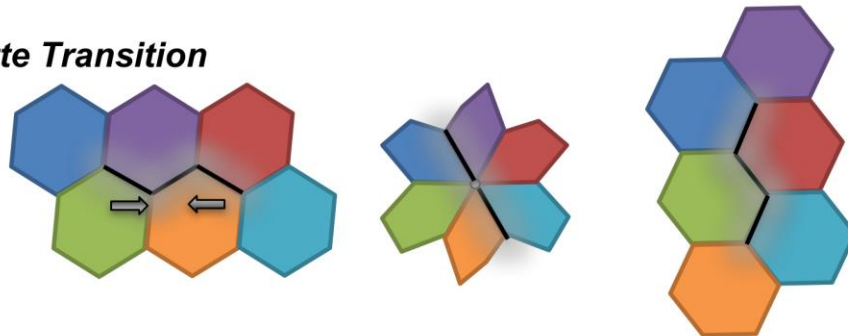


Figure 3. Junction remodeling and cell rearrangement

As cells rearrange, apical cell junctions remodeling. Junctions shrink in one direction and new junctions form orthogonally. Transient high order vertices form in between shrinkage and growth. T1 vertices form when a single shared junction brings 4 cells together. Rosette structures form when multiple junctions shrink to bring 5+ cells together.

The basolateral domain can also facilitate rearrangements through protrusive activity not seen apically (Fig 2). Basal protrusions have been described in ascidian notochord primordium, sea urchin archenteron, *C. elegans* hypodermis, mouse neural plate and most recently, *Drosophila* germband elongation (Hardin 1989, Williams-Masson, Heid et al. 1998, Munro and Odell 2002, Williams, Yen et al. 2014, Sun, Amourda et al. 2017) These protrusions may allow cells to interdigitate and undergo rearrangement in a manner similar to mesenchymal cell intercalation seen in the mesoderm (Shih and Keller 1992). Basal protrusion-based rearrangement and apical junctional remodeling are not mutually exclusive and can occur in conjunction with one another (Williams, Yen et al. 2014, Sun, Amourda et al. 2017). Thus, a given cell behavior, such as rearrangement, may be organized by multiple mechanisms at different levels within the epithelium.

1.1.2 Planar Polarized Behaviors

If an epithelial sheet is to elongate and narrow in the plane, then the cell behaviors that facilitate that movement must also have some planar orientation. During planar polarized cell rearrangement, apical junction remodeling occurs in an oriented manner. For instance, junctions that shrink are usually parallel to the direction of tissue narrowing. New junctions form parallel to the direction of elongation. In *Drosophila*, junctional remodeling is aided in part through asymmetric localization of cytoskeletal and structural proteins like myosin and E-cadherin at shrinking and growing junctions respectively (Bertet, Sulak et al. 2004, Rauzi, Verant et al.

2008, Levayer, Pelissier-Monier et al. 2011). Similarly, in the basolateral surface, protrusions and cell shape are usually oriented parallel the direction of tissue convergence (Williams, Yen et al. 2014, Walck-Shannon, Reiner et al. 2015). Polarized protrusions that form in the direction of tissue convergence may be determined by polarized Rac activity (Walck-Shannon, Reiner et al. 2015, Sun, Amourda et al. 2017).

How do proteins like myosin or Rac become localized to individual sides of cells? Protein targeting or activity can be regulated by molecular signaling pathways such as the core non-Canonical WNT Planar Cell Polarity (PCP) pathway. Targeting or activity is thought to be organized by asymmetric localizations of signaling protein complexes within the plane of the cell. Transmembrane protein complexes anchor to opposite sides of a cell to form mutually exclusive domains. These mutually exclusive domains interact with each other through extracellular coupling and allow translates an intracellular planar polarity between two cells to a tissue wide pattern of planar polarity (Fig 4A). In *Drosophila* wing disk, for example, the PCP transmembrane proteins Van Gogh (Vangl) and Frizzled each go to distinct sides of cells that fall along the proximal-distal axis of the embryo (Strutt, Weber et al. 1997, Usui, Shima et al. 1999). Vangl inserts into the proximal membrane while Frizzled goes to the distal face (Fig 4B). Neither localizes in the perpendicular anterior-posterior axis of the wing along the proximal-distal axis, each cell's proximal face is then connected to a neighboring cell's distal face. Thus, these complexes form complementary and mutually exclusive domains. As cells connect to one another, PCP can provide a larger patterning template through out the tissue. It is thought similar PCP asymmetries form on the anterior-posterior faces of tissues during convergent extension (Jiang, Munro et al. 2005, Ciruna, Jenny et al. 2006, Yin, Kiskowski et al. 2008, Ossipova, Kim

et al. 2015, Roszko, D et al. 2015). Once asymmetric distributions of the PCP signaling components are achieved, downstream effectors of these complexes can also become polarized.

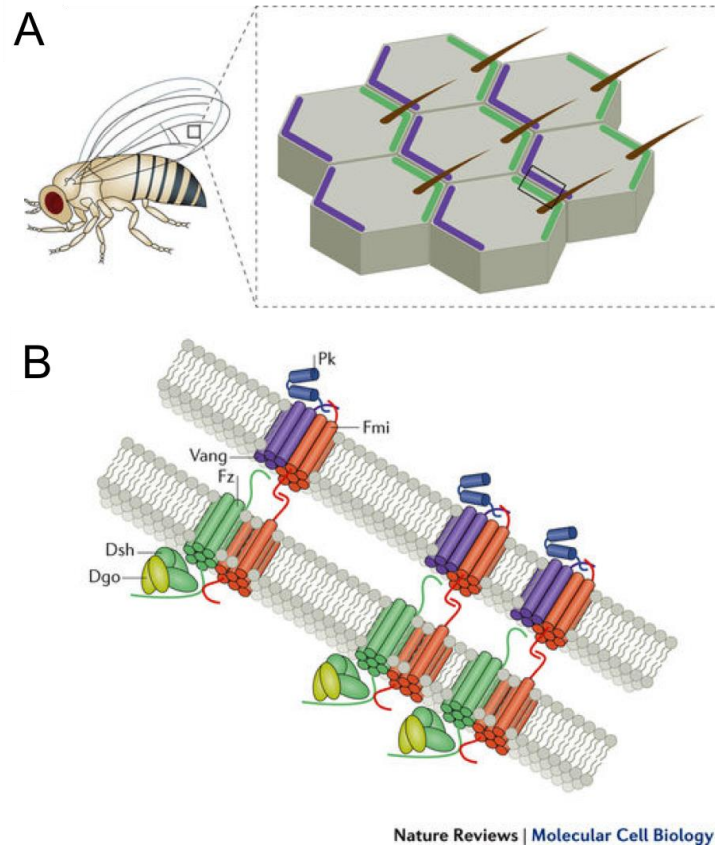


Figure 4. Planar tissue polarity can arise through polarized protein localization

A) Bristles found on *Drosophila* wing blades assume a planar polarized orientation in the proximal-distal axis. Cells within these tissues have asymmetrical localization of PCP protein complexes including the Vangl protein that accumulate proximally (purple) and complement protein complexes containing Frizzled that localize distally (green). B) PCP components form complexes that physically link adjacent cells. The transmembrane proteins Vangl and Frizzled associate with Flamingo (Fmi) which forms a homodimer complex and connect cells across opposing cell membranes. (Modified figure from Figure 1 in (Butler and Wallingford 2017))

1.1.3 Mechanics: a polarizing subject.

Mounting evidence suggests that, in addition to molecular patterning, anisotropic mechanical patterning can direct polarized cell behaviors both during convergent extension as well as other epithelial morphogenetic events. During *Drosophila* germband elongation, detailed analysis of cell shape strain rates compared to local tissue strains revealed that cell rearrangement was not the only strain generating behavior occurring during germband elongation (Butler, Blanchard et al. 2009). During an initial period of germband elongation, cell changed shape and stretch in the direction of tissue elongation. Interestingly, through a series of cell strain and tissue strain analyses of mutant flies, the authors concluded that a pulling force within the tissue likely polarized the cell shape. This study highlights the utility of tracking local tissue and cellular strains to generate mechanistic hypotheses for how mechanics may pattern cell behaviors.

Indeed, physical manipulations of tissues have been useful to demonstrate how mechanics can pattern cell behaviors. Application of exogenous strain or alteration of endogenous strain within tissues can orient or induce cell shape changes (Aigouy, Farhadifar et al. 2010, Etoornay, Popovic et al. 2015), neighbor exchanges (Lau, Tao et al. 2015, Yu and Fernandez-Gonzalez 2016), divisions (Eisenhoffer, Loftus et al. 2012, Campinho, Behrndt et al. 2013), cell protrusions (Weber, Bjerke et al. 2012) , and apical-basal polarity (Jackson, Kim et al. 2017). Mechanical forces may even induce or repolarize PCP molecular patterning (Mitchell, Jacobs et al. 2007, Aigouy, Farhadifar et al. 2010, Chien, Keller et al. 2015). Thus, polarized cell behaviors and tissue deformation may arise from an interplay between molecular and mechanical signaling and patterning (Miller and Davidson 2013, Heller, 2015 #99) (Heller and Fuchs 2015). To describe a complete story of how epithelial morphogenesis is achieved, mechanical cues within tissues must be assessed and controlled.

1.2 CONVERGENT EXTENSION DURING NEURAL PLATE SHAPING

The neural tube is an embryonic precursor structure of the vertebrate central nervous system. Morphogenesis of the neural tube begins with the neural plate, a planar portion of ectoderm on the surface of the embryo that must elongate, bend and fuse into a tubular structure that is internalized within the embryo. Convergent-extension, particularly in the posterior regions of the neural plate that form the hindbrain and spinal cord, initiates this series of deformations during the neural plate shaping phase (Jacobson and Gordon 1976, Keller, Shih et al. 1992). During this time, studies from amphibian, chick and mouse have shown cells rearrange, undergo height changes and later on, begin apically constricting (Burnside and Jacobson 1968, Alvarez and Schoenwolf 1992, Keller, Shih et al. 1992, Elul, Koehl et al. 1997, Williams, Yen et al. 2014). Planar cell polarity mutations, among others, are associated with defects in both convergent-extension tissue deformations, cell behaviors accompanying CE, and cause neural tube defects (Kibar, Vogan et al. 2001, Goto and Keller 2002, Wallingford and Harland 2002, Williams, Yen et al. 2014).

1.3 GOALS AND SPECIFIC AIMS

It remains unclear how PCP mutations act to perturb the cell behaviors and tissue level strains. PCP mutations may directly influence cell behaviors that can no longer produce the forces or behaviors that accommodate convergent-extension. Alternatively, PCP mutations that inhibit convergent-extension may indirectly alter cell behaviors due to a global disruption in the tissue mechanical pattern. Little is known currently, how mechanics might pattern neural plate cell

behaviors. Given the lack of tractable experimental models, prior studies have not been able to test these potential contributing factors. Therefore, we propose to use the experimental model of *Xenopus laevis* neurulation to test the contribution of the neuroepithelium mechanical environment to the polarized cell behaviors and tissue deformation of the neural plate with the following aims:

Aim 1: Characterize the endogenous behaviors of the *Xenopus laevis* neural plate epithelium during neural plate shaping

Aim 2: Assess the role of tissue strains in guiding cell behaviors during neural plate shaping

Aim3: Investigate the role of tissue strain in regulating aberrant cell behaviors in PCP disrupted neural plates

1.4 SIGNIFICANCE

Neural tube defects (NTDs), malformations of embryonic central nervous system structures, are one of the most common congenital disorders affecting nearly 3,000 infants born in the US each year (Williams, Mai et al. 2015). Manifestation of NTDs range in their severity with cranial region defects (anencephaly) often being lethal. The average lifetime cost of treating patients with spina bifida, spinal defects, is estimated to be \$560,000 (Grosse, Ouyang et al. 2008). Over 200 genetic mutations that cause NTDs have been identified in mouse and human, although most

of these mutations in isolation do not display full penetrance (Copp and Greene 2010). The etiology of many defects is thought to be multifactorial and include polygenic interactions, epigenetic and environmental components. Even with the identification of multiple risk factors, the physical mechanisms that prevent the neural tube from properly forming remain unclear.

It has been proposed that the major driver of neural plate CE is directed cell rearrangement via mediolateral intercalation behaviors (Keller, Shih et al. 1992). However, recently an alternative mechanism has been proposed in which planar polarized junctional remodeling drives directed rearrangement. In mouse and chick neurulation, mutations in the planar cell polarity pathway (PCP) inhibit junction remodeling and cause defects in CE (Nishimura, Honda et al. 2012, Williams, Yen et al. 2014). Yet while PCP may be necessary for directed rearrangement, it has not been shown to be wholly sufficient to initiate mediolateral intercalation behaviors. Alternatively, PCP may transduce other patterning cues within the tissues. One possible cue is mechanical patterning, as tensions acting on cells can polarize behaviors such as cell protrusions; anisotropic stresses may pattern neural cell behaviors in a manner similar to that observed in self-organizing epithelia such as the airway epithelium (Weber, Bjerke et al. 2012, Varner, Gleghorn et al. 2015). The neural plate is attached to other tissues such as the mesoderm and non-neural ectoderm that can generate forces and drive stress anisotropies within the plate. For example, the mesoderm underlying the neural plate also converges and extends while the endoderm simultaneously extends to create the archenteron. The neural plate may retain stresses created by earlier morphogenetic movements such as blastopore closure or involution. In addition to external sources of stress, as cells within the plate rearrange, the stress distribution within the tissue changes as well which in turn may alter the behaviors of the cells themselves. **Thus, this work seeks to understand whether mechanical**

cues may instruct cell rearrangement and ultimately convergent extension in neural tube development. To do so we harness the power of the *Xenopus laevis* embryonic model, which gives us the ability to mechanically isolate dorsal tissues and perturb endogenous tissue mechanics in a controlled manner. If successful, we will gain a deeper knowledge about the principles guiding neural plate CE and may understand more about how tissue mechanical environment may regulate neural tube defects. Our findings could allow us to leverage new targets for treatment of NTDs, and also guide tissue engineers who are interested in forming *de novo* tissues that require convergent extension.

2.0 MECHANICS OF NEURULATION: FROM CLASSICAL TO CURRENT PERSPECTIVES ON THE PHYSICAL MECHANICS THAT SHAPE, FOLD, AND FORM THE NEURAL TUBE

The following chapter is a published review on the current state of the biomechanical understanding of neural tube formation. Neural tube defects arise from mechanical failures in the process of neurulation. At the most fundamental level, formation of the neural tube relies on coordinated, complex tissue movements that mechanically transform the flat neural epithelium into a lumenized epithelial tube (Davidson, 2012). The nature of this mechanical transformation has mystified embryologists, geneticists, and clinicians for more than 100 years. Early embryologists pondered the physical mechanisms that guide this transformation. Detailed observations of cell and tissue movements as well as experimental embryological manipulations allowed researchers to generate and test elementary hypotheses of the intrinsic and extrinsic forces acting on the neural tissue. Current research has turned towards understanding the molecular mechanisms underlying neurulation. Genetic and molecular perturbation have identified a multitude of subcellular components that correlate with cell behaviors and tissue movements during neural tube formation. In this review, we focus on methods and conceptual frameworks that have been applied to the study of amphibian neurulation that can be used to determine how molecular and physical mechanisms are integrated and responsible for neurulation. We will describe how qualitative descriptions and quantitative measurements of

strain, force generation and tissue material properties as well as simulations can be used to understand how embryos use morphogenetic programs to drive neurulation.

2.1 A BRIEF HISTORY OF NEURAL TUBE MORPHOGENESIS

Developmental biologists have long debated the physical mechanisms driving neurulation. Early embryologists applied physical analog models to understand the basic mechanical processes that could cause the buckling and folding of a flat epithelial sheet into a tube and then sought to identify the intrinsic and extrinsic sources of force in those processes. In recent years, research has focused more on the genetic and molecular processes that guide neurulation. This latter effort has been successful in identifying numerous cell biological processes essential to neurulation and genes associated with neural tube defects but has struggled to connect these molecular mechanisms to the physical mechanics that directly shapes the neural tube. Both molecular-genetic dissection and physical mechanical exploration have yielded valuable insights into the complexity of neurulation and we are now at a time where molecular and biophysical approaches can be integrated to build a more complete understanding of how neurulation proceeds and how neural tube defects arise. This review will first briefly establish historical perspectives on the mechanical basis of neurulation and then describe modern approaches to synthesizing our current molecular understanding of neurulation with biomechanical analysis.

Tracing the historical formulations and refutation of hypothetical morphogenetic mechanisms provides a valuable perspective on the evolution of ideas as physical descriptions were supplemented with the molecular descriptions of this process. His' descriptions of the different stages of neurulation and experimentation with physical analogs showing how different

material sheets buckled led him to propose that pushing forces generated by the epidermis tissue along the lateral edges of the neural plate could drive neural plate invagination (His 1874). However, this theory lost favor when Roux separated the neural plate from adjacent tissue and saw that folds still formed (Roux 1885). Later embryologists proposed more intrinsic mechanisms that would drive folding through cell shape and volume change (Glaser 1916). While a causative role of intrinsic cell shape change was accepted, theories proposing volume change were refuted (Brown, Hamburger et al. 1941). In 1947, the focus on active physical mechanisms driving neurulation turned to the apical domains of neural epithelial cell sheets when Lewis created a physical analog of the 2D transection of an epithelial sheet with rubber bands and brass bars representing tension bearing apical gel layer (Lewis 1947). Lewis' physical analog models reproduced tissue invagination well and showed how previously observed flask-shaped cells, e.g. apically constricted cells might contribute to neurulation. By the 1960s, electron microscopy revealed the presence of unique subcellular structures, including newly visualized cytoskeletal elements and intracellular vesicles, which were correlated with cell shape changes and patterned within the neural epithelium during neurulation. Together with newly discovered small molecule inhibitors of the cytoskeleton, EM revealed the involvement of F-actin and microtubule cytoskeletal arrays in neurulation (Baker and Schroeder 1967, Karfunkel 1971, Karfunkel 1972, Brun and Garson 1983, Schoenwolf and Powers 1987). Live time-lapse, or cine-microscopy enabled detailed kinematic analysis of tissue shape change during the early phases of neurulation (Burnside and Jacobson 1968, Jacobson and Gordon 1976). These last studies lie at the foundation of modern studies on the physical and molecular mechanisms of morphogenesis and represent a productive methodology that continues today.

Associating actomyosin localization with cell shape change gave credence to the concept that epithelial tissues like the neural plate could autonomously deform through active apical constriction. Lewis' models provided a physical demonstration of the potential role of apical constriction, the concept of apical constriction actively driving epithelial deformation was proposed as early as 1902 (Rhumbler 1902). Apical constriction has since been observed in many cases of epithelial deformation including cell ingression and invagination during gastrulation as well as optic and otic placode formation (Ettensohn 1985). These experimental models of epithelial morphogenesis have enabled the identification of a number of molecular regulators of apical constriction (Sawyer, Harrell et al. 2010) and have suggested other concurrent, potentially redundant mechanisms driving epithelial folding such as basal expansion. These apical constriction independent mechanisms still result in a correlation between apical shape change and tissue folding. In order to understand the contribution of both apical constriction and alternative mechanisms of force generation to epithelial morphogenesis in general and neurulation in specific, a biomechanical framework of analysis is needed.

In 1990, Koehl reviewed the then current understanding of the physical basis for neural tube formation (Koehl 1990). The methodical approach, based on approaches to studying functional morphology (Wainwright, Biggs et al. 1976) and comparative biomechanics (Vogel 2003), offers an excellent introduction to the engineering definitions of mechanics and how biomechanical approaches can further our understanding of tissue morphogenesis (Shawky and Davidson 2015). The goal of this current work is to review efforts to expose the biomechanics of neurulation over the last 25 years and where future efforts are needed.

The 1990 Koehl paper identified five stages of a biomechanical analysis of a morphogenetic process. **#1) Qualitative description** of the process and qualitative statement of physical mechanisms involved. **#2) Qualitative experiments** where components of the physical mechanisms are removed or altered (e.g. removal of structural elements or altered mechanical boundary conditions). **#3) Quantitative analysis** of the process involving (a) morphometric analysis, (b) kinematic analysis, and (c) dynamic force measurements, and (d) measurement of mechanical properties, **#4) Quantitative statement of theories**, and **#5) Empirical tests of model predictions**. In addition to an update on progress in biomechanical analyses of neurulation we add a brief review of molecular pathways, how they may be used to formulate possible physical mechanisms, and how they may relate to the mechanics of neurulation.

2.2 QUALITATIVE DESCRIPTION OF PHENOMENA AND EMPIRICAL EVIDENCE

Primary neurulation can be broken into a series of deformations and tissue movements that convert the flat ectodermal sheet of tissue on the embryo's surface into an internalized tube. Many studies have described and proposed potential mechanical events leading to neurulation and we refer readers to elegant reviews of chick and mouse neurulation (Jacobson 1978, Schoenwolf and Smith 1990, Colas and Schoenwolf 2001). In this review we will describe the tissue movements in amphibians and correlate those movements with cell behaviors observed in both amphibians and other models. These correlations do not necessarily imply causation since cell shape changes and movements can occur in response to forces generated in different tissues

or cells. During the earliest step, known as plate shaping, the neural plate thickens in the dorsal-ventral axis, which is perpendicular to the anterior-posterior and medio-lateral axis of the embryo, and is accompanied by apical-basal height increases within the neural ectodermal cells that are thought to drive this process. At this same time, the lateral edges of the plate begin converging towards the dorsal midline while elongating in the anterior-posterior direction. This convergence and extension of the neural plate is accompanied by mediolateral cell intercalation. Intercalation can occur via polarized junctional remodeling as demonstrated within the mouse and chick epithelium (Nishimura, Honda et al. 2012, Williams, Yen et al. 2014) or through polarized protrusive activity, such as observed in deep mesenchymal cells of the *Xenopus* neural plate as well as in the basolateral surfaces of the mouse epithelium (Keller, Shih et al. 1992, Elul, Koehl et al. 1997, Davidson and Keller 1999, Williams, Yen et al. 2014).

In the next phase of neurulation, neural plate bending, a medial hinge point forms at the dorsal midline and lateral edges of the folds rise and are brought into apposition. The medial hinge-point is marked by wedge shaped midline cells adjacent to non-constricted cells (Schroeder 1970); apical constriction of these cells is thought to provide motive bending forces. Wedging at the midline is coincident with the elevation of lateral edges of the neural plate to produce neural folds. In chick and *Xenopus*, fold formation relies on adjacent non-neural ectoderm (Alvarez and Schoenwolf 1992, Morita, Kajiura-Kobayashi et al. 2012). Throughout this period, the neural plate continues to converge and extend, bringing the folds closer towards apposition as the neural groove deepens. Fold apposition may rely on the formation of dorsolateral hinge points, a line of wedge-shaped cells midway between the medial notoplate and lateral margins of the neural epithelium that may contribute to bringing folds towards the dorsal midline. Whereas medial hinge points are common in vertebrate species, the formation of

dorsolateral hinge points varies between species as well as its precise location within the neural plate. For instance, initial sites of closure at the level of the mesencephalic fold in the chick do not involve dorsolateral hinge points but instead appear to bring folds into apposition progressing ventral to dorsal (Van Straaten, Janssen et al. 1996). Differences in fold apposition between locations in the same embryo and between species suggest developmental programs of mechanics have evolved distinct mechanical solutions to the same problem, operating within a diverse set of physical constraints will still ensuring success of this key step in neurulation.

Shape changes at hinge points and throughout the neural plate and neural groove as the folds rise are accompanied by changes in the cytoskeleton and a rearrangement of intracellular structures. Notable among these changes is the accumulation of actin and myosin along apical cell-cell junctions and within the medioapical cortex of neural epithelial cells. Such an accumulation of actomyosin apical and the narrowing of apical surfaces is collectively referred to as apical constriction (Ettensohn 1985) and has been described in a wide range of epithelial folding events in development and organogenesis (Sawyer, Harrell et al. 2010). Within the *Xenopus* neural epithelium there are additional reductions in apical intermediate filaments and increases in basal-to-apical microtubule arrays (Baker and Schroeder 1967). Beyond cytoskeletal reorganization there is a movement of nuclei from apical domains to basal (Glaser 1914). This last movement, termed interkinetic nuclear migration (Messier 1978), has been observed in avian (Schoenwolf and Franks 1984) and amphibian neurulation (Lofberg 1974) and accompanies many other cases of epithelial folding such as the *Drosophila* ventral furrow (Leptin and Grunewald 1990). Contractile actomyosin networks are often considered the main source of force production within the neural plate but little is known about the contribution of other

cytoskeletal networks or the role of coordinating movement of intracellular organelles such as nuclei.

Once neural folds are apposed new cell-cell adhesions are formed between the apical surfaces of contacting cells in a process known as fusion. Little is known about this process but fusion must involve a carefully choreographed release of neural epithelial cells from their neighboring non-neural ectoderm. Both neural and non-neural ectoderm cells must exchange 'dis-like' neighbors for 'like' cells from the apposing fold, establishing a contiguous sheet of epithelial cells over the dorsal midline of the embryo and a contiguous neural tube beneath the epithelium. It is unclear how the two sides of apposed neural folds are aligned but in some species, fusion is initiated at stereotypical locations and cell adhesions are remodeled in a progressive manner known as zippering. Zippering of the neural folds can occur in both anterior-to-posterior or posterior-to-anterior directions. Where it has been observed in time-lapse or with high resolution imaging in mouse, zippering is accompanied by apical protrusions and membrane ruffles (Pyrgaki, Trainor et al. 2010, Rolo, Savery et al. 2016) that may ensure correct positioning of contacts between apposed folds. By establishing new contacts between the left to right sides of the embryo, cells in the epidermis and neural epithelium appear to resolve into new shapes with a new set of cell-cell contacts after the folds fuse.

Self-assembly of the vertebrate neural tube can proceed via two distinctly different mechanisms; *primary neurulation*, the process described above, involves bending and rolling of a sheet of cells contiguously into a tube whereas *secondary neurulation* involves neural lumen formation within of a solid cylindrical mass of cells (Lowery and Sive 2004). The extent to which these two modes of formation occur is species dependent. Teleosts appear to rely solely on the secondary form (Compagnon and Heisenberg 2013) whereas tetrapods appear to use primary

neurulation in the brain and anterior spinal cord, and secondary neurulation in posterior regions of the spinal cord (Criley 1969). The two modes of neurulation are compatible to the extent that different regions of the neural tube, e.g. dorsal or ventral may rely on secondary- or primary-like modes combined at the same anterior-posterior location (Costanzo, Watterson et al. 1982, Schoenwolf 1984). Such a state might occur during neurulation in the spinal region of *Xenopus* where both rolling and intercalation contribute to the formation of the definitive neural tube lumen (Davidson and Keller 1999). The physical mechanics of these two processes are likely to differ substantially. This review will focus on primary neurulation mechanisms, but a general biomechanical approach could be applied to understand secondary neurulation as well.

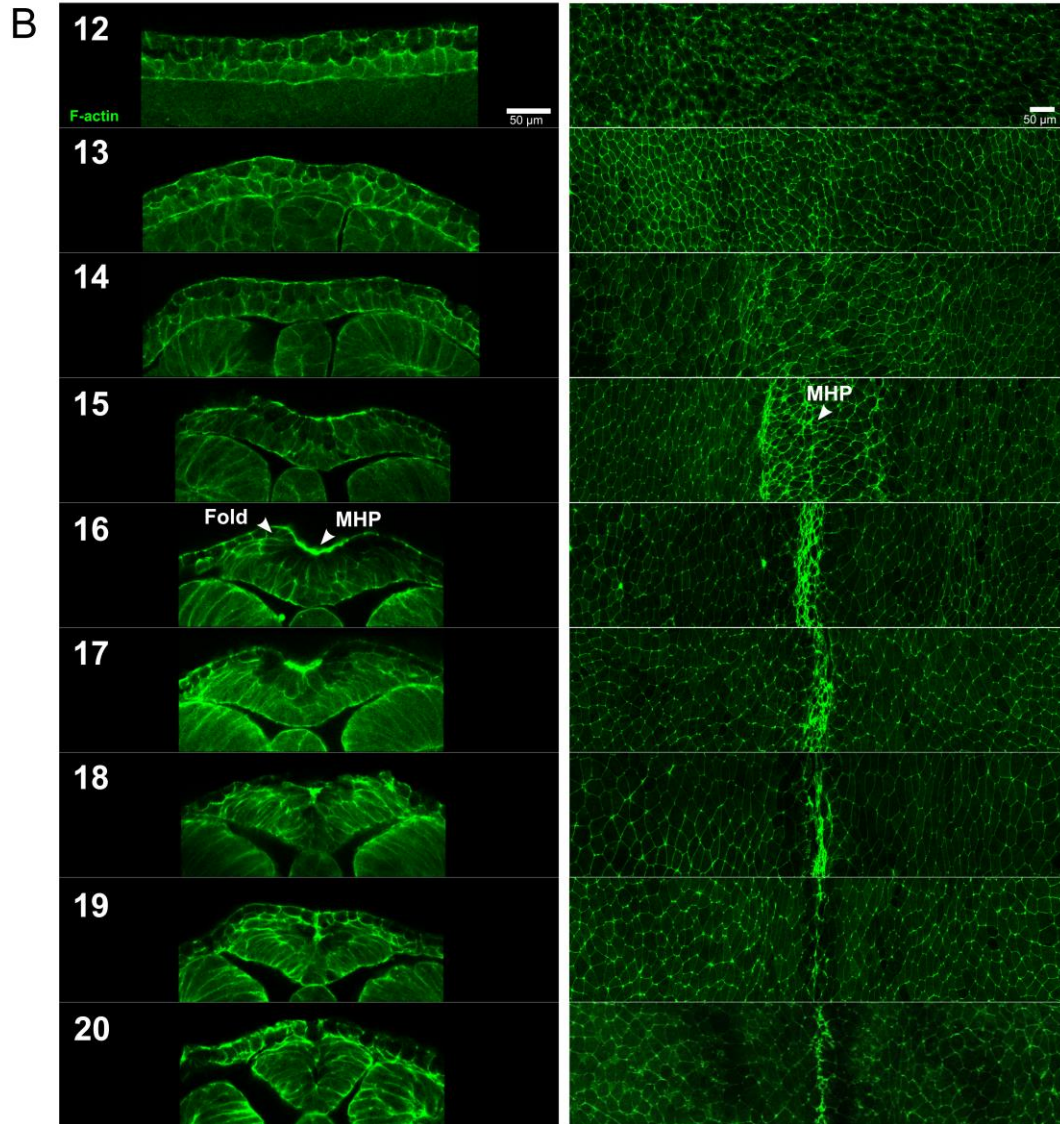
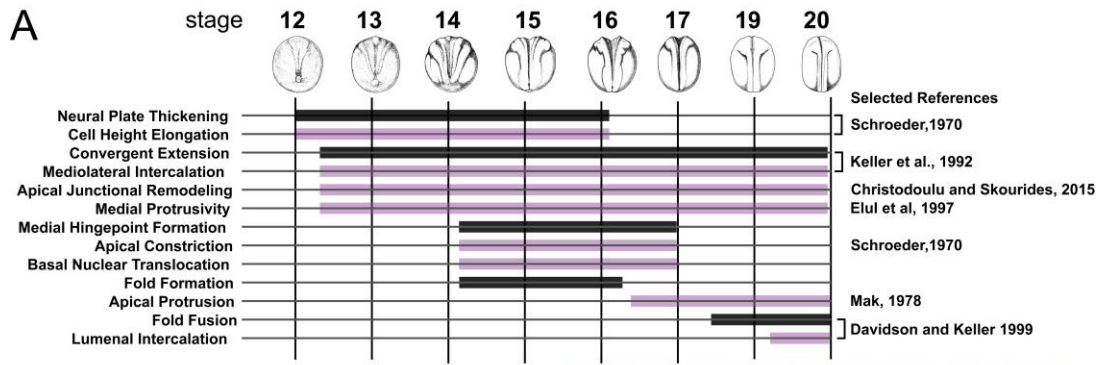


Figure 5. Concurrent mechanical processes shape the neural tube in *Xenopus laevis*.

A) Stage-dependency of specific tissue deforming processes (black bars) and cell behaviors (purple bars) that accompany the different phases of neurulation in *Xenopus laevis*. We refer interested readers to a similar diagram

describing tissue movements and cell behaviors during stages of chick neurulation (Schoenwolf and Smith 1990). B) Transverse sections and maximally z-projected *en face* sections of F-actin stained cell outlines of the posterior neural and non-neural dorsal ectoderm in fixed *Xenopus laevis* embryos showing cell and tissue morphological changes at each stage of neurulation.

2.3 QUALITATIVE EXPERIMENTS WHERE COMPONENTS ARE REMOVED OR ALTERED.

There are strong correlations between lesions in specific molecular pathways and neural tube defects. Just as physical isolation and microsurgical ablation experiments were able to reveal tissues that might contribute to neurulation, removing and altering these pathways using genetic ablation, knock-out, knock-down, dominant-active or dominant-negative overexpression have also informed our hypotheses on the mechanics of neural tube closure. We direct interested readers to a number of excellent recent reviews of genetic and molecular pathways and their involvement in neurulation (Copp and Greene 2013, Wallingford, Niswander et al. 2013) and note that many of these pathways regulate the cell structural components and force generating machinery (Suzuki, Morita et al. 2012). Furthermore, a surprising number of mutations linked to cranial and caudal neural tube defects lie in actomyosin regulators such as cofilin (Escuin, Vernay et al. 2015, Grego-Bessa, Hildebrand et al. 2015), Rac1 (Rolo, Savery et al. 2016), RhoA/ROCK (Kinoshita, Sasai et al. 2008, Nishimura, Honda et al. 2012), ENA/VASP (Roffers-Agarwal, Xanthos et al. 2008), and Shroom (Hildebrand and Soriano 1999, Haigo, Hildebrand et al. 2003, Lee, Scherr et al. 2007, McGreevy, Vijayraghavan et al. 2015). Since neurulation relies on polarized cell deformation, both planar cell polarity (Wallingford and Harland 2002) as well as apicobasal polarity pathways (Eom, Amarnath et al. 2012), which lie upstream of actomyosin

or microtubule dependent processes, are also involved in neurulation (Sokol 2016). The next challenges in these efforts involve understanding how genetic changes alter spatial and temporal protein activities, and how these pathways respond to mechanical cues as well as how they direct cell and tissue mechanics during neurulation.

2.4 INTEGRATING QUANTITATIVE DESCRIPTION OF KINEMATICS AND MORPHOMETRICS WITH MOLECULAR ANALYSIS

To understand the role of mechanics requires both morphometric and kinematic analyses of neurulation. Morphometric analysis is the quantification of static geometric features of cells and tissue in neurulation. Kinematic analysis is the quantification of the direction, magnitude and rates of movement. In combination, morphometric and kinematic analyses are particularly useful to understand the effects of molecular perturbations on tissue shape change. Together they can be used to describe strain occurring in the neural plate at both cell and tissue levels. In a simplified definition, strain is described as the change in length of an object with respect to a reference length.

Generally, when morphological defects are observed after molecular or genetic perturbation, researchers have quantified tissue level morphometrics such as distance between neural folds or width of neural plates as well as changes in overall tissue thickness (Wallingford and Harland 2002, Roffers-Agarwal, Xanthos et al. 2008, Massarwa and Niswander 2013, Itoh, Ossipova et al. 2014, Escuin, Vernay et al. 2015, Grego-Bessa, Hildebrand et al. 2015, McGreevy, Vijayraghavan et al. 2015, McShane, Mole et al. 2015). A number of these studies have gone on to quantify differences in cell level morphological properties to determine any

associations between cell level behaviors and tissue level morphologies. Researchers use transverse sections through the neural plate of fixed embryos to measure ratios between apical to basal width or between apical width and cell height in order to quantify degree of apical constriction between different treatment or conditions (Lee, Scherr et al. 2007, Suzuki, Hara et al. 2010, Eom, Amarnath et al. 2012, Itoh, Ossipova et al. 2014). Cell height changes and nuclear positioning can also be derived from transverse views (Lee, Scherr et al. 2007, Eom, Amarnath et al. 2012). *En face* views of cells allow researchers to determine planar cell elongation and apical area (Elul, Koehl et al. 1997, Lee, Scherr et al. 2007, Morita, Kajiura-Kobayashi et al. 2012, Christodoulou and Skourides 2015, Grego-Bessa, Hildebrand et al. 2015, McGreevy, Vijayraghavan et al. 2015). Techniques to visualize *en face* views of the neural plate in live embryos have been developed and allow researchers to track both cell morphological features such as apical area or cell junction length and tissue level morphology changes over time, providing morphometric and kinematic analyses of both normal as well as perturbed neurulation (Elul, Koehl et al. 1997, Morita, Kajiura-Kobayashi et al. 2012, Massarwa and Niswander 2013, Williams, Yen et al. 2014, Christodoulou and Skourides 2015).

Fixed embryos allow correlation between measured morphometric aspects of the neural plate and surrounding tissues such as cell height with markers that delineate cell identities, patterns of gene expression or protein activity. However, key dynamic or kinematic analyses of neurulation such as the determination of tissue or cell strain or strain rates cannot be measured from fixed samples; without a recording of the trajectory of earlier movement a static analysis provides no initial reference point for the tissue. Differences in static cell shapes and embryo morphology may reflect variability between embryos or variation across a field of cells. Alternatively, live imaging allows direct measurement of strain and strain rates by recording cell

or tissues morphology through time. The following examples describe the utility of live imaging for building mechanics-based hypotheses and exploring the subtle differences between molecular and physical manipulations.

Static and dynamic analyses of neurulation are key elements of both qualitative and quantitative biomechanical analyses. "End point analyses" of neurulation and neural tube defects, e.g. the static description of cell shapes and protein localization or activity at late stages of neurulation, can be useful when correlating phenotypes with different treatments. Extending quantitative analysis to the kinematics and morphometrics as the embryo passes through earlier stages can reveal multiple concurrent mechanisms contributing to the tissue deformation. A recent study of mouse neural plate convergent-extension highlights the utility of this approach (Williams, Yen et al. 2014). During tissue convergent extension, wild type cells display both polarized junctional remodeling apically and basally as well as directed basolateral protrusive activity. Mutations in *Vangl2* and *Ptk7*, both a part of the planar cell polarity pathway, impair tissue level convergent-extension with *Ptk7* mutants generating a larger defect. Morphometric analysis revealed each mutant alters different behaviors within the neural epithelial cells. Whereas *Ptk7* mutants lose all polarized behaviors both apically and basally, they maintain the ability to undergo unpolarized neighbor exchanges; by contrast, *Vangl2* deficient cells are unable to undergo proper neighbor exchange due to impaired apical junctional remodeling.

The forces driving neurulation cannot be inferred from analyses of tissue movements alone. A kinematic description of movement, i.e. characterizing tissue or cell deformation over time, is not sufficient to quantify driving forces, however, such an analysis can form the basis of mechanistic hypotheses for how and where these forces may be generated. Such mechanistic hypotheses can also take into account experimental embryological and biomechanical

observations. For example, analysis using distortion diagrams that describe local patterns of tissue strain in *Xenopus laevis* neural deep cell tissue explants revealed that regions surrounding the midline of the neural plate had high strain rates of both convergence and extension (Elul, Koehl et al. 1997). Subsequently, smaller explants including less lateral tissues showed an increased rate of convergence indicating medial tissues make a major contribution to convergent extension and that lateral tissues may inhibit this process. Further analysis of cell shape within medial tissues indicated cells would periodically become elongated in the mediolateral direction, perpendicular to the direction of tissue level elongation, indicating that cells were not simply passively stretched in the direction of tissue deformation. Together with quantitative descriptions of tissue movements in whole embryos the observations of episodic elongation in cell shape accompanied by polarized protrusive activity suggested that directed cell intercalation drives convergence and extension in the neural plate (Elul, Koehl et al. 1998).

Improvements in live imaging and recent advances in semi-automated image analysis techniques enable analysis of cell and tissue dynamics simultaneously during tissue morphogenesis. By tracking cells and tissues through time, it is possible to calculate strain, which is defined as change in dimensions of an object with respect to a reference. The "tissue tectonics" approach is an ideal platform through which events at the cell-scale can be correlated with global tissue level strain changes (Blanchard, Kabla et al. 2009). This approach involves tracking of local domains of cells through time and space and de-composition of those movements into invariant components of strain and strain rate produced by different cell behaviors, such as cell division, cell intercalation, cell shape change, and rearrangement. Tectonic analysis can reveal subtle patterns in morphology and kinematics that are easily overlooked by end-point or static analyses that focus on localized regions within the neural plate

at specific time points. In *Drosophila*, this and similar techniques, have shown how specific cell behaviors dominate various phases of tissue deformation and how tissue boundary conditions influence cell behaviors (Butler, Blanchard et al. 2009, Etournay, Popovic et al. 2015). Recently, this approach was used to show differences between cell elongation behaviors of the lateral ectoderm versus the early neural plate (Yamashita, Tsuboi et al. 2016). Such techniques increase the sensitivity of perturbation and ablation studies and will be useful in parsing the contribution of individual cell mechanisms in both wild-type and mutant cases of neurulation. A list of select image analysis software are described in Table 1 which are needed to begin these types of analyses.

Table 1 Useful image analysis software to measure cell and tissue morphological changes.

Many software packages allow researchers to quantify kinematic and morphometric data from live images. This table describes advantages and disadvantages of specific software used for general quantitative image analysis and software with specific uses for cell segmentation which allows data for individual cells to be derived in semi-automated or automated fashion and typically used with confocal images of apical cell surfaces. To our knowledge no single method is completely error-free and must allow the user to manually correct erroneously segmented cells.

Program	Usage	
ImageJ/FIJI (Eliceiri, Berthold et al. 2012) (Schneider, Rasband et al. 2012)	General image analysis software	<ul style="list-style-type: none"> • Java based • Established image analysis software used in biological research • Free • Built in graphical user interface (GUI) • Extensive documentation • Provides built in plugins for a number of analysis algorithms • Custom macros or plugins
SeedWater Segmenter (Mashburn, Lynch et al. 2012)	Watershed Algorithm Cell Segmentation Software	<ul style="list-style-type: none"> • Python based • Built in GUI • Semi-automated- allows for user correction of boundaries • Outputs data on select morphological parameters • Tracks cells through time stack • Open Source • Currently provides only 2D analysis • Can be slow with larger image files
MorphoGraphX (Barbier de Reuille, Routier-Kierzkowska et al. 2015)	Watershed Algorithm Cell Segmentation Software	<ul style="list-style-type: none"> • C++ Cuda based • Built in GUI • 2.5D Visualization and segmentation program • Recreates image surfaces based on 3D stack information • Open Source • Requires linux based operating system and special graphics card
TissueAnalyzer (formerly Packing Analyzer) (Aigouy, Farhadifar et al. 2010)	Watershed Algorithm Cell Segmentation Software	<ul style="list-style-type: none"> • Java based • Semi-automated segmentation method- Allows some user correction • Built-in GUI • Easy to install • Works with FIJI • Not open source

Table 1 (Continued).

<p>TissueMiner (Etournay, Merkel et al. 2016)</p>	<p>Cellshape analysis toolkit</p>	<ul style="list-style-type: none"> • R and Python based • Used in conjunction with TissueAnalyzer • Provides database structure for morphology information derived from segmented images • Has built in analysis tool to derive multiscale analyses of deformation and cell tracking • Provides graphical data visualization capabilities • Allows user to create personalized data analysis algorithms to be added to analysis library (require programming knowledge) • Provides 2D analysis • Not fully open source
<p>EpiTools (Heller, Hoppe et al. 2016)</p>	<p>Watershed Algorithm Cell Segmentation Software</p>	<ul style="list-style-type: none"> • Semi-automated segmentation – allows some user correction • Built-in GUI • Provides analysis of cell junctions • Outputs data on select morphological parameters • Interfaces with ImageJ • Accounts for surface curvature • Matlab based GUI
<p>SIESTA (Fernandez-Gonzalez and Zallen 2011)</p>	<p>Watershed Algorithm Cell Segmentation Software</p>	<ul style="list-style-type: none"> • Semi-automated segmentation- allows some user correction • Built-in GUI • Outputs data on select morphological parameters • Accounts for surface curvature • Matlab, DIPImage ToolBox based • Provides 2D analysis • Not open-source
<p>MEDUSA (Zulueta-Coarasa, Tamada et al. 2014)</p>	<p>Active Contour Snake-Based Cell Segmentation Software</p>	<ul style="list-style-type: none"> • Semi-automated segmentation – allows some user correction • Provides analysis of cell junctions • Outputs data on select morphological parameters • Accounts for surface curvature • Provides 3D segmentation • Matlab, DIPImage ToolBox based • Not open source

Table 1 (continued).

Matlab (Mathworks), Mathematica (Wolfram)	Numerical	<ul style="list-style-type: none">• Programmable• Many built in functions• Good handling of matrix operations• Faster debugging rates• Good Documentation• Slow compared to other programming languages• programming knowledge required• Expensive
ITK library	C++ based Bioimaging library for image analysis data processing	<ul style="list-style-type: none">• Many algorithms available for image segmentation, registration, stitching, and more• Can be wrapped in other languages (Python, Java)• Programming knowledge required

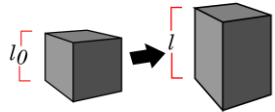
2.5 MEASUREMENT OF FORCES AND MATERIAL PROPERTIES

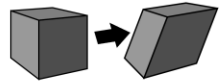
Embryonic tissues, like any material, deform under externally or internally applied loads or forces. The amount and manner in which a tissue or material deforms under a load depends on its material properties such as elastic stiffness and viscosity. Thus, to understand how tissue deformations during neurulation are physically driven one must characterize the forces acting upon and within the neural plate as well as the material properties of the neural plate and surrounding tissues. Given the important role of these properties during neurulation it remains surprising that few studies have quantitatively analyzed the material properties of and forces produced by cells and tissues during neurulation. Currently, most of our knowledge on the mechanics of neurulation comes from experimental mechanical studies on amphibian embryos (Selman 1955, Selman 1958, Wiebe and Brodland 2005, Benko and Brodland 2007, Zhou, Kim

et al. 2009, Zhou, Kim et al. 2010, Zhou, Pal et al. 2015). This is likely due to the large size and relatively simple culture conditions of these embryos making them ideal for physical manipulation and direct mechanical testing. While there are detailed descriptions of morphological changes during neurulation in a few species of amniotes and anamniotes very little is known about the process in human embryos or about the physical mechanics of neurulation in these animal model systems (Colas and Schoenwolf 2001, Araya, Ward et al. 2016). Recently, descriptions of static stages have been supplemented with descriptions of phenotypic changes in mutants and live cell dynamics in mouse mutants. For example, cell morphological and phenotypic changes in cofilin mutants (Grego-Bessa, Hildebrand et al. 2015) have been described, as well as Shroom3 and PCP mutants (McGreevy, Vijayraghavan et al. 2015) and Rho GTPase mutants (Rolo, Savery et al. 2016). Live imaging have described apical protrusion dynamics during fold fusion (Pyrgaki, Trainor et al. 2010 , Massarwa and Niswander 2013) as well as dynamic cellular behaviors during tissue convergent extension (Williams, Yen et al. 2014). Certainly mechanics must play an important role in these events but there have been no comparative studies that shed light on differences in the mechanical processes operating in these groups. To understand the comparative mechanics of neurulation in different animal model systems, researchers must develop novel techniques to manipulate and measure forces and tissue material properties of these tissues.

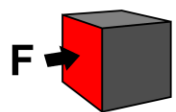
Strain Measurement of the deformation of an object under a load. Change in shape of an object with respect to a reference configuration

$\epsilon = \frac{l - l_0}{l_0}$ **Engineering Strain:** a change in length with reference to its initial configuration where ϵ is strain, l_0 is initial length (m) and l is the final length (m)

 **Normal strain:** Deformation of object due to force applied perpendicularly to surface. Extension or Compression

 **Shear strain:** Deformation of object due to force applied in parallel plane of surface

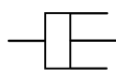
Stress & Force

 $\sigma = \frac{F}{A}$ **Stress:** Force applied over an area where σ is stress (Pa), F is force (N), and A is area (m²)

Tension: Pulling force exerted by a string or cable

Material Properties inherent physical property of a material that describes relationship of a material's deformation response to applied stress

$\sigma = E\epsilon$  **Elasticity:** Ability of deformed material under force to return to original shape after force is removed. Stress (σ) is a function of the elastic modulus (E) and strain (ϵ). Modeled as spring.

$\sigma = \mu \frac{d\epsilon}{dt}$  **Viscosity:** resistance of fluid to stress. Stress (σ), is a function of the viscosity coefficient (μ) and the strain rate ($d\epsilon/dt$). Modeled as dashpot.

Viscoelastic: Materials with both viscous and elastic properties

Figure 6. Formal definitions of mechanical terminology.

Engineering provides specific terms to create mechanical descriptions of biological processes. Provided are commonly used definitions that demonstrate the relationship between strain, stress and material properties.

2.5.1 Measurement of Material Properties

Tension within the neural plate of the axolotl, *Ambystoma mexicanum*, were measured with force-calibrated wires afixed to the apical surfaces of both neural and non-neural ectoderm (Wiebe and Brodland 2005). These tissues were then microsurgically isolated from the embryo and pulled apart while tissue deformations were tracked. A stiffness modulus could then be calculated (as the slope of the force resultant versus strain curve) and compared between different stage samples as well as between different tissue types (ie. neural vs. epidermal ectoderm). The stiffness modulus measured in these studies depends on tissue geometry. To translate the geometry-dependent stiffness modulus to a geometry-independent Young's modulus requires measurement of the cross-sectional area. Assuming a constant tissue thickness, the Young's modulus of neural tissue was estimated at 20 Pa. These studies demonstrated the existence of material anisotropy, regional differences, and stage-dependent differences in stiffness modulus based on tissue location within the anterior posterior axis but could not separate stiffness changes from positional or stage-dependent shape changes within the neural plate.

The mechanical properties of the neural plate and dorsal tissues of the African claw-toed frog, *Xenopus laevis*, were measured with an unconfined uniaxial compression test (also known as a creep or stress-relaxation test (Findley, Lai et al. 1989); (Zhou, Kim et al. 2009)). This method yields a measurement of the geometry-independent Young's modulus of dorsal tissue explants that contain all three germ-layers including the neural plate. This study revealed a stage-wise increase in axial tissue modulus (e.g. residual modulus). Furthermore, perturbation of actin and myosin through acute drug treatment revealed the role of the cytoskeleton in establishing a tissue's Young's modulus; however, disruption of actomyosin reduced the modulus but only 50%

indicating actomyosin accounts for some but not all of the ability of a neural stage embryo to resist mechanical tension and compression. In these tests the stiffness of the neural plate was estimated to be 40 to 60 Pa, similar to that of the underlying notochord. With these and other studies (Rolo, Skoglund et al. 2009, von Dassow, Strother et al. 2010, Zhou, Kim et al. 2010) revealing the dependence of neural mechanical properties on F-actin and myosin, it is highly likely that many of the upstream regulators of actin and myosin affect tissue mechanical properties.

2.5.2 Measurement of Force Production and Stresses within the Neural plate

In the 1950s, Selman measured the force of neural fold convergence using magnetic dumb-bells that were placed against the inside of folds of the alpine newt *Ichthyosaura alpestris*, and the axolotl (Selman 1955, Selman 1958). By creating magnetic repulsion between the dumb bells, Selman could estimate the force needed to stall fold convergence. These forces were variable but Selman found neural folds could produce 0.40 to 0.45 μN (40 to 45×10^{-3} dynes) in the newt and 0.8 to 1.1 μN (80 to 110×10^{-3} dynes) in the axolotl. In both species, Selman noted that the force needed to stall convergence increased over time.

Most recently, extensional stresses produced during neurulation were measured for *Xenopus laevis* tissues (Zhou, Pal et al. 2015). This approach utilized a gel based stress sensor in which dorsal tissue explants were embedded in an agarose gel. As the explant converges and extends, it pushes against the gel, generating stress within and causing deformation of the gel. Gel deformations tracked by observing the movements of microbeads embedded within the gel were converted into displacement and strain. Using the known material properties of the gel, the

mean stress generated along the anterior-posterior axis of the extending tissue was found to be ~ 5 Pa, or roughly 0.6 μN of force distributed over the transverse cross-sectional area of a dorsal tissue. Inhibiting rho-kinase (ROCK)-mediated myosin activity reduced stress production of these tissues. Surprisingly, no changes in the rates of tissue convergence and extension could be observed in ROCK-inhibited explants cultured outside the gel. In the absence of a mechanical 'phenotype' a conventional genetic interpretation would suggest ROCK is not involved. However, biomechanical analysis allowed the separation and quantification of two physical mechanical properties of the embryo, e.g. force production and mechanical resistance. Each of these mechanical aspects of convergent extension are co-affected and that their interaction after ROCK inhibition does not generate an obvious changes in neurulation. These studies also revealed that isolated neural plate isolates alone could generate extensional stresses similar to those produced by dorsal explants containing all three germ layers.

2.5.3 Estimating the mechanical status of contractile epithelia using microdissection via microsurgery or laser ablation.

Microsurgery has long been used qualitatively to distinguish active generation of forces from passive tissue deformation during morphogenesis (Schechtman 1942, Townes and Holtfreter 1955, Keller and Jansa 1992) but has been adapted recently for more quantitative analyses. Stress resultants within the early neural plate of axolotl embryos were measured using a force-calibrated set of steel wires (Benko and Brodland 2007). After affixing steel wires, the neural ectoderm was dissected from the remainder of the embryo and the position of the wires adjusted to minimize changes in shape of the newly released neural plate. This approach was used to estimate the tension exerted by the plate *in vivo*. Using a finite element model analogous to a

spherical pressure vessel, the authors estimated that non-neural ectoderm was under isotropic tension and that interior of the embryo during neurulation was under 1100 Pa pressure.

In animal models where physical manipulations are not possible, laser ablation can be used to probe tension within the embryonic epithelium. Laser ablation provides a semi-quantitative platform to understand stresses acting within tissue sheets. This method is analogous to early experiments involving cutting tissues to observe tissue recoil (Belousov, Dorfman et al. 1975, Jacobson and Gordon 1976). The advantage of the laser ablation technology in combination with modern imaging techniques is that one can accurately control where cuts are made and allow analysis of recoil within the first few seconds, which reduces the confounding influence of wound healing. Recoil in the first few seconds reflect the degree of tissue strain which is a function of both tissue tension and tissue stiffness (Ma, Lynch et al. 2009). Laser ablation can reveal differences in directional strain along boundaries and within the cortex of cells. Although absolute values for tension cannot be measured, most studies assume constant tissue stiffness and rely on instantaneous recoil velocity as an index of tension. These experiments are particularly useful in describing local and directional differences in strain within cell junctions or the cortex. However, it should be noted changes in recoil velocity might alternatively reflect changes in material properties of the cells. Though laser ablation has not yet been used in studying tensions within early neural ectodermal cells, it has been used to interrogate the mechanical status of the epidermis during processive neural fold fusion in *Ciona intestinalis* ascidian embryos (Hashimoto, Robin et al. 2015); ascidian neurulation appears similar to vertebrate neurulation and offers a unique comparative model for neural fold fusion.

2.6 SIMULATING NEURAL TUBE FORMATION

2.6.1 Physical Analog Models of Neurulation

Where mechanical testing of embryonic tissues may not be possible, physical analogs can provide a way to recreate the deformations seen in the neural ectoderm using materials of known material properties that could approximate the properties of embryonic tissues. Embryologists have mainly used physical analog models to test the plausibility of biomechanical theories on the origin of a particular deformation or what type of material properties cells and tissues might be an important factor in these deformations. Physical analog models can be built to represent tissue mechanics at different scales. Wilhelm His proposed compressive forces exerted by the lateral ectoderm could neural plate invagination similarly to how laminate sheets buckle under lateral compression. In this case, His viewed the neural plate as a contiguous material (His 1874). Lewis was one of the earliest investigators to consider the discrete cell mechanics of neural folding and invagination using brass bars and rubber bands representing individual cells and specific compartments in the neural plate (Lewis 1947). Rubber bands exerted a contractile force in the “apical” compartment of the model causing the system to become concave. This model demonstrated how differential contractility in the apical compartment could drive an entire epithelial sheet to buckle. Another model demonstrated how tissue extension may be sufficient to cause buckling by demonstrating the formation and convergence of ridges after pulling on a rubber sheet (Jacobson 1978). The simplicity of physical analog models remain attractive and can easily demonstrate biomechanical processes of folding (Fig. 7A). Scaled physical models can also be used to test different assumptions of experiments that test cell and tissue properties; for instance, a rubber band-connected model of a multicellular array can be dissected with "laser"

ablation and provide intuition about anisotropic conditions of tension and stiffness exposed by biophysical and embryological manipulations of embryonic epithelial sheets (Fig. 7B).

Whereas researchers have increasingly turned towards computational simulations to model biological processes, physical analogs can still play an important role in building the mechanical intuition needed to implement more complex computer simulations. Physical analogs can inform the biologist about the process of building models, the roles of implicit constraints such as boundary and initial conditions, and how models might be used with experiment. Recently, this approach proved to be illuminating in understanding the mechanical behavior of the curled embryonic gut (Savin, Kurpios et al. 2011). Early exploratory work with a physical model, where there are few obstacles to model development and modification, should be more broadly adopted in biomechanical studies of development in general and of neurulation in specific.

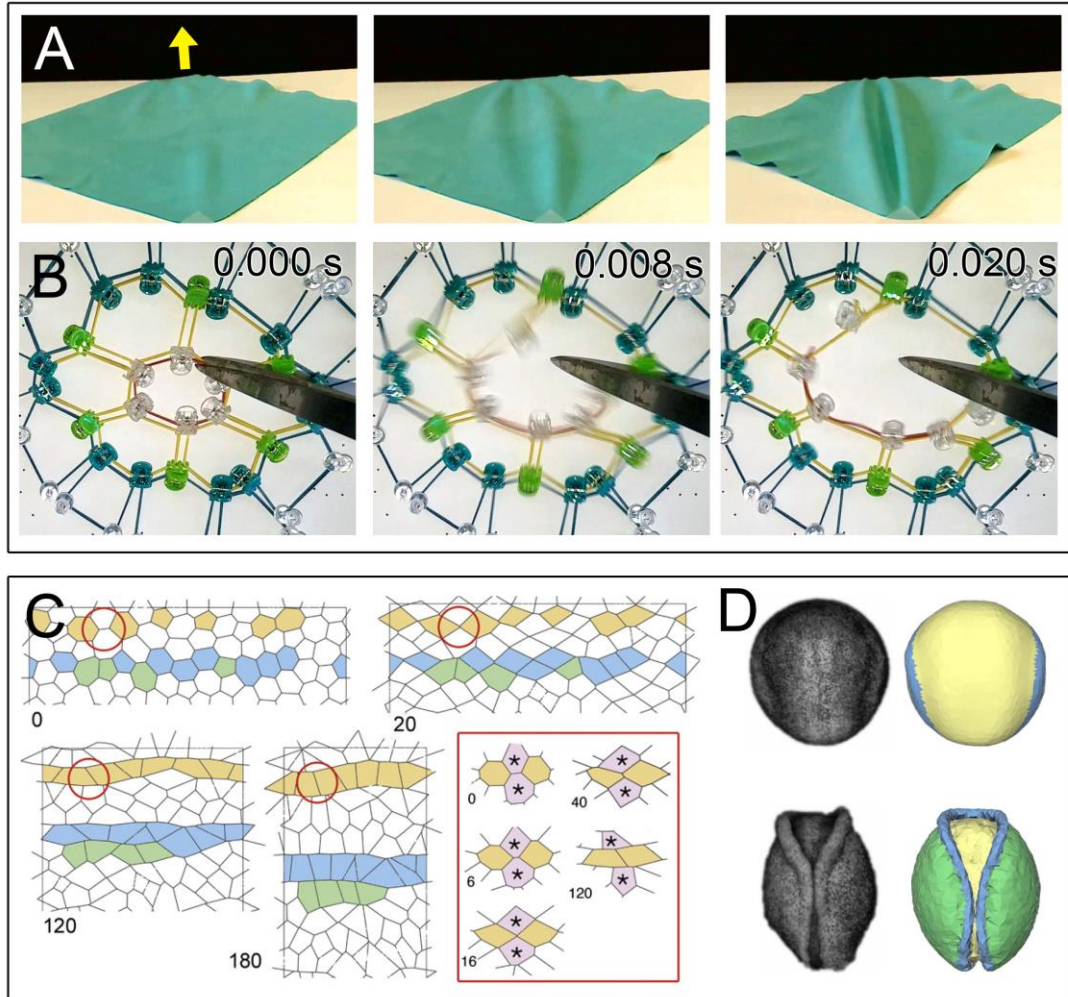


Figure 7. Simulating the mechanics of neurulation with physical analogs and computational models.

A) Physical analog model of fold formation in an elastic sheet. Tensile force is applied (yellow arrow) causing lateral buckling and fold formation. B) Physical analog model of laser ablation. Cells boundaries represented by network of elastic rubber bands under differential tension and with differential elasticity. When a single rubber band is cut, tension is released and network recoils. The instantaneous velocity of recoil reflects both the tension and mechanical properties of cell sheets in laser ablation experiments. C) Computational vertex-model of cell rearrangement during neural plate shaping in the chick. Patterns of cell-cell adhesion are predicted to produce aligned rows through directed cell rearrangement (modified from Fig. 2 in Nishimura et al., 2012; with authors' permission). D) Continuum model of axolotl neurulation. Finite element model based on image-acquired 3D geometry (modified from Figure 9 in Chen and Brodland, 2008; with authors' permission).

2.6.2 Computational Models of Neurulation

Just as physical analog models guided early embryologists current biomechanical analysis of epithelial morphogenesis is informed by computational models. Like physical analogs, these models can be constructed to test the roles of specific mechanical assumptions or theories of force-generation. A wide range of biomechanical and computational models have been developed to study epithelial morphogenesis and these can be broken down into several categories based on the level of detail at the cell and tissue levels (Davidson, Joshi et al. 2010). Two-dimensional models of the apical face of the neural plate or transverse sections across the neural plate can be assembled by connecting vertices representing cell-cell junctions by springs and dashpots (vertex-models; (Nishimura, Honda et al. 2012)). Vertex-models combined with material conservation laws can be constructed to recapitulate the complex elastic and plastic behavior of epithelial tissues and mimic the appearance and dynamic behaviors of living epithelial sheets. Few models have been developed to represent species specific mechanics of neurulation and have instead taken the form of more generic tests of convergence and extension (Weliky, Minsuk et al. 1991, Zajac, Jones et al. 2003, Brodland and Veldhuis 2006) and epithelial folding (Odell, Oster et al. 1981, Davidson, Koehl et al. 1995, Chen and Brodland 2008). Vertex-models (Fletcher, Osterfield et al. 2014) have been particularly useful in testing biomechanical hypotheses of "in-plane" movements, e.g. two-dimensional epithelial morphogenesis (Farhadifar, Roper et al. 2007), and the methodology has recently been extended to three-dimensional cases of morphogenesis (Murisic, Hakim et al. 2015).

Extending computational models to explore the complex dynamics of 3D tissue movements in complex composite tissues has proven challenging. For instance, vertex-models use spring-like struts (incorporating contractility and adhesion) to represent structures such as

adherens junctions in 2D models but do not represent sheet-structures that compose basolateral cell-cell contacts, dispersed point-like desmosomes, or extracellular matrix found along the basal surface of most epithelial sheets. To side-step these difficulties two different modeling strategies have been taken: 1) particle based 3D models in which each cell in a tissue can be represented by a set of self-interacting particles or discrete virtual cells (Sandersius, Weijer et al. 2011, Palm and Merks 2015), or 2) continuum 3D models in which cell-cell interfaces and internal structures are lumped within finite element models (Taber 1995).

Both continuum- and vertex-models have been useful tools to extend experimental intuition concerning mechanics-based hypotheses of neurulation. The cellular focus of vertex-models has been most compatible with cell-focused analyses of morphogenesis. By contrast, continuum-methods are more robust in representing large-deformations and complex nonlinear materials that compose the embryo. Ideally, future modeling approaches will need to incorporate hybrid formulations combining continuum methods with discrete representation of cells, complex extracellular interfaces, and extracellular matrix. Such hybrid models would be more flexible and able to predict the roles of intracellular programs of force generation and their impact on macroscopic processes of force transmission and collective tissue movement involved in neurulation.

2.7 MECHANICS AS COMPONENT IN THE SIGNALING NETWORKS OF NEURULATION

Ongoing studies in mechanobiology suggest a complex interplay between mechanics, cell and subcellular protein activity, and subsequent tissue deformation (von Dassow and Davidson 2011, Heisenberg and Bellaiche 2013, Sasai 2013). Not only do cell behaviors drive mechanical events within tissues, but mechanics can feedback to cell signaling pathways and influence cell behaviors both passively and actively. Growing evidence supports the role for mechanics as a patterning cue during development (Heller and Fuchs 2015). Central to the patterning function of mechanical cues is the establishment of anisotropic tissue strain fields that can orient cell divisions, initiate shape change, and guide protrusive activity (Aigouy, Farhadifar et al. 2010, Weber, Bjerke et al. 2012, Campinho, Behrndt et al. 2013, Chien, Keller et al. 2015, Etournay, Popovic et al. 2015, Lau, Tao et al. 2015). Recent work in both fly and frog suggests anisotropic tissue strain can directly regulate planar tissue polarity via non-canonical WNT or PCP signaling pathways. Cells isolated from wing hinge contraction in the drosophila pupal wing can prevent the endogenous reorientation of PCP complexes needed to instruct polarized cell behaviors (Aigouy, Farhadifar et al. 2010). More recently, studies using *Xenopus* skin ectoderm showed that isolating early gastrula ectoderm from large scale movements in the embryo prevents efficient PCP polarity stabilization at later stages (Chien, Keller et al. 2015). This defect can be rescued with the application of exogenous strains onto tissue explants showing that strain may orient PCP components in a timely manner. The authors suggest that, *in vivo*, strains generated by gastrulation guide this process. Such studies set a precedent for exploring how mechanics may influence signaling networks that control PCP or apico-basal polarized cell behaviors in neural tube morphogenesis. As planar cell polarity genetic mutations are found in neural tube

defects, our understanding of how these genetic defects are manifested may benefit from evaluating the mechanical background against which they act and vice versa. Should mechanical regulation operate during neurulation, an important question is how these mechanical cues are transduced to affect cell behaviors. Cell culture studies have identified a number of mechanosensitive proteins including those associated with cell adhesion and mechanically gated ion channels that could allow cells to sense mechanical cues and use these cues to direct morphogenetic processes (Miller and Davidson 2013).

2.8 BIOMECHANICS OF NEURULATION, NEURAL TUBE DEFECTS, AND ROBUST DEVELOPMENT.

The ultimate goal of building a mechanical description of neurulation is to understand the origins of human neural tube defects. Since all neural tube defects are mechanical in nature, an understanding of neurulation mechanics should allow us to attribute these defects to specific cell biological sources that result in defects in tissue mechanical properties, cell force generation, or patterning. Over the last 125 years, the plausibility of many hypotheses on the mechanical processes contributing to neurulation have been demonstrated in physical analogs, computational models, or through qualitative embryological manipulation, however, little is known about contribution of specific biomechanical processes to maintaining robust neurulation. Biomechanical lesions underlying birth defects, either through genetic or environmental perturbations, remain unknown. To understand the incidence of birth defects will require a quantitative understanding of how phenotypic changes in neurulation vary with genotypic and environmental perturbations. Forging this linkage between genetics, mechanics, and functional

morphology remains a major challenge to understanding developmental biomechanics (von Dassow and Davidson 2011). With the broader availability of experimental biomechanical tools, advanced cell biological methods, and predictive conceptual frameworks we anticipate the predictive power of computational simulations of neurulation will be combined with experimental biomechanical analyses to build more complete understanding of the mechanics of neurulation and the origin of neural tube defects.

3.0 NEUROEPITHELIUM CELL BEHAVIORS DURING *XENOPUS* NEURAL PLATE SHAPING

3.1 INTRODUCTION

The formation of the vertebrate central nervous system begins with the morphogenesis of the neural tube early in embryonic development. The neural tube starts as the neural plate, a flat sheet of dorsal surface ectoderm that is specified during late gastrulation (Gilbert 2000). At the end of gastrulation, the neural plate undergoes a series of deformations that converts it from a planar tissue into an elongated, tubular structure that is internalized within the embryo. During the first step of this process, the neural plate shaping phase, the lateral edges of the neural plate begin converging towards the dorsal midline while the tissue simultaneously elongates in the perpendicular anterior posterior axis. At the end of plate shaping, folds elevate at the lateral border of the plate and the plate bends at the dorsal midline. These bilateral folds continue to converge and eventually meet in apposition at the dorsal midline at which point they release from neighboring non-neural ectoderm and fuse into the neural tube. The non-neural ectoderm fuses over the neural tube to internalize it within the embryo. Failure of convergent extension may lead to failure of fold apposition and/or fusion (Wallingford and Harland 2002).

Like any deforming material, forces may act upon or within the neural plate to drive the requisite tissue shape changes. As tissues in the embryo undergo self-assembly, internal forces

may arise from the coordinated behaviors of the constituent embryonic cells. Studies on cellular behaviors concomitant with neural plate shaping have spawned a number of hypotheses responsible for cellular force generating mechanisms of tissue CE. Seminal work applying morphometric analyses in *Taricha taorsa*, newt, embryos showed the neural plate cells increase in apical-basal cell height (Burnside and Jacobson 1968). This height change correlated with a simultaneous narrowing of the cell apical surface was proposed to drive convergence of the neural plate.

However, subsequent computer models, suggested cell shape change alone could not account for the “keyhole” or elongated shape of the tissue (Jacobson and Gordon 1976). Further observations from this work raised the possibility that oriented cell rearrangements within the neural plate midline, where wide arrays of cells intercalate into long narrow arrays of cells, may provide the motive force for elongation. Similar cell rearrangements have been proposed to occur in chick neural plates where an additional role for oriented cell divisions has been suggested (Alvarez and Schoenwolf 1992, Sausedo, Smith et al. 1997)

Directed cell rearrangement also occurs in fish, frog, and mouse embryos. In mesenchymal cell populations such as the deep cell layer of the bilayer *Xenopus* neural plate, cells display mediolateral intercalation behaviors utilizing polarized protrusive activity that facilitates cells rearrangement with their neighbors (Elul, Koehl et al. 1997, Davidson and Keller 1999, Ezin, Skoglund et al. 2003). In simple epithelia, like the chick neural tube, apical junctional remodeling events have also been observed (Nishimura, Honda et al. 2012). Directed apical junction remodeling has been traditionally viewed as the driving mechanism of cell rearrangements in other systems of epithelial convergent-extension. Pioneering work in *Drosophila* germ band elongation found that cell-cell junctions shrink in a preferred direction to

form an intermediate state where 4 or more cells meet at a single vertex; new junctions then grow in a perpendicular fashion causing an exchange of cell neighbors (Bertet, Sulak et al. 2004, Blankenship, Backovic et al. 2006). Observations from converging and extending mouse neural plates suggests that neuroepithelial cells actually use both directed apical junctional remodeling as well as basolateral protrusive activity (Williams, Yen et al. 2014). Recent, more detailed observations during *Drosophila* germ band elongation suggested that the basolateral protrusive activity drives rearrangements basally first with apical cell junction remodeling following (Sun, Amourda et al. 2017). Thus, even in the case where directional junction remodeling was first described, basal rearrangements may predominate.

It remains unclear whether a dominant mechanism exists within the neuroepithelium as the work in mouse suggested both “apical first” and “basal first” rearrangements occurred in equal frequency. Regardless of the apical or basal origins, directed cell rearrangement is widely considered the driving mechanism for CE as it frequently accompanies elongating tissues not just neural tube formation but a host of other tissues undergoing convergent extension (Keller 2002)..

This chapter investigates the endogenous behaviors of *Xenopus laevis* neuroepithelial cells as the posterior neural plate is shaped. We have adapted and developed imaging and image analysis tools to segment and extract cell shape and topological maps for fixed and live image sequences of developing neural plates. Using these tools, we analyze patterns of cell level and tissue level strains that accompany neural plate convergent extension. Cells at the lateral border of the neural plate elongate in the direction of tissue extension. Cells medially within the neural plate have varied strain patterns that do not match tissue strain patterns, ruling out shape change as a driving mechanism for tissue deformation. Medial neural plate cells undergo directed rearrangements, which initiate in the basolateral domain of cells and then propagate apically

where cell junctional remodeling occurs. Rearrangements are accompanied by basolateral protrusions. Together, these results reveal distinctive programs of cell shape change and rearrangement during neural plate convergent extension.

3.2 RESULTS

3.2.1 Regional patterns of cell shape across dorsal ectoderm and neural ectoderm during plate shaping

To establish the timing of cell shape changes that accompanied neural plate shaping we fixed embryos at four stages from late gastrula (Nieuwkoop and Faber (1967), NF; NF stage 12.5) through early groove stages (NF stage 15) (Fig 8A). F-actin was labeled with bodipy-phalloidin, and we collected confocal z- stacks of the apical dorsal surface. We segmented F-actin cell outlines in z-projected maps of the posterior spinal region of the neural plate (Fig 8B). The neural plate is contiguous with non-neural ectoderm on each of its lateral edges but these boundaries are not initially apparent in cell morphology. To confirm the identity of cells across this field and to estimate the neural plate width at each stage, we tracked the limit of cytokeratin filaments that are enriched in the apical domains of non-neural ectoderm and demarcate the boundary between the neural and non-neural ectoderm beginning at stage 13 (Fig 8C). We confirmed cytokeratin reliably marked the neural plate boundaries by comparing it to similar staged neural plates stained for Sox3, a positive marker of neural cells (Fig 8D). Using the cell boundary-segmented images we measured cell shape parameters describing apical area and apical elongation as a function of cell distance from the dorsal midline region.

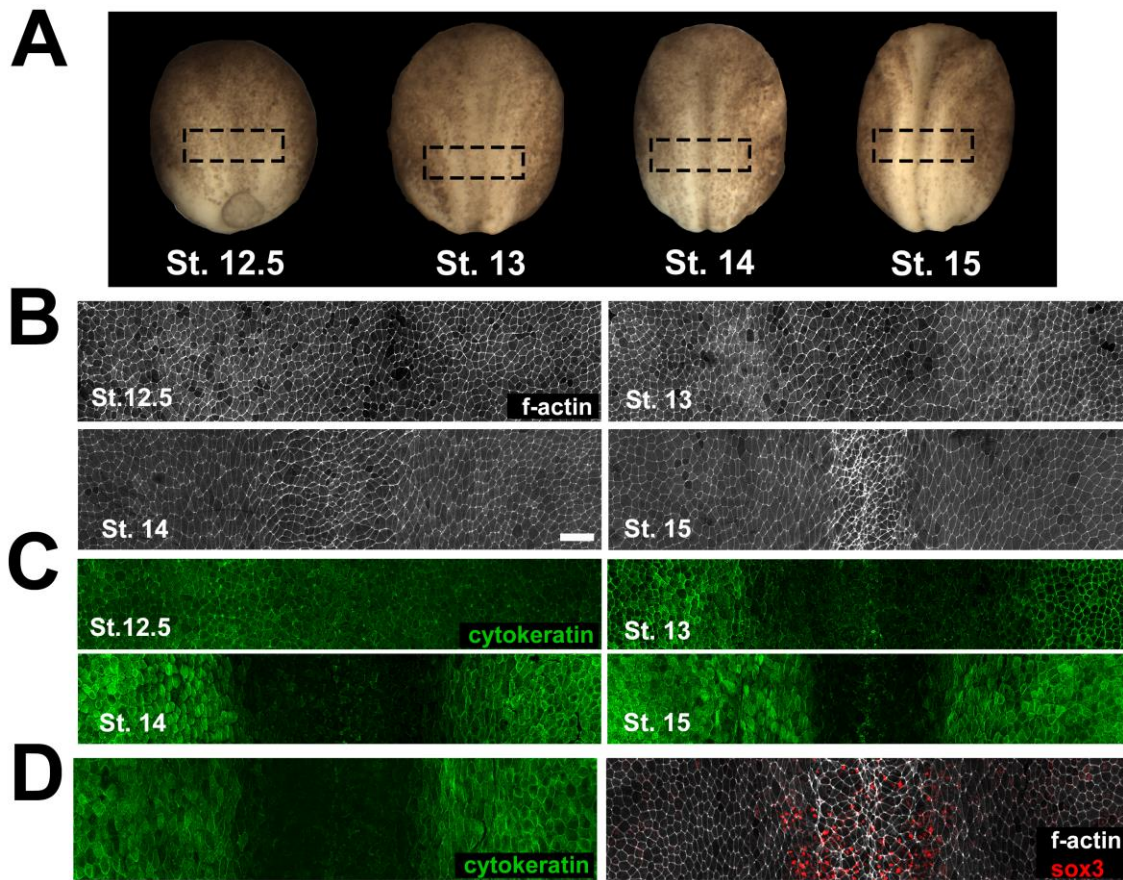


Figure 8. Spatiotemporal changes in cell shape during plate shaping.

A. Embryos fixed at 4 stages during neural plate shaping from end of gastrulation (stage 12.5) to the end of the neural plate phase (stage 15). Box indicates approximate location of cell analysis in the posterior axis b) Z-projection of f-actin cell outlines on the apical dorsal surface of phalloidin stained embryos. Cell outlines are segmented for morphology and vertex order analysis. Scale bar 100 μm . C. Z-projected map of keratin in the apical dorsal surface of embryos. In stages 13-15, neural ectoderm has reduced keratin. D. Keratin and Sox3 staining in stage 14 neural plates.

Through shape analysis of fixed samples, the apical area of cells at the midline of the neural plate becomes progressively constricted by stage 15 (Fig 9A). Additionally, by stage 14 cells at the border of the neural plate become significantly elongated compared to cells at the midline (Fig 9B). At the border, elongated cells, with an aspect ratio greater than 1.5, align in the with the anterior-posterior (AP) axis. Interestingly, cells within the medial neural plate were less elongated and become less aligned with the AP axis at stage 14 (Fig 9C).

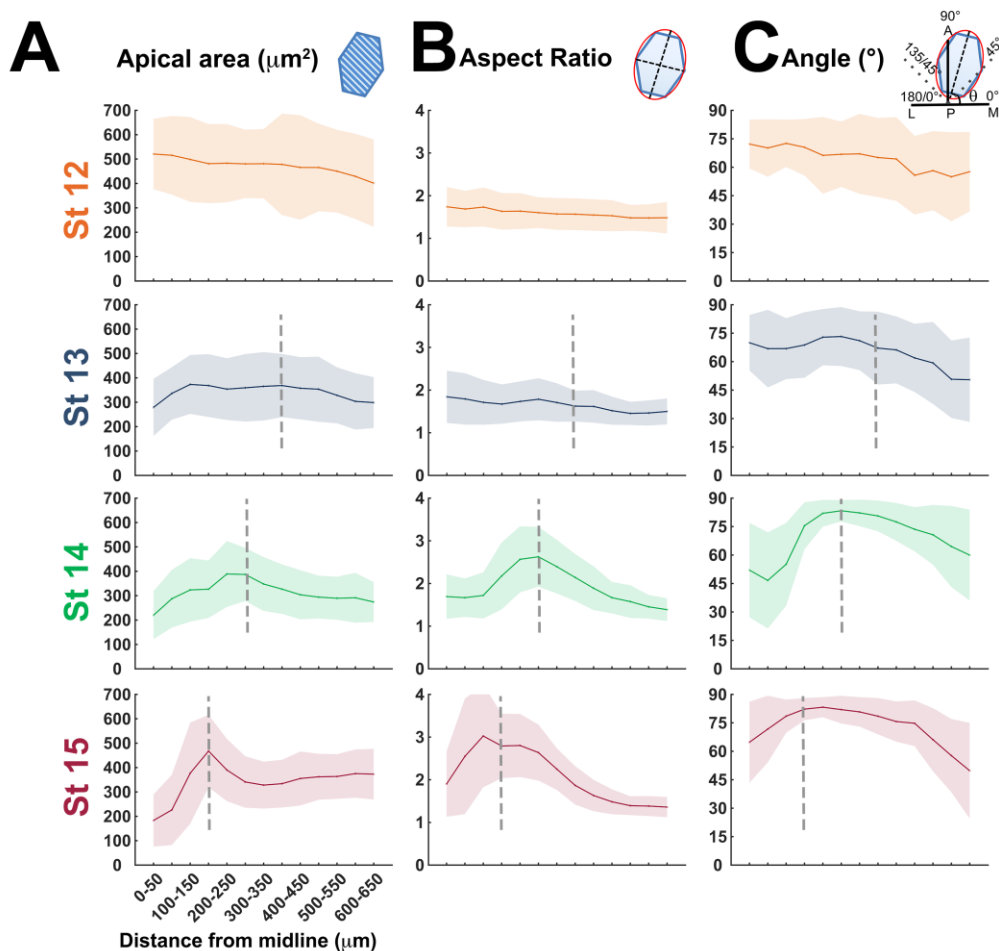


Figure 9. Morphometric measurements of cells at different stages reveal distinct patterns of cell shape.

A) Average cell apical area is plotted for each stage as a binned distance from the neural plate midline. Bins are 50 μ m. 200-300 cells per bin. Data pooled from 4 embryos per stage. Ribbon indicates standard deviation. Dotted line indicates estimated border of neural plate from keratin staining. B) Cell aspect ratio (major/minor axis of fit ellipse) patterns as a function of distance from midline and stage. C) Cell orientation (angle of major axis of fit ellipse) patterns as a function of distance from midline and stage. Angles measured for cells with aspect ratio > 1.5. AP axis is 90° and ML axis is 0°

To determine whether cell shapes reflect tissue strains, confocal time-lapse image sequences were made of the posterior neural plate in transgenic whole embryos (n=2) and dorsal isolate explants (n=3) that express a membrane-GFP marker in all cells. Dorsal isolates are tissue explants that contain all three germ layers including the neural plate and have been shown to converge and extend even in isolation from the embryo (Zhou, Pal et al. 2015). From timelapses, we tracked cells over an hour between stages 13 and 14 (Fig 10A). We then performed a tissue tectonics analysis (modified from (Blanchard, Kabla et al. 2009) where we calculate the strain in local tissue domains, called coronas, and contrast tissue strain to shape strains of individual cells within that domain (Fig 10B-E). This analysis reveals a complex pattern of cell and tissue 'concordance', e.g. where cell and tissue strains align in the same direction. Concordant strains suggest that either cell shape changes drive tissue shape changes or that tissue strains guide cell strains. Alternatively, if the direction of cell strain does not match the direction of tissue deformation, e.g. that cell and tissue strain are 'discordant', it is unlikely cell shape change guides tissue deformation. We called this a “discordant” relationship between cell and tissue strain.

Tissues samples showed highly variable spatial patterns of strain (Fig 10 F-G). There were some general trends: (1) mediolateral tissue strain rates revealed the neural plate converged at a rate ranging from -10% to -40% per hour (Fig 10H); (2) the medial region tended

to converge than more lateral tissues. Strikingly, cell level ML convergence rates showed cells either converged much less compared to tissues or in some cases actually elongated in the ML direction, discordant with tissue level convergence. AP tissue strain rates reveal patterns of tissue elongation in the AP direction with rates ranging from about 10% to 40% per hour (Fig 10H). Strain rates are highest in lateral regions. Cell strain rates near the midline showed cells either shrank in the AP axis, discordant with tissue elongation, or did not elongate much at all (Fig10H). Laterally, however, most neural plates had cell AP strain rates that were concordant with, albeit of lower magnitude than tissue AP strain rates.

In the midline, both AP and ML cell strains are discordant to tissue level strains and thus suggest that cell shape change is unlikely to be a driving mechanism for tissue CE in this region. Similarly, in lateral tissues, ML cell shape strain does not always reflect ML tissue convergence. However, AP cell elongation in this region is concordant with AP tissue elongation. In this case, it is possible that cell elongation is contributing to tissue elongation or alternatively, cells are passively stretched by the tension anisotropies generated by tissue elongation. Overall, live imaging corroborates observations of static fixed neural plates that showed at stage 14, cells more at the border of the neural plate become highly elongated in the AP direction where as elongated cells at the midline became less aligned with the AP axis. Since midline cell shape does not reflect the tissue strain, we propose these cells undergo rearrangement to facilitate CE.

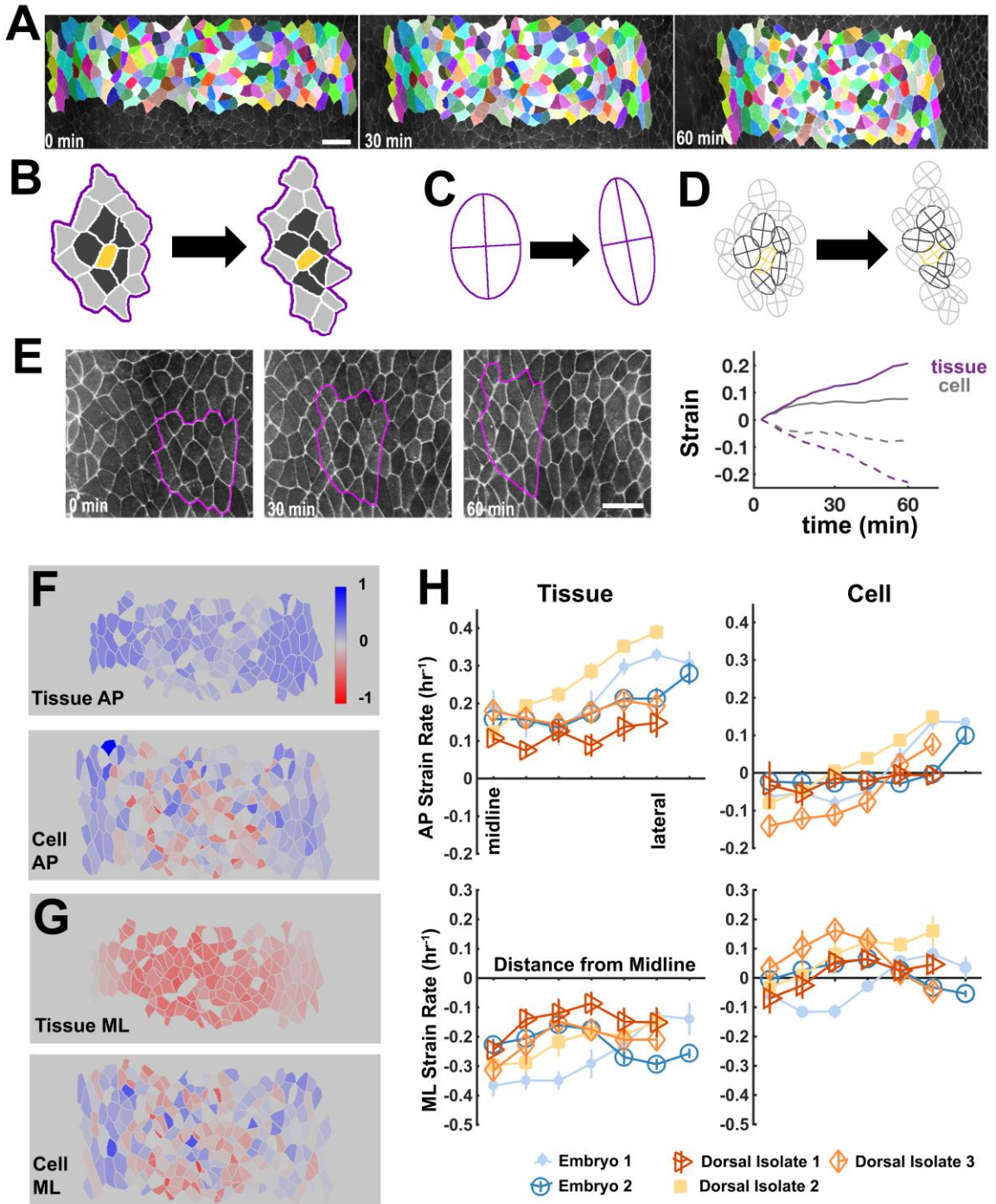


Figure 10. Tissue tectonic approach to quantify cell and tissue strains.

A) Stills from timelapse of neural plate within membrane-gfp labeled transgenic embryos. Pseudocolor indicates cells tracked over time. Scale bar 100 μm B) Schematic of cell and tissue strain analysis. Clusters of

cells as well as bounding corona, purple outline, are tracked over time. Corona is defined 1 to 2 layers of neighbors for central cell within the cluster. E) Tissue strain found from changes to an ellipse fit to the bounding corona over time F) Cell strains found from ellipse of each cell outline over time. G) Example of corona tracked over time and plot of corresponding strains. Purple solid line indicates AP corona strain over time. Grey solid line is average AP cell strain within cluster. Purple dashed line indicates ML corona strain. Grey dashed line indicates average ML cell strain in. F. Representative spatial map of cumulative AP strains at 60 minutes for tissues (top) and individual cells (bottom) G. Representative spatial map of cumulative ML strains at 60 minutes for tissues (top) and individual cells (bottom) H. Average AP strain rates for tissues (left) and cells (right) as function of distance from midline. Rates were calculated for 2 whole embryos and 3 dorsal isolates. Each tissue is plotted separately. CI Average ML strain rates for tissues (left) and cells (right) as a distance from midline. Rates were calculated for 2 whole embryos and 3 dorsal isolates. Error bars indicate 95%

3.2.2 Distinctive patterns of 4-cell and higher order multicellular rosettes during neurulation.

The number of cells that meet at a single vertex is a measure of multicellular morphology. Four-cell and higher-order cell vertices are a leading indicator of directed cell rearrangements. From staged fixed neural plates, we analyzed patterns of cell vertex topology to see if high order vertices were present (Fig 11A). We observed both T1 vertices, where 4 cells meet, as well as rosettes, where 5+ cells meet, within the neural plate at late gastrula, the earliest stage we tested, and noted their increasing abundance concentrated within the area surrounding the midline of the neural plate in later stage embryos (Fig. 11B). Occasional rosettes were also observed in the border cell region however at a lower frequency compared to the neural plate. These results suggested that neural plate cell rearrangement begins at the onset of neural plate shaping and increases in frequency near the neural plate midline.

Recent analysis of cell rearrangements in other models suggest that the formation of high order vertices in converging and extending tissues is driven by the contraction of planar polarized actomyosin cables found at junctions parallel with the direction of tissue convergence (Bertet, Sulak et al. 2004, Fernandez-Gonzalez, Simoes Sde et al. 2009, McGreevy, Vijayraghavan et al. 2015). Both actin and myosin have been shown to be upregulated at these junctions in other systems of CE and actin cables have been qualitatively described in *Xenopus* neural plates (Ossipova, Kim et al. 2015). To confirm their presence, so we measured intensity of actin at junctions that were parallel to the AP and ML axes in stage 14 neural plates. We found that there was an increase in intensity in ML junctions over AP junction (Figure 11C). Observation of these cables and high order vertices highly suggested the neural plate epithelium undergoes cell rearrangement.

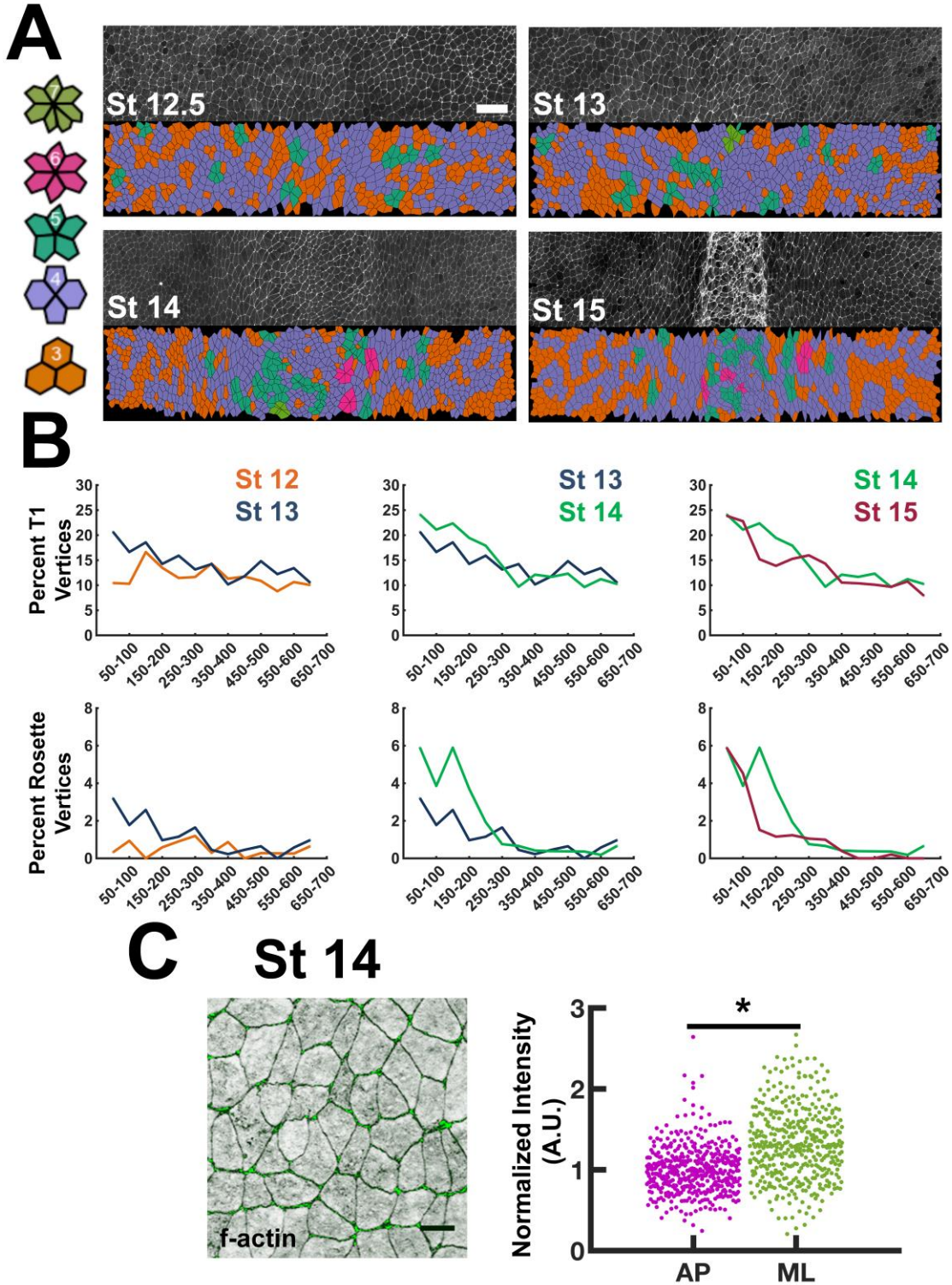


Figure 11. High order vertices, indicative of rearrangement, increase medially with stage.

A) Cell vertex order, the number of cells meeting at a single vertex, assessed at 4 stages in fixed analysis. Cells are pseudocolored coded to indicate the largest order vertex they participate in. Scale bar 100 μm . B) Stagewise

quantification of percent T1 vertices (4-cell vertex) and of rosettes (5+ cell vertex) binned as function of distance from neural plate midline. Bins are 50 μ m. Data pooled from 4 embryos at each stage. C) F-actin intensity quantified in stage 14 neural plates at junctions within 30 degrees of AP axis and 30 degrees of the ML axis. Data from 4 embryos. Junction intensity normalized to mean AP intensity per embryo. (n= 450 junctions, *p<0.001. Mann Whitney-U)

3.2.3 Neuroepithelial cells undergo directed rearrangements and apical junctional remodeling

To assess cell rearrangement, we analyzed the time-lapsed image sequences of neural plates in whole embryos and dorsal isolates. We tracked loss of a neighbor and gain of a neighbor, separately then calculated the percentage of cells that lost neighbors, gained neighbors, or both (Fig 12A-C). On average across the five neural plates, 44.5% of cells both lost and gained neighbors, 20.8% of cells lost but did not gain neighbors, 17.9% of cells gained a neighbor but did not lose neighbors. Together, on average 83% of cells we observed participated in some aspect of rearrangement during the hour of plate shaping we observed. Additionally, some cells lost and gained multiple neighbors over period of observation (Figure 12A-B). Formally, a loss or gain of a new cell-cell junction results in a loss or gain of a neighbor. Thus, to determine if rearrangements were oriented, we quantified the direction of gained and lost junctions (Figure 12D). We found that shrinking junctions were more aligned with the ML axis, the direction of tissue convergence, than new junctions that grow more parallel the AP axis, the direction of tissue extension (Figure 12E-F). It should be noted, our analysis excluded dividing cells; divisions also facilitate cell neighbor exchanges but may reflect intracellular mechanics rather than active cell rearrangement (Stooke-Vaughan, Davidson et al. 2017). Occasional divisions were seen during neural plate shaping but are not thought to play a large role in *Xenopus*

neurulation (Harris and Hartenstein 1991). Further analysis of the final angle between daughter cell centroids indicate they align more with the AP axis following division (Fig 12G). Thus far, our analysis supported the hypothesis that apical junctional remodeling facilitates cell rearrangement in the neuroepithelium.

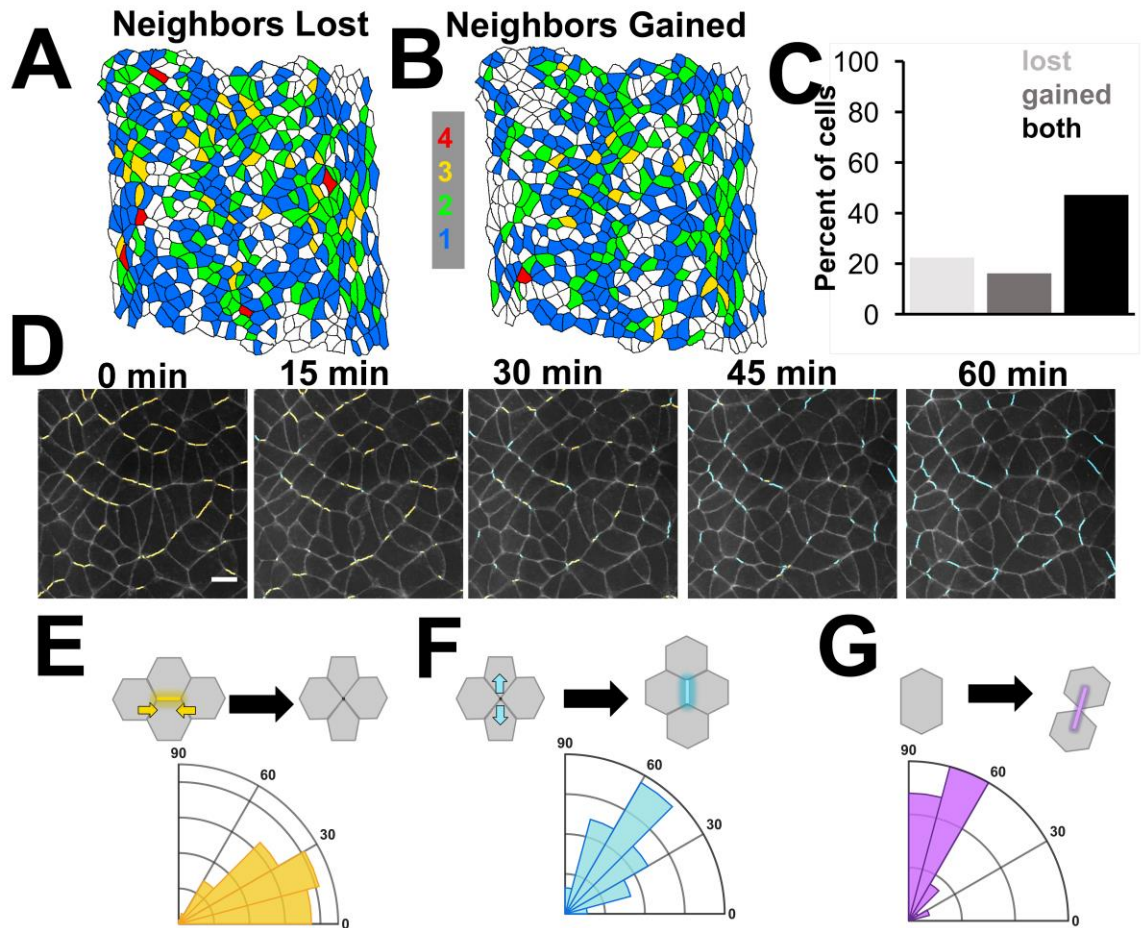


Figure 12. Neuroepithelial cells undergo oriented rearrangements.

A) Example map identifying cells from representative embryo neural plate that lost neighboring cells due to junctional shrinkage. Pseudocolor represents number of neighbors lost over an hour. B) Example map identifying cells that gained neighbors due to new junction growth. Pseudocolor represents number of neighbors gained over an hour. C) Quantification of the percentage of total cells tracked that only lost neighbors, only gained neighbors or both lost and gained neighbors indicative of the pervasiveness of cell rearrangement. D) Demonstration of cell junctions tracked within a neuroepithelium over an hour. Junctions that shrink are pseudocolored orange. New junctions that grow are pseudocolored blue. E) Polar histogram showing shrinking junction directionality F) Polar histogram of new junction growth directionality. G) Polar histogram of cell division orientation. AP axis is 90° . ML is 0°

3.2.4 Basal first mechanism of rearrangement

Epithelial rearrangement may be driven by basolateral cell behaviors. To determine if *Xenopus* epithelial rearrangements initiated first apically or basally within the neural tissue, we collected confocal timelapses at an apical and basal level 5-7 μ m into the tissue. Neural plates expressing mem-mcherry and tricellulin-gfp. reveal the location cell vertices at the tight junction level (Figure 13A). We detected high order vertices both in the apical slice and basal slice. Surprisingly we found nearly 90% of vertices we formed basally first (n=79; 3 explants Figure 13B). The average time-lag between basal first formation and apical formation was 21.25 minutes. In the four cases of apical first formation we observed average lag of 7.7 minutes (Figure 13C).

We also compared the average duration of all T1 junctions found apically or basally to see if vertices resolve faster apically or basally. In two of the neural plates, we found a significant decrease in basal vertex duration (Figure 13D). Thus, cells both initiate rearrangement basally and complete neighbor exchanges faster than at apical surfaces.

Scatter labeling of cells reveals basal rearrangement is accompanied by basolateral protrusions, corroborating what has been observed in other systems of basal rearrangement (Williams-Masson, Heid et al. 1998, Williams, Yen et al. 2014, Sun, Amourda et al. 2017). Although not quantified, protrusions seemed to orient in mediolateral direction (Fig 13E). On occasion, we noticed intrusions of deep cells into the basal epithelial layer (Fig 13F). We were careful to avoid including these intrusions in our analysis. We suspect the cells are from the underlying deep cell layer, as they would move in and out of deeper confocal sections. Dual labeling embryos with a scatter of mem-gfp expressing cells against a background of mem-

mcherry expressing cells reveal small extensions of deep labeled suggesting deep cells may interact with the superficial epithelial layer possibly influencing the epithelium's behavior (13G). Alternatively, deep cell incursions may also indicate that the basolateral surface of the epithelium is "loose" allowing basolateral protrusions from in plane and out-of plane neighbors. Taken together, we hypothesize that directed cell rearrangement in *Xenopus* neuroepithelium may be driven by mediolateral directed protrusions in a fashion similar to that observed in mesenchymal mesoderm during gastrulation.

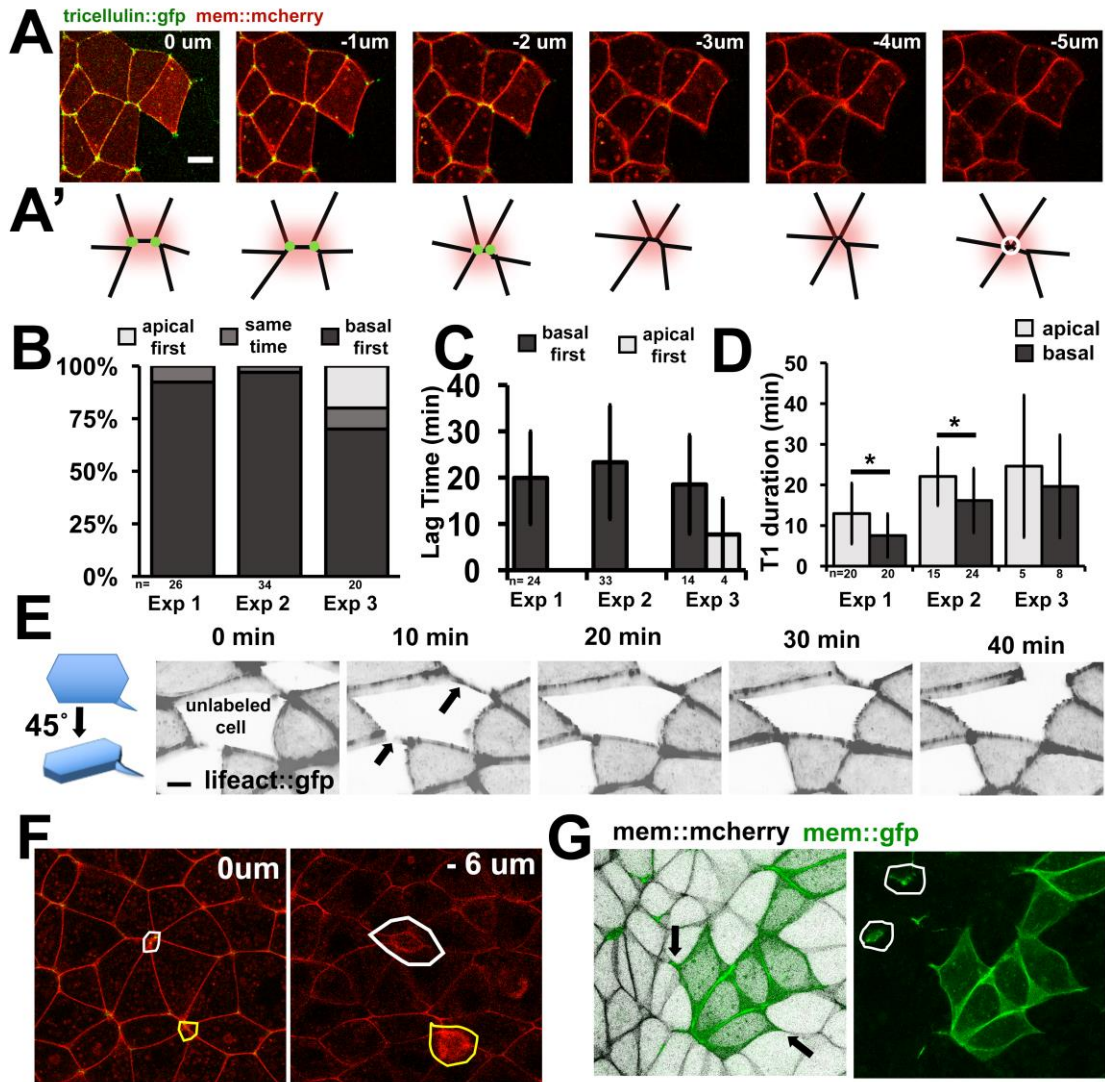


Figure 13. Basolateral rearrangement precedes apical junction remodeling.

A) Still from timelapse of *mem-mcherry* expressing embryo showing junction organization at different depths(z) from apical surface. Apical surface demarcated by tight junctional protein *tricellulin-GFP*. A') Stick diagram showing the location of cell junctions in each slice. Red highlighted region shows junction shrinks basally. B) Percent of high order vertices that form basally first, apically first or simultaneously. C) Quantification of time lag between basal vertex formation and apical vertex formation. D) Average time of of T1 junction persistence before resolution in apical and basal domains. (* $p < 0.05$, Mann-Whitney-U). E) a 45° 3D projection of scatter labeled cells expressing actin label, *lifeact-GFP*. Scale bar 10 μm. F) Apical (0 μm) and basal (-6 μm) slice of cells expressing *mem:mcherry*. Circled areas indicate “intrusions” within basal surface from underlying deep cells. G) Z-projected

Scatter label of mem::gfp against background of mem::mcherry expression reveals mediolateral protrusions (black arrows) as well as intrusions from labeled deeper cells (white circles, right).

3.3 DISCUSSION

3.3.1 Regional difference in cell shape strains

Through the application of the tissue tectonics approach, we were able to parse out how well changes in shape at the cell level reflected strains at the tissue level. In the lateral neural plate, we observe cells elongate in the direction of tissue elongation. Within the neural plate, shape change seems to be negligible and potentially even counter act the AP elongation and ML convergence observed in the tissue. This description suggests neuroepithelial cells resist local strain anisotropies. If neuroepithelial cells were a passive elastic material we would expect they either stretch and narrow with the tissue or at the minimum, if they are very stiff, not change shape. The fact that their shape counter acts tissue strains likely means they are not both passive and elastic. Neuroepithelial cells, thus, could be actively changing their shape and/or may be better modeled as a viscoelastic or viscous material where strains are dissipated through rearrangements. Here it is also important to consider timescales. Viscous dissipation occurs over longer time periods. These tissues strain in either direction 10-40% per hour. Larger strain rates may elicit different, potentially more elastic behaviors from cells.

More laterally, near the epidermal border of the neural plate we observe cells that are stretched in the AP direction. It is tempting to attribute the elongated shape of border cells to potential anisotropic tensions within the tissue. If these cells were truly passive however, we may

expect to see cells have a negative strain rate in the ML direction, reflecting tissue convergence. In most cases, we observed either positive or near zero cell strain rates in the ML direction, suggesting that cells are actually stretching mediolateral. The major difference between lateral and midline tissues, however, seems to be in the AP strain rates. If the midline were driving extension, we would expect the lateral tissue strain rates to at best match, the rates of midline extension, assuming no dissipative loss. Surprisingly, we see in several instances an increase in the AP strain rate in lateral tissues compared to midline. Perhaps it follows then that cells within this lateral region stretch in the AP direction as they are subject to larger strains. Alternatively, active cell elongation in the AP direction could be contributing to tissue strains. In either case, there is clear distinction between cell shape strains between midline and border cells.

3.3.2 Cell rearrangement as a conserved behavior in converging and extending tissues

We have also shown that the *Xenopus* neuroepithelial cells undergo directed rearrangements. This is a rather unsurprising finding considering the ubiquity of this cell behavior in other epithelial converging and extending systems studied. What is surprising however, is that mechanism of epithelial cell rearrangement may not be necessarily be driven by apical junction remodeling despite the observation that the neuroepithelial cell form and resolve high order vertices and the fact that actin may be upregulated at shrinking junctions. If apical junction remodeling drives cell rearrangement we would expect to see basal rearrangement following this or at least occurring simultaneously. In the vast majority of cases, we observed basal first rearrangement suggesting that, in fact, basal activity initiates rearrangement. This is contrary to what has been reported in mouse where it was reported that apical first and basal rearrangements have an equal likelihood of occurring (Williams, Yen et al. 2014). One possible reason for this

discrepancy could be due to the metric of rearrangement we measured. Williams et al. tracked the timing of resolution, our analysis detected the timing of formation of high order vertices. Another discrepancy is that they limited their analysis to resolution of rosettes (vertices where 5+ cells meet) whereas the majority of our data comes from T1 transitions (where 4 cells meet). A recent analysis in fly suggests that 70% of rosettes that form during germ band elongation are basal first (Sun, Amourda et al. 2017). Ultimately, force generation may arise from both apical and basal processes and may be implemented differentially according to evolutionary and selective pressures embryonic morphogenesis dictates.

Basal protrusions may be common in apparently quiescent epithelial cells undergoing morphogenesis. Qualitatively, cells protrude more in the mediolateral direction. We have seen these protrusions interact across neighboring cell boundaries as those boundaries shrink, potentially implicating them in long-range communication with non-neighboring cells. Alternatively, directed protrusive activity in mesenchymal cell populations like the mesoderm and deep neural cells are thought to produce tractions for moving (Keller, Shih et al. 1992, Elul, Koehl et al. 1997). In mesoderm, protrusions constantly emanate in both the medial and lateral directions. The sum of the tractions produced by these constant protrusions has been proposed to cause intercalations. In deep neural tissues, cells episodically become mediolaterally elongated, protrude and then shorten, combining cell shape change and tractions generated by protrusions to intercalate in between neighbors, similar to a motile cell (Elul, Koehl et al. 1997). Thus, neural epithelial cell protrusions could be mechanically involved in traction generation and intercalation.

There is a possibility that basal protrusions do not drive rearrangement at all. For example, during *C. Elegans* hypodermis intercalation, a mutant that inhibits rearrangement does

not affect the formation of directed basolateral protrusions (Heid, Raich et al. 2001). Even in the *Drosophila* germ band elongation study, a mutant that resulted in a near 5 fold reduction in protrusive activity only lead to around a 20% reduction in tissue elongation (Sun, Amourda et al. 2017) . Further examination will be required both to understand the mechanism of basolateral protrusion and rearrangement and to understand how apical and basolateral surfaces act in conjunction to facilitate rearrangement.

3.3.3 Limitations

There are several potential limitations to our experimental approach. First, the surfaces of the embryos and explants have 3D topographies. Most of our image processing is done on Z-projected images of the neuroepithelium, potentially overlooking the effects of a 3D surface. For example, cell shapes may be distorted if cells are at an angle relative to the imaging plane. Others have tried to correct for the 3D surface by modeling the embryo as an ellipsoid estimating a radius of curvature within the tissue (Blanchard, Kabla et al. 2009) This may work for whole embryos that are considerably more spherical than dorsal isolate explants that maintain a “brick” like shape. New image processing and segmentation approaches are necessary for cell tracking cells in both time and depth and will be useful for these types of tissue surface analyses.

3.4 EXPERIMENTAL PROCEDURES

3.4.1 Embryo Handling, Histology, Immunostaining and Imaging

Xenopus laevis embryos were obtained by standard methods (Kay 1991) fertilized in vitro and cultured in 1/3X Modified Barth's Solution (MBS) (Sive 2000). For explants: Embryos are cultured to stage 12.5 (Nieuwkoop and Faber 1956) at which time dorsal axial and paraxial tissues (dorsal isolate) are microsurgically removed from the embryo using hair loops and knives in DFA solution (Danichik's For Amy; (Sater, Steinhardt et al. 1993)). Before microsurgery, small (~1x5mm) pieces of glasses are cut from a #1.5 glass slide using a diamond pen. After isolation, tissue explants are transferred to a clean dish filled with DFA and gently and minimally compressed under a precut small piece of glass using vacuum grease at the ends for half an hour prior to experimentation to allow healing without tissue folding/bending. For microinjection of mRNAs, embryos are placed in 1X MBS containing Ficoll.

For F-actin staining, embryos were devitellinized and fixed for 30 minutes in 4% Paraformaldehyde + 3.7% Gluteraldehyde. Embryos were then permeablized in 0.1% TritonX in PBS (PBST) for 30 minutes. A 2.5:1000 concentration of Bodipy-Phalloidin in was applied for 1 hour and then rinsed 3 times in PBS.

For kertain staining, embryos were devitellinized and fixed overnight in Dent's Fixative at -20°C. Embryos were then washed 3x and rehydrated in PBS. Embryos were blocked for 1 hr in PBS + 10% Goat Serum (PBS+GS). Immunofluorescence staining was carried out with primary antibody 1h5 (Type II keratin, Developmental Studies Hybridoma Bank) at a 1:500 concentration.

For maps of apical surface, fixed embryos were bisected and flattened under a slip of coverglass within a custom imaging chamber. Imaging was performed on a spinning disk confocal (Yokagawa CSU-X1) using a 25x Water Objective to produce tiled z-stacks (2 μ m, Zstep size) images of the tissue.

For live imaging, confocal stacks were collected at 3 minute time intervals, 2 μ m z-intervals. We imaged apical surface of dorsal isolate explants held under a glass coverslip or of whole embryos mounted in 1% ultra-low melting agarose (type IX-A; Sigma) gels in custom imaging chambers.

3.4.2 Microinjection

For live visualization of apical surface, mRNA encoding fluorescent protein constructs were injected at the one-, two-cell stage or four-cell stage to visualize plasma membrane (CAAX-GFP, CAAX-mCherry), F-actin (LifeAct-GFP), tight junction tricellulin (Tricellulin-GFP). Tricellulin-GFP plasmid generously provided by Dr. Anne Miller (Higashi, Arnold et al. 2016).

3.4.3 Image Processing and Segmentation

F-actin and fluorescent membrane outlines were segmented using SeedWater Segmenter, a semiautomated watershed algorithm based segmentation software (Mashburn, Lynch et al. 2012) (Fig 14A,B). The binary cell outline (Fig14C) as well cell identity maps output (Fig14D) by the program were processed with custom written ImageJ macros to extract individual ROIs for each cell, detect the location of cell vertices and cell-cell junctions (Schneider, Rasband et al. 2012).

Further analysis quantifying cell morphology parameters, cell neighbor exchanges, division angles and rates, was performed in Matlab (Mathworks).

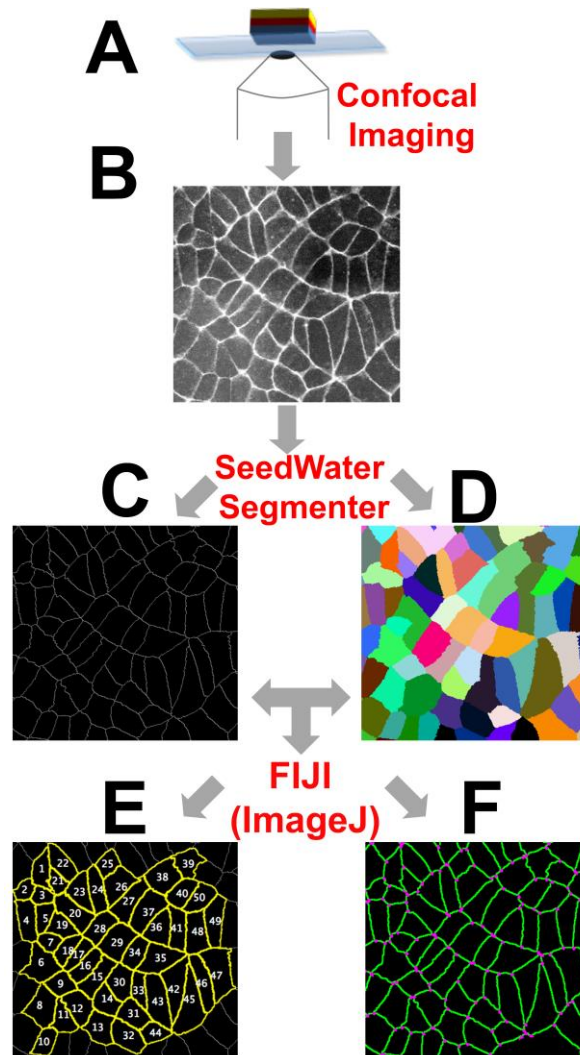


Figure 14. Image Processing Workflow

A) Cell outlines of apical surface are visualized using confocal microscopy. B) Raw image of cell outlines are processed in SeedWater Segmenter to produce C) binary outline of cell membranes or D) Identity map of cell in which each cell is assigned a unique identity. E) Binary outline can be used to extract individual regions of interest for each cell in ImageJ. F) Further processing on the outline and identity map can be used to detect cell-cell junctions and cell vertices.

3.4.4 Tissue Tectonics strain analysis

The tissue tectonics method was adapted from Blanchard et al (Blanchard, Kabla et al. 2009). We calculated strains for local tissue domains surrounding a central cell, also called coronas, A corona was defined as the one to two layers of cells neighboring the central cell (Fig 10B) Coronas were determined using a custom written ImageJ macro and the outputs of SeedWater Segmenter (Mashburn, Lynch et al. 2012). Coronas and individual cells were tracked over time . To describe shape changes and determine strains, we fit an ellipse to each corona domain as well as for individual cells (Fig 10 C,D). Lagrangian strains, where the initial configuration of the shape is used as a reference, were calculated based on ellipse deformation between 3-minute time intervals. Linear regression was used to find per hour corona strain rates as well as an area weighted average of constituent cell strain rates in each corona. We used the following method to calculate strain of an ellipse.

The general form of an ellipse can be defined by the following equation:

$$(Ax + By)^2 + (Cx + Dy)^2 = 1$$

where

$$A = \frac{2\cos\theta}{a}, B = \frac{2\sin\theta}{a}, C = -\frac{2\sin\theta}{b}, D = \frac{2\cos\theta}{b}$$

‘a’ is the length of the major axis, b length of the minor axis, and θ is the angle of the major axis.

We define the initial configuration of the ellipse at time $t-1$ as:

$$(\Lambda x + B y)^2 + (C x + D y)^2 = 1$$

We define the current configuration of the ellipse at time t as

$$(a x + b y)^2 + (c x + d y)^2 = 1$$

The initial configuration of the ellipse can be mapped to the current configuration through using the deformation gradient tensor, F :

$$\begin{bmatrix} \Lambda & B \\ C & D \end{bmatrix} = \begin{bmatrix} a & b \\ c & d \end{bmatrix} * F$$

$$F = \begin{bmatrix} a & b \\ c & d \end{bmatrix}^{-1} \begin{bmatrix} \Lambda & B \\ C & D \end{bmatrix}$$

We can use the deformation gradient tensor to then find the Lagrangian finite strain tensor.

$$\varepsilon = \frac{1}{2} F^T F - I = \begin{bmatrix} \varepsilon_{xx} & \varepsilon_{xy} \\ \varepsilon_{yx} & \varepsilon_{yy} \end{bmatrix}$$

Importantly, we align the AP and ML axis of the tissue with the X and Y-axis of the Cartesian coordinate system. Therefore, ε_{xx} is the strain in the ML direction while ε_{yy} is the strain in the AP direction.

3.4.5 Apical Basal Vertex Analysis

Z-stack confocal sections were collected using a 63x oil objective on a Leica SP5 laser-scanhead mounted on an inverted compound microscope. Slices in stacks were collected at 1 μ m-intervals. Timelapse sequences were collected using 1 minute intervals. Vertex and junctional analysis were performed on segmented images of cell outlines in apical and basal surfaces using custom Imagej macros and Matlab scripts. For the vertex duration study, to ensure that we were detecting the full duration of the vertex, we excluded any vertices that were detected in the first frame of the timelapse and those that did not persist beyond a frame. Additionally, we did not include any vertices that resolved in the final 3 minutes to ensure the vertices were fully resolved as sometimes there is a gap in detection. Finally, we excluded any vertex that became part of a higher order vertex, as this is not true resolution.

3.4.6 Statistical analysis

All statistical analysis was performed in IBM, SPSS version 22. Mann-Whitney U was chosen when independent samples Levene's test of homoscedasticity was rejected. For spatiotemporal pattern descriptions, 4 embryos per stage

4.0 STRAIN-DEPENDENT AND INTRINSIC CELL BEHAVIORS WITHIN THE NEURAL PLATE

4.1 INTRODUCTION

Which, if any, cell populations within the neural plate generate the force for convergent extension? To address this question, tissues must be physically manipulated (Koehl 1990). Ex vivo approaches where tissues are isolated from the embryo have given insight into location, magnitude and direction of force generation within tissues. For instance, newt neural plate explants only converge but do not extend once isolated from other tissues. However, extension proceeds in neural plates attached to underlying notochord (Jacobson and Gordon 1976). This contrasts with experiments done in *Xenopus laevis*, where neural plate sandwiches do converge and extend. Neural plate sandwiches also exhibit similar material properties and similar force production to dorsal tissue explants that contain all three germ layers (Zhou, Kim et al. 2009, Zhou, Pal et al. 2015). *Xenopus* explants containing just the deep neural plate cells also have the intrinsic capacity to undergo limited convergence and extension as well as cell rearrangement in isolation (Elul, Koehl et al. 1998). It remains to be seen if the neuroepithelium maintains the same convergence and extension capability.

Physical manipulation of tissues is also useful to probe how cells respond to altered mechanical conditions. During development, anisotropies in tissue mechanics can guide cell behaviors including oriented cell shape changes (Aigouy et al., 2010, Etournay et al., 2015), neighbor exchanges (Lau et al., 2015), divisions (Campinho et al., 2013), cell protrusions (Weber et al., 2012), and polarity (Chien et al., 2015, (Jackson, Kim et al. 2017) . Thus, it is possible that the anisotropic converging and extending strain field generated during neural plate shaping orients the observed cell shape changes or rearrangements. There are few precedents for these experiments beyond efforts in *Xenopus* where cell behaviors are routinely studied in mechanical isolation (Shih and Keller 1992, Weber, Bjerke et al. 2012).

In this chapter, we investigated the interplay between neural plate cells and their mechanical environment. We first prevented tissue elongation by embedding dorsal isolate explants in stiff agarose gels and found that cells at the neural plate border lose their elongated morphology. Interestingly, cells within the medial neural plate continue to undergo oriented rearrangements. To understand if rearrangement was intrinsic to the neuroepithelium, we excise and grafted portions of neuroepithelium into non-neural ectoderm, a tissue that do not undergo convergent extension. Strain analysis revealed small amounts of tissue convergent extension still occurred within the grafts. Cells continued to initiate rearrangement by shrinking junctions and forming high order vertices; however, we found resolution from these vertices appears inhibited. Instead, graft elongation may have occurred in part through active cell shape change.

4.2 RESULTS

4.2.1 Embedding dorsal isolates in agarose gels alters tissue strain

Since cells can change their behaviors based on their local mechanical environment, neuroepithelial cell shape change or rearrangement may require the strains generated during tissue convergence and extension. To understand the relationship between tissue strain and cell behaviors, we developed an assay in which stage 12.5 dorsal isolate explants were physically constrained in an inert non-adhesive agarose hydrogel used previously to measure extensional forces (Zhou, Pal et al. 2015). These gels offer mechanical resistance to tissues elongation but do not inhibit the generation of stress (Fig 15A). We quantified strain changes from stereoscopic timelapse image sequences of gel-embedded explants and control explants that were free to elongate (Fig 15B) . Since the neuroepithelium of the *Xenopus* embryo is pigmented, we are able to use an automated image registration based method to track displacements of the tissue in the stereoscopic images (Kim, Hazar et al. 2014). AP and ML strains from the displacements mapped the medial and lateral portions of the dorsal isolate neural plates. After 80 minutes of culture, gel confinement effectively abolished AP elongation strain at the midline and significantly reduced the average AP strain laterally by 50% (Fig 15C,C') There was a slight but not significant reduction of ML convergence strains at the midline (Fig 15C). Laterally, however we found the average ML strain was reduced nearly 75% (Fig 15C').

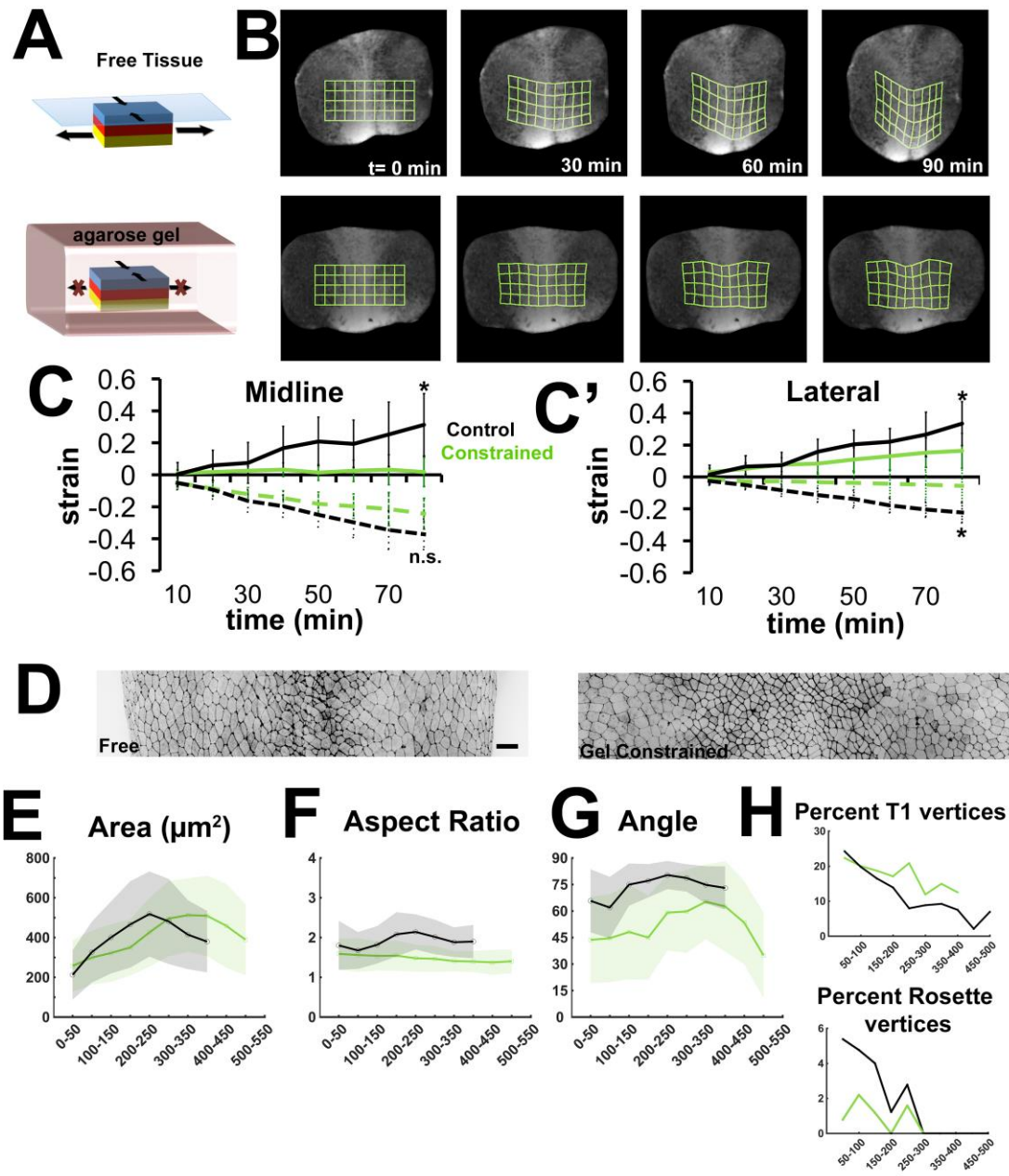


Figure 15. Confinement alters tissue strain patterns and cell morphology.

A) Schematic of experimental set up. Free control explants (top) are allowed to converge and extend under piece of coverglass. Confined explants (bottom) are set in a 1% low-melting agarose gel. B) Stills from stereoscopic timelapse image sequences of free explant (top) and gel confined explant (bottom) . 100 x 100 μm deformation grids mapped on to surface of explant showing strain patterns. C) Average strains within medial neural plate plotted over time. Solid lines are AP strains. Dotted lines are ML strains. Controls plotted in Gel constrained plotted in green. Mean strain at 80 minutes was compared ($n=6$ explants $*p < 0.05$, Mann-Whitney U) D) F-actin labeled free and gel

constrained neural plates of dorsal isolates. E) Average apical area plotted against distance from midline. Bins are 50 μm . F) Average cell aspect ratio plotted against distance from midline. G) Average orientation angle of elongated cells plotted against distance from midline. H) Percentage of T1 or rosette vertices in 50 μm binned regions plotted against distance from midline.

Using gel confinement we quantified cell morphology within confined and free dorsal isolates after 2 hours of culture (Fig 15D-G). Neural plate border cells in gel-confined tissues displayed reduced aspect ratios and were less aligned with the AP axis compared to controls (Fig 15F). This suggested that local strain patterns of border cells were altered by gel-confinement. To resolve cell strain we collected confocal timelapse sequences of mem-GFP expressing explants. To compare tissue and cell level strain rates we tracked cells for 60 minutes at three-minute intervals and extracted AP and ML cell and tissue (corona) strains. We found considerable variation between different replicates (Fig 16A). In one experiment, the medial neural plate converged in both the ML and AP directions. In another experiment, AP convergence was still present but diminished. Laterally, the tissues showed either reduced convergence or expansion in the ML direction. (Fig 16B)

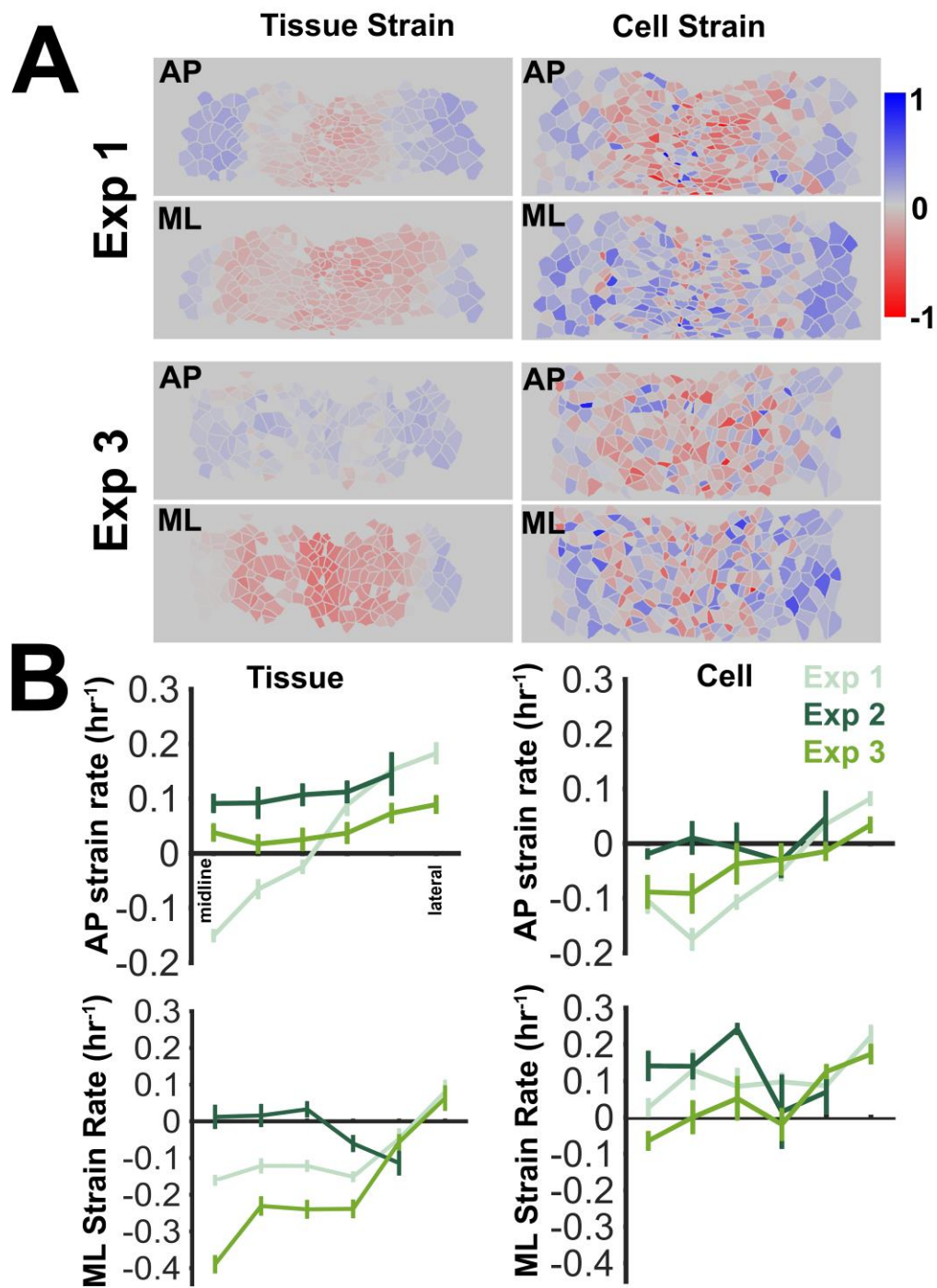


Figure 16. Strain patterns of gel-confined tissues.

A) Cumulative cell and tissue strains after one hour of confinement mapped onto tracked cells show. Two examples of differing strains. B) Average regional strain rates for tissues (left) and cells (right) plotted as function of distance from midline. Bars are 95% CI.

To understand why the border cells were AP elongated in the free but not confined explants, we considered the strain patterns needed to generate anisotropic shapes starting from an isodiametric one (Fig 17A). For AP elongation to occur, three possible scenarios exist: (1) A cell might elongate in AP direction with either no strain or net positive expansion in the ML direction. AP elongated shapes will be generated as long as AP expansion is greater than ML expansion. (2) The cell might be narrowing in the ML direction and either not straining or narrowing in the AP direction as well. If the amount of ML narrowing is greater than AP narrowing, the cell will appear AP elongated; (3) a cell might be elongating the AP direction while simultaneously narrowing in the ML direction such that both cell strains contribute to the elongated appearance of the cell. These three conditions are reversed when shapes elongate mediolaterally. To limit anisotropic shape changes, the magnitude and direction of AP strain must roughly be equal to the magnitude and direction of ML strain.

We applied this logic to understand the differences between the cell shapes seen within the border cells of gels and freely elongating explants. Border cell aspect ratio and cumulative AP and ML strains were extracted from the timelapse sequences of the gel-confined and free explants.

Initially, the border cell shapes are slightly elongated and aligned with the AP axis in both the gel-confined and freely elongating control tissues (Fig 17B). By the end of one hour, cell aspect ratio decreased within the gel-confined tissues and cells were less AP aligned. Whereas in controls, aspect ratio and orientation was maintained or became more AP aligned. This suggested that border cells had undergone expansion in the ML direction to produce a less elongated AP shape. We found that while AP and ML cell strain patterns showed considerable variation in the controls, border cells in constrained tissues were consistently more likely to have

either near equal AP and ML strains or slightly larger positive ML strains than AP strains indicating cells stretched in the ML direction during confinement (Fig 17C). ML stretch could account for the decrease in the aspect ratio and the orientation angle of gel confined border cells.

Local tissue-level strains described by corona analysis revealed that small variations among the controls reflected greater variances in cell strain patterns. For example, in one experiment (Exp #1, Fig17C) there was a clear distinction between the corona strain patterns of the free tissue and the gel confined explant. In the free tissue, AP strains were largely positive and ML strains were negative or close to zero. By contrast, in the gel-confined tissue, AP strains were lower, nearly half the magnitudes of the control with largely positive ML strains.

These patterns are reflected at the cell level where we observed a cluster of cells with positive AP strains and negative ML strains in the control tissue, suggesting these cells elongated and narrowed. Cells in gel-confined tissues have mostly positive ML strains and either equivalent or lower positive AP strains suggesting these cells stretched in the ML direction or remained isodiametric (Exp #1, Fig17C). The cell strain patterns were reflected in the changes in cell aspect ratios. In the free explant, the average cell aspect ratio increased slightly and the orientation angle remained around the same. In the gel confined tissue, cell aspect ratio and angle both decreased suggesting cells stretched in the ML direction (Exp #1, Fig17B).

By contrast, in another experiment (Fig 17C; Exp #3), corona strain patterns were more similar between both the gel-confined and free explants. AP corona elongation strains were around the same magnitude. ML strain patterns, however, were slightly different between confined and free tissues. Free tissue ML corona strains were more negative suggesting coronas narrowed where as gel-confined ML corona strains were slightly positive suggesting ML corona expansion. Changes in border cell aspect ratio and angle once again reflect this pattern. In

control cells, there was effectively no change in both elongation and orientation. In the gel-confined cells, aspect ratio decreased about 10% and the cell orientation angle decreased as well suggesting cells stretched in the ML direction.

Unfortunately, one experiment (Fig 17C; Exp #2) lacked corona strain data in the gel confined case as the cells within this tissue had larger areas and thus did not have the requisite number of neighbors to track a corona of cells. Within the spread of cell level strains, there a distinct separation between control cells, that exhibit positive AP strains and negative or near zero ML strains and gel confined cells that exhibit negative AP strains and positive ML strains. We might predict the tissue level strain patterns for the gel would show positive ML stretching and either zero or negative AP strains. Cell level strains in free explants follow a similar pattern as the tissue coronas. Both cells and coronas have net positive AP strains and mostly negative ML strains. Overall, the gel confinement experiments suggest cell shape strains and tissue strains are directly coupled at the neural plate border.

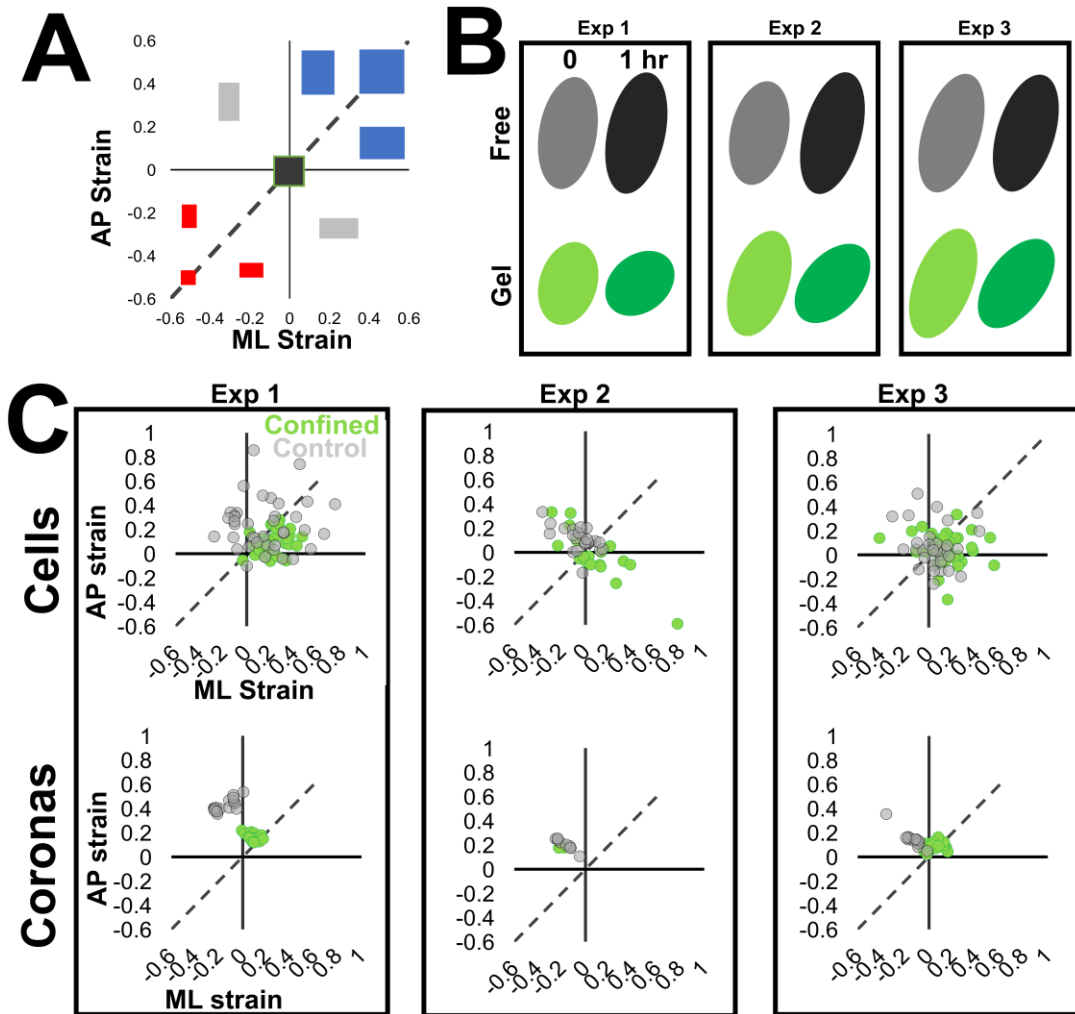


Figure 17. Gel confinement alters cell and tissue strain patterns in the lateral neural plate.

A) Schematic of theoretical combinations of AP and ML strains that produce elongated cell shapes when applied to an isodiametric shape (center square, green outline). Dotted line indicates where AP and ML strains are equal. Shapes above and to the left of dotted line have strain combinations which make them appear AP elongated. Shapes below and right of the dotted line have strain combinations that make them appear ML elongated. Colors indicate strain patterns that increase (blue) or decrease (red) shape area. B) Visual representation of average shape and angle of lateral plate cells at start and end of hour long timelapse. C) Cumulative AP strain plotted against ML strain for individual cells (top) and tissue coronas (bottom) of control (grey) and gel confined (green) tissues. Dotted line indicates where AP and ML strains are equivalent. Each dot represents individual cell or tissue corona.

4.2.2 Cell rearrangements persist in gel confined tissues

The persistence of tissue level convergence and discordant cell and tissue strain patterns in the medial region of confined neural plates suggested that rearrangement might still occur. Analysis of fixed samples indicated the percent of rosettes, but not T1 vertices was reduced in confinement suggesting a possible change in rearrangement dynamics (Figure 15H). We suspected in the medial tissues, where cell rearrangement is the dominant behavior, gel confinement may alter rearrangement orientation. We would predict that abrogating AP strains through confinement may affect the direction in which new cell-cell junctions grow (Lau, Tao et al. 2015, Yu and Fernandez-Gonzalez 2016). Because tissues converge but are unable to elongate in confinement, it was also possible that cells may initiate a rearrangement by shrinking their cell-cell junctions into a high-order vertex, but may be unable to resolve out from that configuration. If the orientation of rearrangements were different, the direction in which cell-cell junctions shrink to form a high order vertex or resolve to form a new cell-cell contact would be altered.

To test these predictions, we analyzed live confocal data of gel-confined and free explants expressing mem-GFP. Cell rearrangements continue in confined explants. In both control and gel confined explants, the angle of junction growth was more aligned with the AP axis than the angle of junction shrinkage (Fig18A-A') Furthermore, in two of the three experiments, we observed no significant difference in the angle of junction growth or junction shrinkage between gel-confined and free explants even though tissue level AP strains were disrupted in the gels. Thus, gel confinement does not abrogate directed junctional remodeling.

Because directed junctional remodeling accompanies cell rearrangement in free tissues and whole embryos, this suggested rearrangement persists in confined tissues.

To confirm that local cell rearrangements continued in confined samples, we identified the numbers of cells that gained new neighbors and the amount that lost neighbors in gel confined and free tissues was quantified. The percent of cells that lose neighbors indicates how many cells initiate a rearrangement through the shrinking of a shared cell boundary. The percent of cells that gain new neighbors indicates of how many cells complete a rearrangement through the growth of a new boundary. Each replicate yielded slightly different results (Fig18B-B’). In the first experiment there was no significant in the percent of cells that lost neighbors or gained neighbor between the control and gel-confined explant (Fig 18B). This meant an equal fraction of cells in both the tissues participated in a rearrangement. In a second experiment, the percentage of cells gaining a new neighbor significantly decreased in the gel-confined tissue suggesting fewer cells completed a rearrangement compared to the cells in the control tissue (Fig 18B’). In the third experiment, both the percentage of cells that lost and gained neighbors in the gel confined explant was lower than the control suggesting that the rearrangement process might have been slightly inhibited (Fig18B’). Thus, though the experimental variability precludes any conclusion on the amount of rearrangement, we nonetheless find cell rearrangements can still occur within confined tissues.

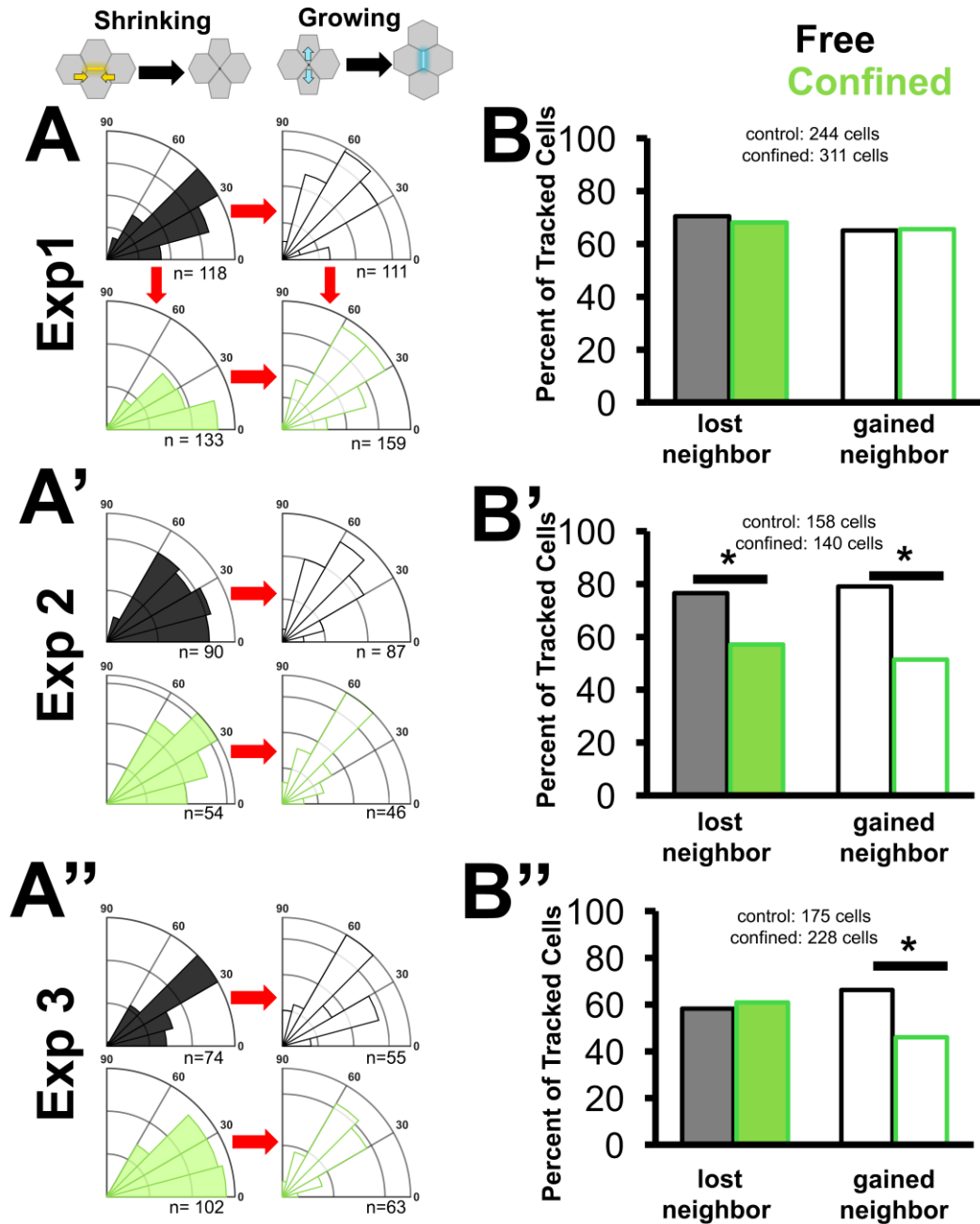


Figure 18. Orientation of rearrangements preserved in gel-confined tissues.

A'-A'') Polar histograms display angles of shrinking junctions (left) and growing junctions (right) within control (grey) and gel-confined (green) tissues. Red arrows indicate significant difference in mean angle, $p < 0.05$ Mann-Whitney-U. B-B'') Quantification of number of cells that lost or gained a neighbor due to junction shrinkage within free and gel-confined explants. ($p < 0.05$, Pearson's Chi Square)

4.2.3 Gel confined tissues exhibit increased cell division

In the course of analyzing cell topology we observed confinement resulted in a significant increase in cell division. This was a surprising and potentially confounding factor, as our junctional analysis ignores cell-cells boundaries shared with cells that divide. In that analysis we excluded dividing cells from neighbor change analysis but did not rule out cells that may have divided earlier. Free explants had little to no cell division during the hour of observation, 7-15% of gel-confined cells divided (Fig 19). We speculate that an increase in cell division might reflect a feedback mechanism within the tissue to reduce stresses built up by frustrated elongation. Recent studies in MDCK and fish skin demonstrated tissue compression can cause cell extrusion from epithelial monolayers (Eisenhoffer, Loftus et al. 2012) and that tissue tension can induce cell division (Gudipaty, Lindblom et al. 2017). A similar mechanism may be acting within the confined explants; further evaluation will be necessary to dissect how these divisions are induced and whether mechanics or some other environmental cue is responsible.

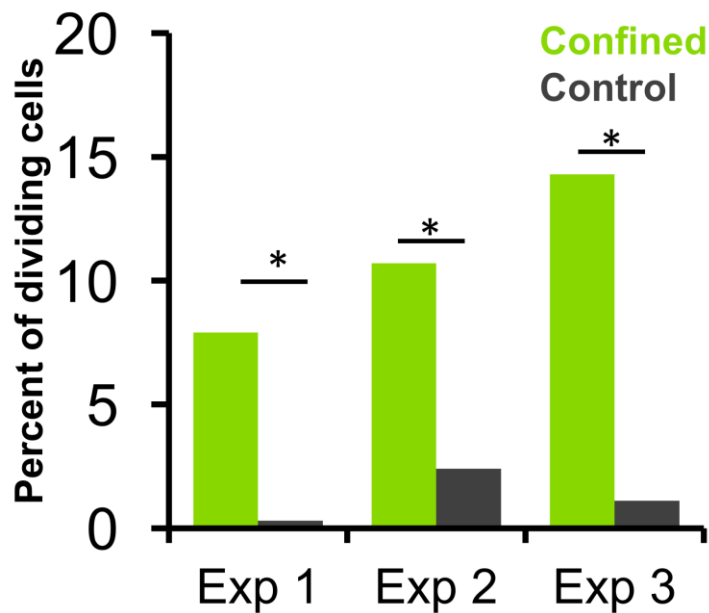


Figure 19. Cell Division Increases in gel confined tissues.

Quantification of percentage of tracked cells that divide during an hour of confinement compared to free controls. (p<0.05; Pearson’s Chi Squared).

4.2.4 Convergent extension and cell rearrangement is intrinsic to the superficial layer of the neuroepithelium

Gel confined tissues retain the ability to generate anisotropic stress (Zhou, Pal et al. 2015) and we have shown cells retain the ability to rearrange locally. Thus, anisotropic tissue strain and local tensions persist in the gel-confined tissue suggesting local anisotropic tensions are sufficient to orient cell rearrangements. These anisotropic tensions could either be produced intrinsically by the superficial neuroepithelium itself, or result from forces generated by the movements of other tissues including the underlying deep neural ectoderm or the attached mesoderm that also undergo convergent extension. To remove or minimize contribution from movements of other germ layers in the tissue, we performed tissue grafting experiments in which

the single cell layered neuroepithelium was isolated from the converging and extending tissue environment of the dorsal axis and grafted into a quiescent host tissue. We grafted late gastrula (stage 12.5) neuroepithelial midline tissues labeled with a rhodamine-conjugated dextran into the ventral ectoderm of unlabeled stage-matched host embryos (Fig20A). Ventral ectoderm does not undergo CE until tailbud stages (Larkin and Danilchik 1999, Jackson, Kim et al. 2017). Grafts were allowed to heal for 30 minutes at which point ventral host ectoderm containing the graft was isolated and plated on fibronectin coated coverslips. Removal of host and graft tissue eliminated influence of embryo wide mechanical cues from host environment. Ventral ectoderm isolates usually spread radially outwards on these coverslips but these movements are slow (25-50 μm per hour) and isotropic (Song, Shawky et al. 2015). After two hours, we assessed cell morphology and vertex topology in the graft and compared to host ectoderm at least 200 μm away from graft edge (Fig20B).

Grafted neural cells differed significantly from the surrounding host ectoderm in morphology and topology. Cell apical area was significantly reduced in grafted tissues compared to hosts, suggesting the cells maintained the apical constriction program of neuroepithelial cells (Fig 20C). Grafted cells were also more elongated on average compared to host (Fig 20D). Based on staging and our analysis of whole embryos, these patterns matched stage 15 neural plate midlines cells which were apically constricted and more elongated compared to lateral non-neural ectoderm.

Since the timing of cell morphology changes seemed to be preserved within the grafts, we wondered whether cells formed T1 or rosettes. From fixed tissues, we assessed whether high order vertices were present within the tissue. Surprisingly, we found a significant increase in

both T1s and rosette vertices compared to the host tissue suggesting cells continued to rearrange within nonneural ectoderm host environment(Fig 20E).

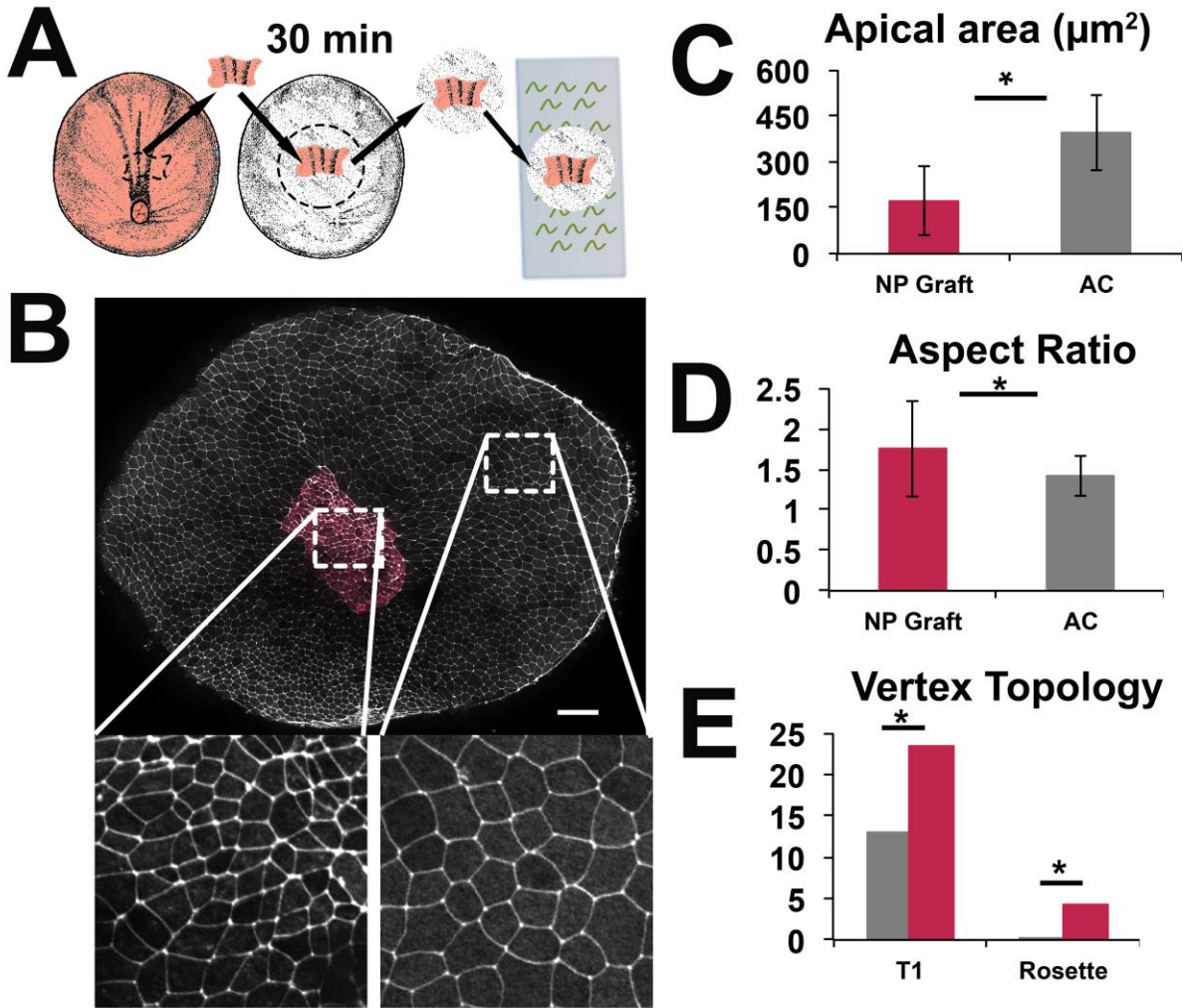


Figure 20. Neuroepithelial cells grafts show altered cell morphology compared to host tissue cells.

A) Schematic of experimental set up. Portions of rhodamine-dextran labeled embryos were removed from neural plate and transferred into ventral tissues of unlabeled host embryos. After 30 minutes of healing, host tissue containing graft is excised from embryo and placed onto fibronectin coated cover slip. B) Phalloidin stain of grafted neuroepithelium (red) in host ventral tissue. Scale bar 100 um. Magnified sections of tissue demonstrating cell morphologies. C) Quantification of average apical area and D) Aspect ratio for graft and host cells (AC) cells. (n= 683 graft cells, 395 host cells. Data pooled from explants. p<0.05 Mann-Whitney U). E) Percentage of T1 and rosette vertices within graft (pink) and host tissue (grey). (*p<0.05, Pearson's chi squared)

To confirm that dynamic rearrangements in grafts represented neural behaviors and to understand the strain pattern within the grafts, we collected confocal time-lapse image sequences of membrane-mcherry expressing grafts. Remarkably, grafted tissues continued to converge and extend in both the tissue and cell level strains within the graft (Fig21B). The mosaic pattern of mem-mcherry expression within the tissue allowed us to identify the AP axis within the graft. (Note: In *Xenopus*, mRNAs can be targeted to specific blastomeres of the 4-cell or later stage embryo that will give rise to the dorsal tissues including the neural plate. Injecting at these stages causes mosaic expression of the mRNA within the tissues, and often results in increased mRNA expression in strips of cells that span the AP axis. Thus, stripes of grafted cells in host allowed us to align the AP axis of the tissue for strain calculations (Fig 21A). After one hour of culture, tissues exhibited a 6 to 10% ML convergence strain and a 7 to 10% AP extension strain (Fig 21B). We note that magnitudes of strain in grafts were 2-4 fold lower than strains observed in whole embryos and dorsal isolates, but this anisotropy of CE strains were retained by the superficial neural ectoderm removed from their native mechanical environment.

Surprisingly, mean cell AP strains (18% and 13%, respectively) were larger than mean tissue AP strains (7% and 10% respectively; n=2 grafts). Patterns of high cell-level strains in grafts are the reverse of strain patterns observed in intact dorsal isolates and whole embryos, where tissue strains are much greater than cell strains suggesting that AP cell expansion drives neural tissue elongation in grafts. In the ML direction, cells also expanded (12% and 16% mean ML strain, respectively) where as tissues converged (-9.8% and -6.6% mean ML strain). This suggests tissue convergence may not be driven exclusively cell shape change.

Instead, live time lapse analysis indicates that neural convergence in grafts is achieved through cell rearrangements. Roughly 50% of cells in both explants lost neighbors and only

around 30% of cells gained new neighbors (Fig 21D) fewer cells completed rearrangement than initiated it. Overall however, rearrangement remained oriented, as the average direction of junction shrinking was more ML than the average direction of new junction growth (Fig 21C). Taken together, the patterns of rearrangement and tissue strains remain within the grafted neural epithelium, however constraints imposed by the host ectoderm may prevent effective resolution of new junctions where AP elongation is directly driven by cell shape change, unlike in host tissue where AP elongation results from rearrangement.

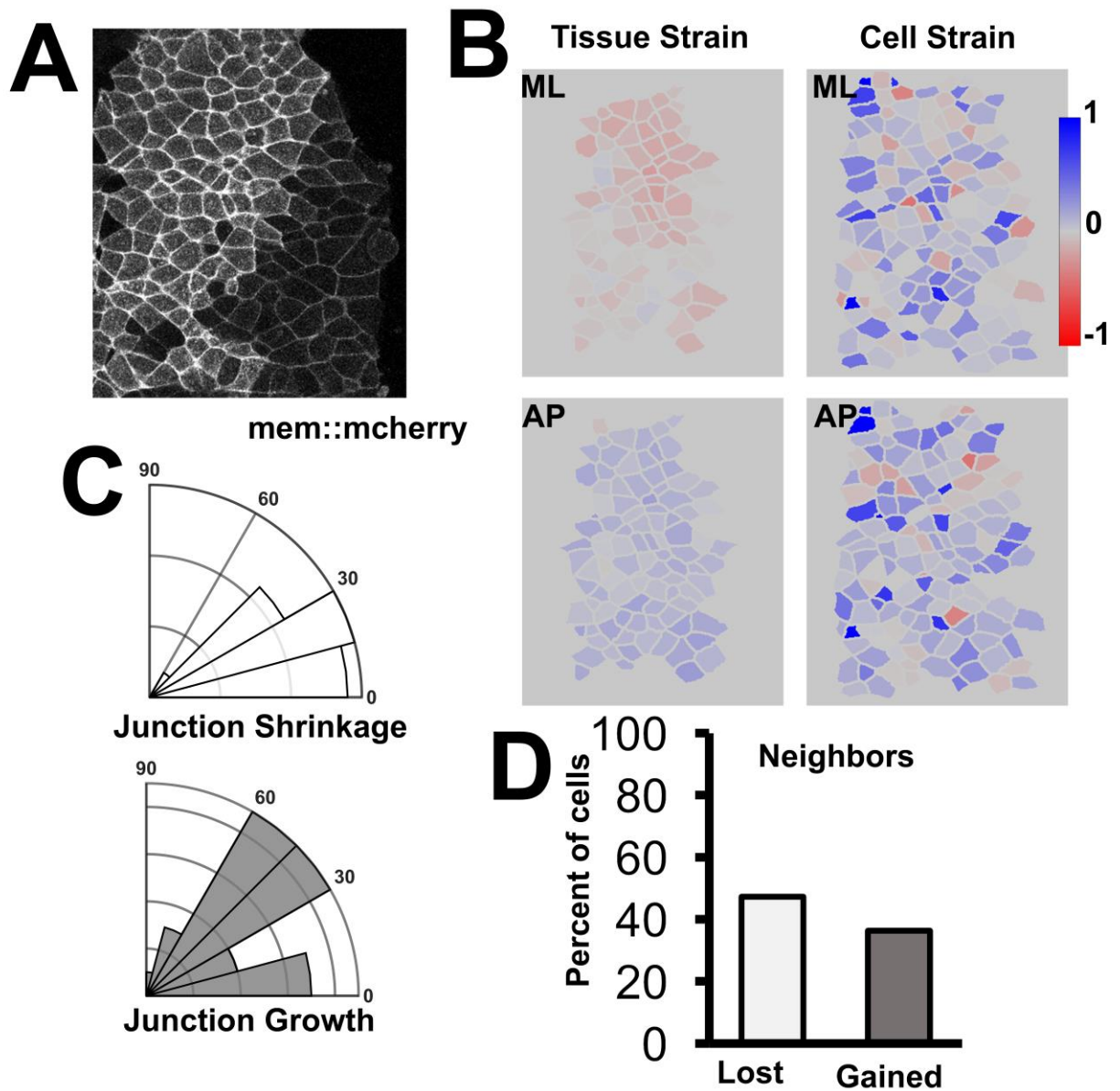


Figure 21. Grafted neuroepithelia converge and extend.

A) Still from timelapse of mem-GFP expressing graft demonstrating mosaic labeling where some regions are brighter than others. B) Map of tissue and cell level AP and ML strains within representative graft. C) Polar histogram of junction shrinking and growth orientations within graft. D) Percentage of tracked cells within graft that lost or gained a neighbor due to junctional remodeling.

4.3 DISCUSSION

4.3.1 Strain dependent cell morphologies of the lateral neural plate

The interplay between neuroepithelial cell morphologies and constraints from their mechanical environment is complex and spatially varied. As the gel confinement assay demonstrated, the AP elongated morphology of lateral neural plate cells is a response to mechanical strain patterns within the tissue. When tissue elongation is prevented within the gel, the lateral cells no longer appear elongated in the AP direction compared to controls. Interestingly, analysis of tissue strains suggested gel confinement not only reduced AP elongation strains of the lateral plate tissue but also either reduced ML tissue convergence or resulted in ML stretching. ML tissue stretch may have contributed to cells losing their AP elongated appearance, as lateral cells in confined tissues also exhibited positive ML strains.

What might cause the tissue, and subsequently the cells, to stretch mediolaterally? Tissue confinement only blocks bulk level tissue strains. Tissues and cells within the gel can continue to generate local tensions and anisotropic stress (Zhou, Pal et al. 2015). Furthermore, confinement may redirect stresses within the tissue that would normally be dissipated through strain mediated cell rearrangements or AP cell elongation. Lateral height may be altered by deep medial tissues that continued to converge within the gels.

4.3.2 Cell rearrangement and tissue CE is intrinsic to the neuroepithelium

The convergence of the medial tissue is robust, unperturbed by both preventing tissue elongation in gels or isolating the neuroepithelium from the embryo. It has been previously shown that deep mesenchymal neural cells are capable of driving limited CE in deep neural plate isolates. Extensive studies have described deep neural explant CE and intercalation behaviors in isolation (Keller, Shih et al. 1992, Elul, Koehl et al. 1997, Ezin, Skoglund et al. 2003). Here, through tissue grafting, we provide evidence that the neuroepithelium does not entirely rely on the deep cells to deform. Within the grafted neural epithelial sheets, convergent extension persisted, concomitant with oriented cell rearrangement. This does not prove epithelial cell rearrangements cause tissue CE, but suggest they contribute to CE. These experiments demonstrate that directed cell rearrangement is intrinsic to the neuroepithelium. Even in the confined explants that could not extend, cells continued to exchange neighbors. A similar experiment from CE during *Drosophila* germband elongation suggests that rearrangement is also intrinsic to the germband epithelium and not dependent on extensional forces potentially generated by attached mesoderm tissues undergoing invagination (Bertet, Sulak et al. 2004). In that study, the *folded-gastrulation* (*fog*) mutant that blocked mesoderm invagination effectively confined the germband tissue preventing elongation, in a similar manner to our explants embedded agarose gels. Cell junctional remodeling of the germband cells in the *fog* was still observed despite this extensional obstruction. Instead of elongating, the germband tissue folds. It would be interesting to see if these mutant flies also exhibit excess cell division in the germband as we observed in *Xenopus* confined tissues. Recent studies have suggested increased tension applied to of epithelial tissues can induce cell division such as in *Drosophila* wing discs (Etournay, Popovic et al. 2015) and MDCK monolayers (Gudipaty, Lindblom et al. 2017).

4.3.3 Limitations

In the gel confinement experiments, it is hard to predict and recreate repeatable strain patterns when we rely on the endogenous strain production of the dorsal isolate. Thus, there were large variations in our live experiments although there were similar variations when gels were used for stress measurements (Zhou, Pal et al. 2015). Furthermore, live imaging of free dorsal isolates requires that these explants be mildly compressed under a coverglass for a flatter imaging surface. Similar limitations exist in *Drosophila* studies where embryos are routinely dehydrated slightly to enable ‘flatter’ fields of view during time-lapse imaging. It is possible, that tissues became constrained due to the coverglass and may account for some of the observed variations in tissue strains. As we now have demonstrated neural epithelial tissues can continue converge and extend in isolation. Adapting these tissues for use with a tissue stretching device that can apply defined strains to the tissue may provide more reproducible data. However, even under defined strain conditions, irregular healing of the grafts may contribute to variation of tissue behaviors. Ectoderm tissue explants that are induced to form neural tissue may be able to recapitulate

Another limitation of this work arises from our ability to quantify junction remodeling in tissues that undergo high rates of cell division. Our algorithm does not currently include a way to distinguish between new cell junctions produced from a cell division event versus a cell rearrangement event. Because of this, we ignore all junctions shared with a dividing cell at all time points throughout our timelapses thus losing data on potential non-division related cell junction remodeling.

4.4 EXPERIMENTAL PROCEDURES

4.4.1 Embryo Handling, Immunofluorescence and Microinjection

Xenopus laevis embryos were obtained by standard methods (Kay 1991) fertilized in vitro and cultured in 1/3X Modified Barth's Solution (MBS) (Sive 2000). For explants: Embryos are cultured to stage 12.5 (Nieuwkoop and Faber 1956) at which time dorsal axial and paraxial tissues (dorsal isolate) are microsurgically removed from the embryo using hair loops and knives in DFA solution (Danichik's For Amy; (Sater, Steinhardt et al. 1993)). Before microsurgery, small (~1x5mm) pieces of glasses are cut from a #1.5 glass slide using a diamond pen. After isolation, tissue explants are transferred to a clean dish filled with DFA and gently and minimally compressed under a precut small piece of glass using vacuum grease at the ends for half an hour prior to experimentation to allow healing without tissue folding/bending. For microinjection of mRNAs, embryos are placed in 1X MBS containing Ficoll.

For F-actin staining, embryos were devitellinized and fixed for 30 minutes in 4% Paraformaldehyde + 3.7% Gluteraldehyde. Embryos were then permeablized in 0.1% TritonX in PBS (PBST) for 30 minutes. A 2.5:1000 concentration of Bodipy-Phalloidin in was applied for 1 hour and then rinsed 3 times in PBS.

For live visualization of apical surface, mRNA encoding fluorescent protein constructs were injected at the one- or two-cell stage to plasma membrane (CAAX-GFP).

4.4.2 Gel Confinement assay

Following the protocol in Zhou et al (2015), dorsal isolates were excised at stage 12.5 and allowed to heal for 30 minutes under glass coverslips. A 1% solution of Ultra-low melting

agarose (type IX-A; Sigma) was dissolved in DFA solution at 65°C, Explants were then transferred into slurry of 1% low melting agarose in DFA solution within a custom imaging chamber. For live imaging, explants were positioned close to the bottom of the chamber with minimal agarose between the neuroepithelium and the glass. Chambers with agarose and explants are set in a 14°C incubator for 15 minutes. For fixed tissue analysis, explants were fixed within the gel.

4.4.3 Tissue grafting

Donor embryos were injected with rhodamine-dextran or membrane-mcherry mRNA. Host embryos were unlabeled or injected with tricellulin-GFP mRNA. Single layer neuroepithelial tissues were cut from labeled donor embryos and played into holes created in the ventral ectoderm tissues of sister embryos (Edlund, Davidson et al. 2013). The graft was allowed to heal for 30 minutes after which the ventral ectoderm of the host, containing the graft, was excised from the embryo and placed onto fibronectin coated glass coverslips. For fixed analysis, explants were cultured for two hours before fixation. For live imaging, explants were allowed to heal and adhere to glasscover slip for 60 minutes before imaging.

4.4.4 Image Processing

Image processing techniques for cell morphology analyses and tissue tectonic analysis were described in a previous section (See section 3.4.2 and 3.4.3)

4.4.5 Statistical analysis

All statistical analysis was performed in IBM, SPSS version 22. Mann-Whitney U was chosen when independent samples Levene's test of homoscedasticity was rejected. Chi Square was chosen for contingency analysis for percent of high order vertices.

5.0 PLANAR CELL POLARITY AND NEUROEPITHELIAL CELL BEHAVIORS

Convergent extension is an anisotropic deformation with elongation and narrowing occurring in perpendicular embryonic axes. The cell behaviors accompanying convergent extension are also oriented. How these behaviors and strains become oriented is an open question. While anisotropic mechanics may play a role, molecular patterning can also confer polarity.

The core planar cell polarity (PCP) molecular pathway is compelling to study as mutations of several PCP components are associated with neural tube defects and disrupt tissue convergent extension (Heisenberg, Tada et al. 2000, Tada and Smith 2000, Kibar, Vogan et al. 2001, Goto and Keller 2002, Wallingford and Harland 2002). Yet, the exact role PCP plays in regulating CE remains unclear. Polarization of the structural and force generating components within cells is particularly important if cells are to undergo directed behaviors like rearrangement, junction contraction, and cell shape change. Indeed, the PCP pathway interacts with modulators of actomyosin contractility such as Rho GTPases Rho Kinase (Strutt, Weber et al. 1997, Habas, Kato et al. 2001, Winter, Wang et al. 2001, Nishimura, Honda et al. 2012) and can permissively regulate actin contractions (Kim and Davidson 2011). Yet, regulation of actomyosin may also be upstream of PCP (Mahaffey, Grego-Bessa et al. 2013) (Ossipova, Kim et al. 2015) and anisotropic tissue mechanics may even localize PCP components (Aigouy, Farhadifar et al. 2010) (Chien, Keller et al. 2015) (Aw, Heck et al. 2016). Thus, a complex

picture emerges where molecular signaling and mechanical anisotropy may feedback on to one another to break symmetry in cell and tissue behaviors.

In this chapter we sought to understand the relationship between tissue strain and PCP defects in the neural plate. We overexpressed the PCP protein Vangl2 in the neuroepithelium which is known to disrupt convergent extension (Goto and Keller 2002) and tracked morphology defects concomitant with CE defects. Following lines of investigation carried out in prior chapters, we tested whether the observed cell morphology changes were due to perturbed tissue level strains. After Vangl2 overexpressing cells are subject to native strains, cells become elongated in the AP axis but when confined in agarose gels, tissue explants that contained patches of Vangl2 overexpressing cells display reduced elongation. This suggests, that Vangl2 overexpression inhibits the ability of neuroepithelial cells to maintain or restore their shape when subject to anisotropic tensions.

5.1 RESULTS

5.1.1 Vangl-2 Overexpression disrupts CE and alters cell morphology

Vangl-2 overexpression (OE) during neural plate shaping was characterized. Vangl2 mRNA was targeted to the dorsal blastomeres of the 4-cell stage embryo so that was only over-expressed Vangl2 in the neural plate and dorsal tissue (Fig 22A). The amount of mRNA injected was titrated down to allow the embryo to complete gastrulation but was sufficiently high to induce defective CE (see: (Goto and Keller 2002) “mild/moderate phenotype). To quantify CE strain differences we created stereoscopic timelapses of both Vangl2-OE embryos and uninjected

controls during neural plate shaping (Fig 22B). Over 90 minutes between stages 12.5 and 14, we observed less AP elongation and ML convergence in the Vangl2-OE embryos than stage-matched controls (Fig 22C,D).

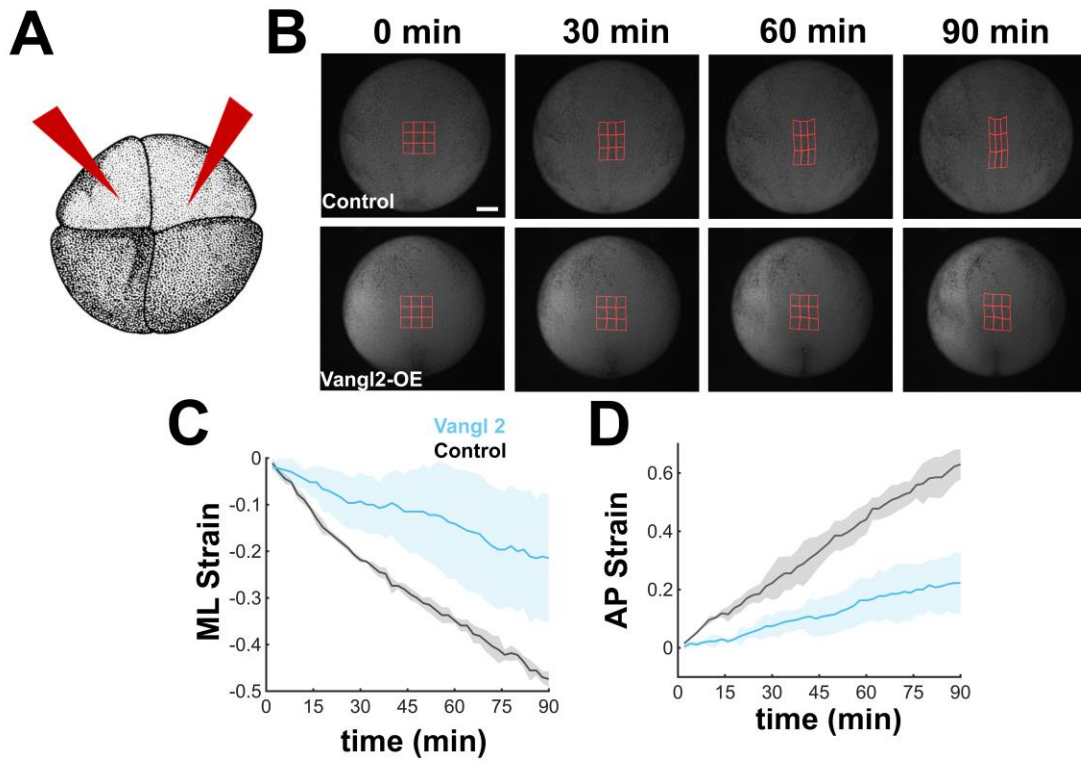


Figure 22. Vangl2 overexpression inhibits neural plate convergent extension.

A) Vangl2 mRNA was injected into the 2 dorsal blastomeres of the 4-cell stage embryo. B. Stereoscopic timelapse image sequences of uninjected, control embryos (top) and Vangl2-overexpressing embryos (bottom) with deformation grids overlaid. Scale bar 200 μ m C) ML strains quantified for control and Vangl2-overexpressing tissues (n=3 embryo each). D) AP strains quantified for control and Vangl2-overexpressing tissues (n=3 embryo each).

Cell morphology was quantified in stage 15 control and Vangl2-OE embryos within the medial neural plate (Fig 23A). Apical area was significantly larger in Vangl2-OE embryos compared to controls (Fig 23B). While there was no change in average aspect ratio, the orientation of elongated cells was significantly more aligned with the AP axis in the Vangl2-OE embryos compared to control embryos (Fig 23C,D). Components of the PCP pathway have been shown to alter rearrangement in mouse neural plates (Williams, Yen et al. 2014). We found a significant reduction in rosettes but not T1 junctions suggesting that rearrangement still occurred but potentially not as efficiently as in controls (Fig 23E).

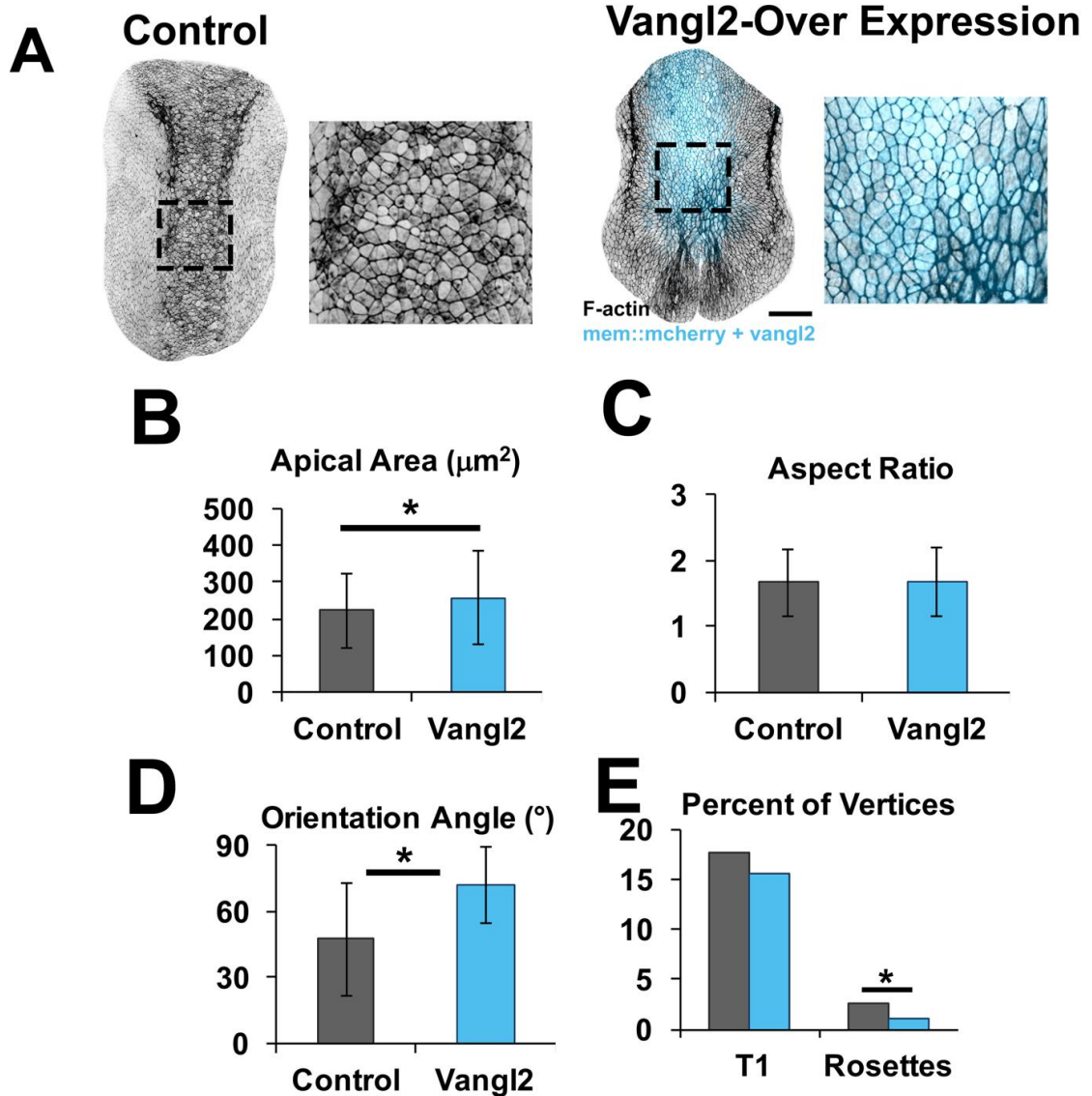


Figure 23. Global Vangl2 overexpression within the neural plate alters cell morphology.

A) Apical surface of whole control embryo (left) and embryo overexpressing vangl2 (right). Vangl2 mRNA was coinjected with mem::mcherry. Close up cell morphologies shown of dotted region. B. Quantification of apical area for control and Vangl2 overexpressing embryos (data pooled from 4 embryos; $*p < 0.05$, Mann-Whitney U). C) Quantification of cell aspect ratio. D) Average orientation angle of cell major axis. ($p < 0.05$; Mann-Whitney U). E). Quantification of high order vertices as percent of total vertices. ($p < 0.05$; Pearson's chi square).

5.1.2 Vangl-2 Overexpression causes cell AP elongation

Although severely diminished, neural plates in Vangl2-OE embryos still underwent a residual amount of CE. We hypothesized that elongated Vangl2-OE cells may have oriented with the AP axis in response to tissue strain. If Vangl2-OE cell elongation was strain dependent, then we reasoned cells should appear more AP elongated when introduced to the larger strain rates in control embryos. Alternatively, because the aspect ratios of cells in experimental and control embryos were the same, Vangl2-OE may alter the direction of cell orientation but not affect cell elongation. To preserve normal tissue strain rates, we overexpressed Vangl2-3xGFP in small clusters of cells within the neural plate rather than through out the whole tissue. We achieved this limited expression by targeting the injection of Vangl2-3xGFP mRNA into one dorsal blastomere of the 8-16 cell embryo. This caused mosaic expression of the mRNA within the neural plate, limiting the domain of expression to narrow strips of cells that spanned the AP axis. If tissue strain causes Vangl2OE cells to elongate and align with the AP axis, we would expect that cells in stage 12.5 embryos would have a less elongated morphology compared to control cells than stage 14 embryos that have undergone more CE strain. To test this, Vangl2-OE mosaic and control embryos were fixed at stage 12.5 and stage 14, after the embryos had undergone CE (Fig 24A). At stage 12.5, Vangl2-OE cells in mosaic embryos have a small but significant increase in apical area compared control neuroepithelial cells (Fig 24C). By stage 14, Vangl2-OE cells are roughly 50% larger than control cells suggesting Vangl2-OE disrupted normal apical constriction (Fig 24D). At both stages, Vangl2-OE cells had significantly larger aspect ratios compared to controls (Fig24C,D). Stage 12.5 Vangl2-OE cells were 13% more elongated than control cells. By stage 14, Vangl2-OE cells were 48% more elongated compared to controls supporting the hypothesis that these cells would appear more stretched as CE progressed. At

both stages, Vangl2-OE elongated cells oriented more towards the AP axis than control cells, with the disparity in angle increasing at stage 14 (Fig 24C,D).

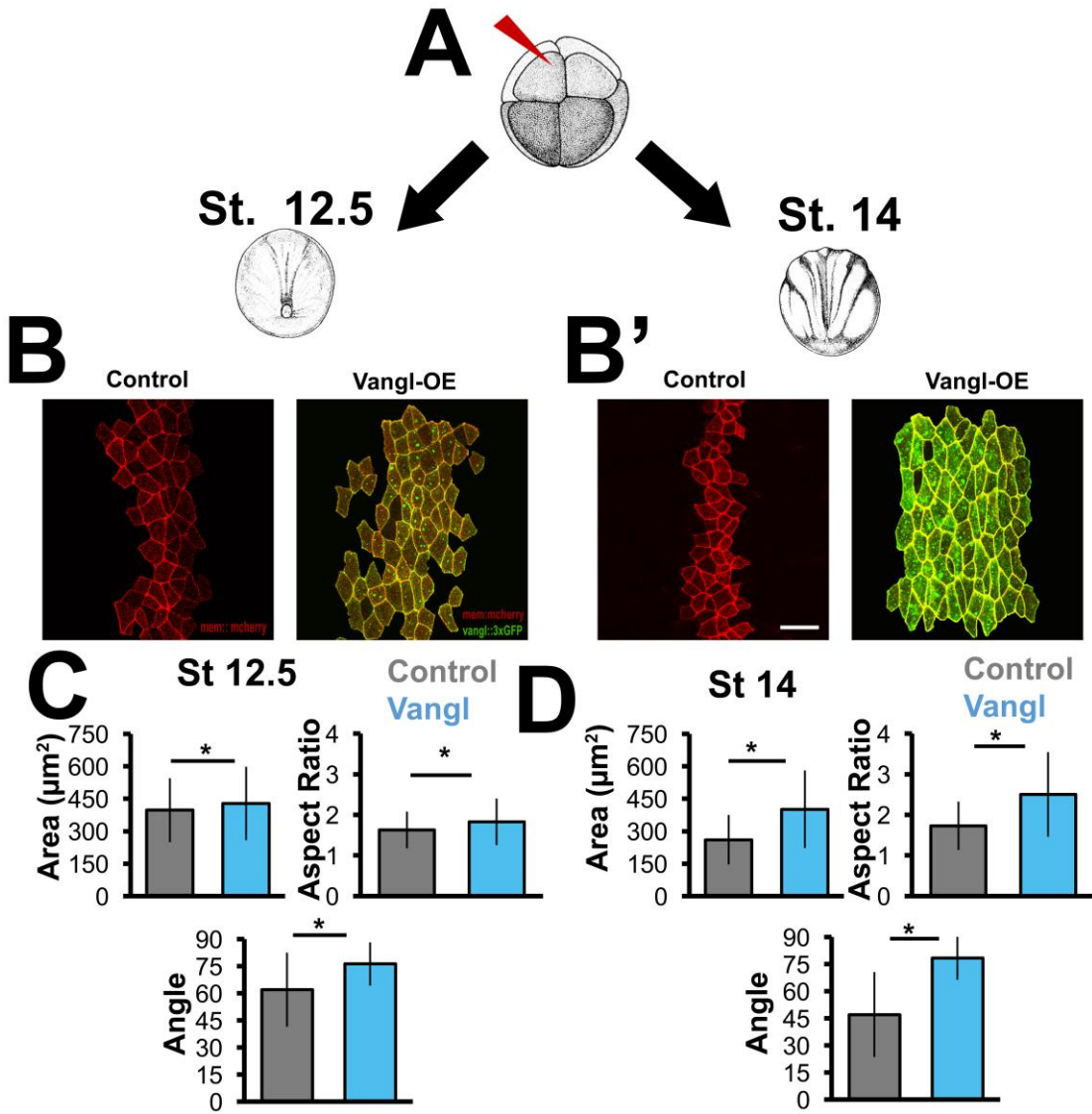


Figure 24. Elongation of Vangl2 overexpressing cells increases at later stages.

A) Vangl2-3xGFP mRNA with mem-mcherry mRNA or mem-mcherry mRNA alone was injected into one dorsal blastomere of the 8-16 cell stage embryo for mosaic expression in tissue. Embryos were cultured to stage 12.5 or 14 before being fixed and imaged. B) Apical surface of stage 12.5 neural plate mosaically labeled with mem-mcherry (left) or mem-mcherry and overexpressing vangl2-3xGFP (right). B') Apical surface of stage 14 neural plate mosaically labeled with mem-mcherry (left) or mem-mcherry and overexpressing vangl2-3xGFP (right). Scale bar 50 μm . C) Morphometric parameters comparing cell morphologies of control and vangl2 overexpressing cells in stage 12.5 embryos. D) Morphometric parameters comparing cell morphologies of control and vangl2 overexpressing cells in stage 14 embryos. ($P < 0.05$; Mann-Whitney U test)

Fixed analysis did not confirm that tissues were undergoing CE, so we collected 1-hour long confocal timelapse image sequences of 2 live stage 13 dorsal isolate neural plates expressing stripes of cells overexpressing Vangl2-3xGFP against a background of membrane-mcherry expressing cells (Fig 25A; data for one tissue show). Cell were tracked within the stripe of Vangl2-OE and AP and ML strains at tissue and cell scales were quantified. The two dorsal isolates had mean AP tissue strains of $24.5 \pm 10\%$ and $23.4 \pm 6.5\%$, respectively. The mean AP cell strains for each tissue was $14.1 \pm 18.4\%$ and $15.8 \pm 14.9\%$, respectively. Therefore, in both tissues, AP cell strains were concordant with tissue elongation strain (25B,C). In the ML direction, tissue strains varied more with one tissue converging $17.9 \pm 6.7\%$ and the other barely converging $0.7 \pm 5.1\%$ on average. ML cell strains were $-2.8 \pm 15.2\%$ and $13.8 \pm 16.5\%$, respectively; suggesting ML strains were less concordant.

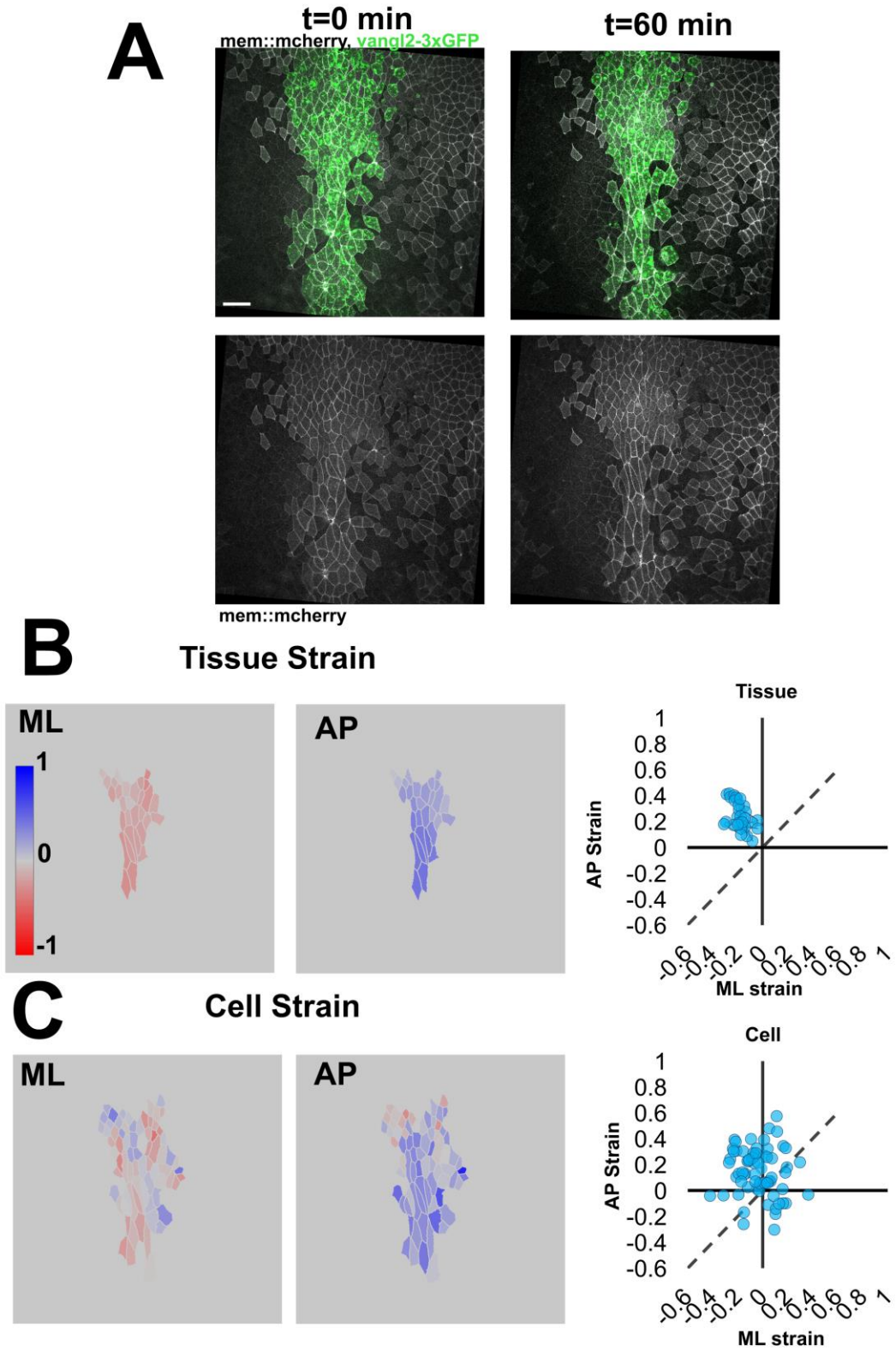


Figure 25. Strain patterns in mosaic Vangl2-Overexpression tissues

A) Still from beginning and end of timelapse of Vangl2-3xGFP overexpressed in strip of neural plate. B) Spatial map of quantified cumulative tissue strain in AP and ML direction. Graph shows relationship between AP and ML strain for individual tissue coronas C) Quantification of cell level AP and ML strains. Graph shows relationship between AP and ML strain for individual cells.

To test if the AP tissue elongation guided the AP cell elongation, we embedded dorsal isolates with Vangl2-OE patches within agarose gels. After 2 hours, we fixed the gel-embedded tissues along side free extending controls and evaluated cell morphology (Fig26A,B). Apical area of cells were unaltered (Fig 26C) however Vangl2-OE cells within confined tissues were significantly less AP elongated than cells in free tissues (Fig 26D,E). These results preliminarily suggest Vangl-OE cell elongation is a response to tissue elongation. Further characterization will be necessary, particularly in live samples, to understand the mechanism behind this cell elongation Here, we conclude that PCP patterning may allow neuroepithelial cells to maintain isodiametric shapes in the face of AP elongation tensions.

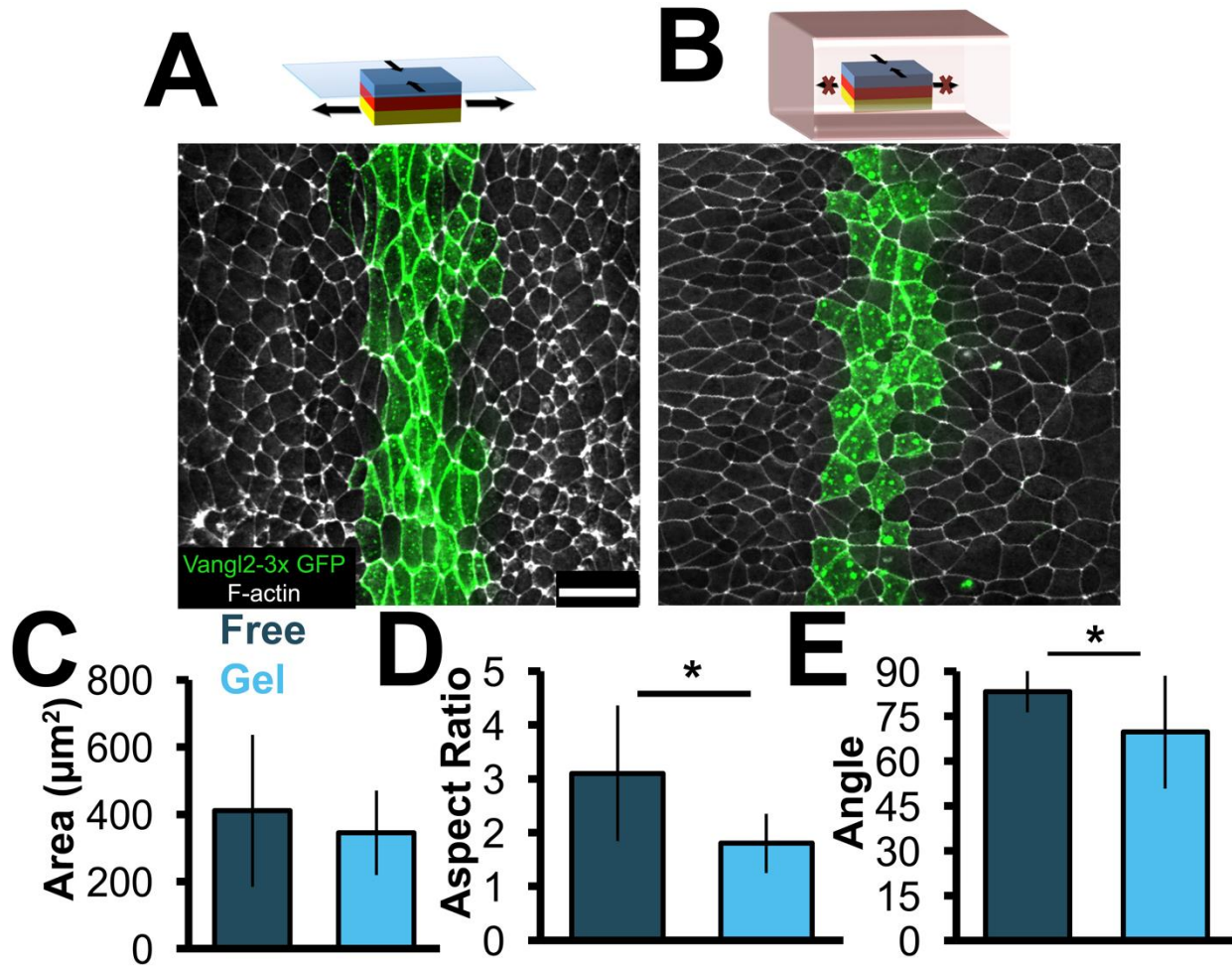


Figure 26. Gel confinement reduces Vangl2-overexpressing cell elongation

A) F-actin labeled free explant with strip of Vangl2-overexpression. Scale bar 100 μm B) F-actin labeled gel-confined explant with strip of Vangl2-overexpression. C) Quantification of apical area of Vangl2-OE cells in gel-confined and free tissues. (n=100 cells per group; 5 explants) D) Quantification of apical area of Vangl2-OE cells in gel-confined and free tissues. (n=100 cells per group; 5 explants; $p < 0.05$; Mann-Whitney U). E) Quantification of orientation angle of elongated Vangl2-OE cells in gel-confined and free tissues. (n=65 cell in gel. 96 cells in free; 5 explants; $p < 0.05$ Mann-Whitney-U)

5.2 DISCUSSION

The aim of this chapter was to establish a framework through which the interplay between molecular and mechanical regulation of neural plate morphogenesis could be tested. While most of the data is preliminary, our results suggest that Vangl2 or PCP plays a role in maintaining cell morphology during convergent extension.

Interestingly, although neural plate convergent extension and neuroepithelial cell rearrangements were reduced in Vangl knockdown mice, cells did not assume the same anisotropic elongate shape seen in the *Xenopus* vangl2 overexpressing cells (Williams, Yen et al. 2014). Perhaps these morphology defects only obviously manifest when strains within the tissue more closely match wildtype CE strains.

Why might Vangl-OE cells elongate under strain? It is possible that the contractility at cell-cell junctions may be altered. If junction stiffness decreases, then cells may be more compliant. PCP is thought to regulate polarized junctional contractility in chick neural plate. (Nishimura, Honda et al. 2012). Vangl2 plays a role in apical constriction as well and we confirm that Vangl2-OE cells are less constricted at stage 14 than control cells. Lack of constriction could also contribute to increased compliance within the cortex (Ossipova, Chuykin et al. 2015). Perhaps, overexpression alters basal activities within the cells. In *Xenopus*, mesodermal and deep neural populations that overexpress Vangl2 during CE fail to acquire polarized protrusive activity (Goto and Keller 2002). It is possible that Vangl2 overexpression may play a similar role within the neural plate. If polarized protrusive activity confers some ability to dissipate strain through basal rearrangements, then reducing these behaviors may force the stresses of tissue extension to act exclusively on the apical junctions and cause the cell to

stretch out. Our *Xenopus laevis* model system is ideal for testing these hypotheses, as we are able to image basal activities and probe what cells may do in different mechanical environments.

5.2.1 Limitations

As mentioned, most of the evidence provided here is preliminary data. Further characterization is needed of tissue and cell strains as well as cell behaviors in both cases where Vangl2 is locally and globally overexpressed. We have yet to confirm that rearrangement is abrogated within the global overexpression of Vangl2. This will be necessary to address if the defective cell morphologies arise from an inability of cells to properly rearrange. There is also limited molecular analysis of the action of Vangl2 within these tissues. How might Vangl2 be changing actomyosin or other cytoskeletal machinery that may be important for shape maintenance? Can the elongation defect be rescued by Vangl2 knock down? Furthermore, we must perform live imaging of explants in gels to see if Vangl2 cells no longer elongate AP or if they might be stretching mediolaterally.

5.3 EXPERIMENTAL PROCEDURES

5.3.1 Embryo Handling, Immunofluorescence and Microinjection

Xenopus laevis embryos were obtained by standard methods (Kay 1991) fertilized in vitro and cultured in 1/3X Modified Barth's Solution (MBS) (Sive 2000). For explants: Embryos are cultured to stage 12.5 (Nieuwkoop and Faber 1956) at which time dorsal axial and paraxial

tissues (dorsal isolate) are microsurgically removed from the embryo using hair loops and knives in DFA solution (Danichik's For Amy; (Sater, Steinhardt et al. 1993)). Before microsurgery, small (~1x5mm) pieces of glasses are cut from a #1.5 glass slide using a diamond pen. After isolation, tissue explants are transferred to a clean dish filled with DFA and gently and minimally compressed under a pre-cut small piece of glass using vacuum grease at the ends for half an hour prior to experimentation to allow healing without tissue folding/bending. For microinjection of mRNAs, embryos are placed in 1X MBS containing Ficoll.

For F-actin staining, embryos were devitellinized and fixed for 30 minutes in 4% Paraformaldehyde + 3.7% Gluteraldehyde. Embryos were then permeabilized in 0.1% TritonX in PBS (PBST) for 30 minutes. A 2.5:1000 concentration of Bodipy-Phalloidin in was applied for 1 hour and then rinsed 3 times in PBS.

For live visualization of apical surface, mRNA encoding fluorescent protein constructs were injected at the one- or two-cell stage to plasma membrane (CAAX-GFP).

For Vangl2 overexpression: the Vangl2.S mRNA sequence was based on Goto et al (Goto and Keller 2002). For the Vangl2-3xGFP, the Vangl2 gene was fused in frame to a 3x eGFP cassette which contained a concatenation of three eGFPs with 6 nt linkers in between each eGFP. 90-360 pg Vangl2 or Vangl2-3xGFP mRNA was injected into dorsal blastomeres of the 4 or 8-cell stage. Embryos were allowed to develop to the appropriate stages (12.5 or 14) and were either fixed or explanted into dorsal isolates for live imaging or gel confinement. Vangl2-3xGFP was used for scatter-labeled overexpression as overexpression phenotype could be visually identified through the appearance of punctate spots of GFP (Fig 26A,B).

5.3.2 Image Processing

Image processing techniques for cell morphology analyses and tissue tectonic analysis were described in a previous section (See section 3.4.2 and 3.4.3)

5.3.3 Statistical analysis

All statistical analysis was performed in IBM, SPSS version 22. Mann-Whitney U was chosen when independent samples Levene's test of homoscedasticity was rejected. Chi Square was chosen for contingency analysis for percent of high order vertices.

6.0 CONCLUSIONS

6.1 SUMMARY OF FINDINGS

Through this work, we sought to understand the interplay of tissue strain patterns and cell behaviors that accompany neural plate shaping in the *Xenopus laevis* neuroepithelium. First, we hypothesized there would be spatiotemporal differences in cell behaviors during neural plate convergent extension. In Chapter 3, we established the timing and spatial patterns of cell behaviors and strains during neural plate convergent extension. Within the medial neural plate, cellular strains do not follow the pattern of local tissue convergent-extension strain, suggesting that cell shape change does not drive tissue deformation in this region. Instead, medial neural plate cells increasingly participate in directed cell rearrangements accompanied by apical junctional remodeling and basolateral rearrangement. We observe that basolateral rearrangement precedes and occurs more rapidly than apical remodeling. These results suggest that basolateral activity may drive epithelial cell rearrangement. Within the basolateral domain, neuroepithelial cells emanate cell protrusions that span the junctions of neighboring cells. It is possible that this protrusive activity mediates the basal rearrangement.

At the border of the neural plate and non-neural ectoderm, tissues continue to converge and extend. However, as tissue CE proceeds, cells within this region assume AP elongated morphologies. Cell shape strains in the AP direction are concordant with tissue level AP strains.

Second, we hypothesized that tissue CE drives border cell shape changes. In chapter 4, we confined tissue explants containing the neural plate and prevented them from elongating. We confirm lateral cells in confinement no longer assume an AP elongated shape. In part this may be due to a reduction in AP tissue strain, however we also observe that tissue convergence within the lateral region is diminished and in some cases tissues exhibit mediolateral stretch. Therefore, it is possible cells are being pulled mediolaterally within confinement and are therefore losing their AP elongated shape.

Through tissue confinement, we also tested the hypothesis that the orientations of neuroepithelial cell rearrangement depend on the endogenous tissue strain field. We find this is not the case. Despite abrogating tissue elongation at the midline, cell rearrangements continue to proceed in an oriented manner. Interestingly, confinement induces an excess of cell division. Gel confinement suggested neural epithelial cell rearrangement might be a programmed behavior within the neural plate. Tissue grafting experiments confirm that both cell rearrangement and tissue convergent-extension can occur autonomously within the neuroepithelium without the presence of the other tissues within the dorsal axis.

Third, we hypothesized that cellular defects observed planar cell polarity pathway mutants were in part a response to aberrant tissue strain patterns. In Chapter 5, we tested the role of planar cell polarity in neural plate shaping through the overexpression of Vangl2. We found that overexpression globally within the neural plate prevents native levels of convergent-extension strain and causes cells to become larger apically and more aligned with the AP axis. To understand whether Vangl2 mutant cell shape change occurred due to perturbed strain, we mosaically overexpressed Vangl2 in patches of cells within neural plates. These preps maintained native tissue strains. At the cellular level, Vangl2 overexpressing cells became

elongated in the AP axis. This suggested PCP may serve to maintain cell shapes when cells are subject to native convergent extensions strains. Constraining tissues with Vangl2-overexpressing patches supported this hypothesis as cells no longer become AP elongated.

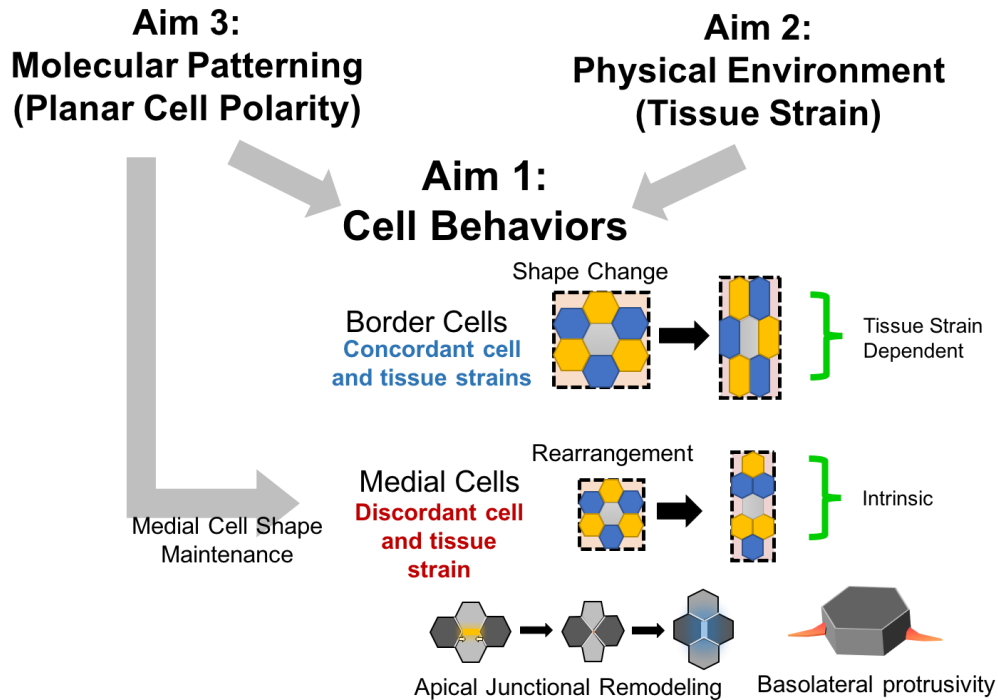


Figure 27. Framework to investigate mechanical and molecular controls of cell behaviors

Both the physical environment and molecular patterning influence cell behaviors during morphogenesis. This dissertation has explored both aspects during neural plate shaping. Aim 1 established spatiotemporal patterns of cell strain and behaviors as well as tissue strain within the neural plate. Aim 2 manipulated the physical environment of the neural epithelium, described through changes in tissue strain and then assessed changes in cell strain patterns or behaviors. Aim 3 assessed how the planar cell polarity molecular pathway alters cell and tissue strain patterns as well as cell behavioral changes. Combined with mechanical manipulation techniques, we find that this pathway may play a role in cell shape maintenance.

6.2 SIGNIFICANCE OF FINDINGS

This work establishes the *Xenopus laevis* neuroepithelium as an ideal model to study epithelial cell behaviors during convergent extension and more broadly, neurulation. Many of the cell behaviors observed in other models of tissue CE such as cell rearrangement through apical junction remodeling and basolateral protrusivity, and shape change occur within *Xenopus* (Bertet, Sulak et al. 2004, Blankenship, Backovic et al. 2006, Nishimura, Honda et al. 2012, Williams, Yen et al. 2014, Sun, Amourda et al. 2017). A major advantage of our model is the ability to perform mechanical manipulations on tissues. As demonstrated in chapter 4, we can alter mechanical components like tissue elongation and assess cell defects. We can remove tissues from native environment and assess intrinsic cell behaviors. Finally, Chapter 5 showed how we could combine mechanical manipulation with molecular disruption to reveal the subtle differences between mutant and native cell behaviors subject to similar mechanical environments.

Strides have made in *Drosophila in* assessing the role of mechanical regulation of cell behaviors during epithelial cell morphogenesis (Rauzi, Verant et al. 2008, Butler, Blanchard et al. 2009, Fernandez-Gonzalez, Simoes Sde et al. 2009, Aigouy, Farhadifar et al. 2010, Collinet, Rauzi et al. 2015, Etournay, Popovic et al. 2015, Yu and Fernandez-Gonzalez 2016). By adapting some of these approaches that combine whole field analysis of cell and tissue strains with mechanical manipulations, we were able to tease apart spatial and temporal behavioral differences of cell behaviors within the neural ectoderm. One question that arises asks are changes in cell behaviors a direct response to changes in strain? This is likely not the case. Strain is a manifestation forces acting within or upon cells and tissues which have specific material properties. Ultimately, cell shape changes or tissue strains are readouts of the changes in

the mechanical forces acting on or within the cell and tissue or changes of their material properties. It is likely changes in force or material properties that influence cell behaviors. Thus, mechanical manipulations of tissues, such as confinement, change force or material properties the within the tissue and the resulting behavioral changes are likely responses to this new mechanical state. This research creates a framework through which we can now assess how these behavioral differences arise.

6.3 FUTURE DIRECTIONS

While this work has provided insights into the deformations and cell behaviors that shape the *Xenopus* neural plate, many new questions have arisen. First, we have observed regional differences in the relationship between cell and tissue strain. Lateral cells shape strains and tissue strains are concordant where as medial cell and tissue strains are not. What permits or causes these behavioral and morphological differences between the medial and lateral cell populations? As we address this question, we likely must explore the molecular mechanisms that control cell shape including elements of the cell cytoskeleton and how planar cell polarity may play a role in cell shape maintenance. Beyond cell shape changes, open questions remain as to how cell rearrangement is driven. Our observations of basal protrusions that precede apical junction remodeling particularly warrant further investigation, namely trying to understand if basal activity drives rearrangement.

6.3.1 What controls the spatial differences in cell behaviors? Why do lateral cells undergo strain dependent elongation while medial cells remain more isodiametric?

From a mechanical standpoint, it will be interesting to determine what permits and prevents strain dependent stretching within the neuroepithelium. While lateral neuroepithelial cells stretch under convergent-extension forces acting within the tissue, cells in the medial neuroepithelium resist such stretching. These cells may be actively generating constricting forces so as not to elongate or may be much stiffer than lateral cells and thus resist deforming as much. To see if there are mechanical differences between medial and lateral cell junctions, we can assess if cell level junctional tensions or stiffness through laser ablation as has been done in fly (Rauzi, Verant et al. 2008). If the neuroepithelium is actively contracting to prevent tissue stretching, then tensions within these cells might be higher. A recent study utilized an actinin based FRET tension sensor and demonstrated that the neural plate cells may be under more tension than lateral cells (Yamashita, Tsuboi et al. 2016). While these results do not definitively suggest the mechanism as to why tension is greater it does suggest that the medial and lateral cell populations have some mechanical difference. Cells may constrict or alter their material properties through controlling actomyosin contractility. As described in Section 2.3, a number of mutations of actin regulators are linked to neural tube defects. Using techniques to modulate these actin regulators (such as overexpression, knockdown or small molecule inhibitors) in combination with mechanical manipulations such as grafting or tissue confinement, we may further uncover how these actomyosin activity is different within the medial neural plate cells compared to the lateral cells.

6.3.2 How does planar cell polarity maintain neuroepithelial cell morphology?

Our preliminary results suggest that PCP compromised cells (via Vangl2 overexpression) are unable to maintain isodiametric shapes when subject to native tissue strains. Certainly this must be explored further and bolstered by more live data on the dynamics of Vangl2 overexpressed cells. Future work on this problem specifically, might benefit from an experimental set up in which defined amounts of exogenous strains are applied to the neural plate. As grafting confirmed, the cells of the neural plate maintain their behavioral programs and ability to deform the epithelium in isolation. Thus, explanting the neural plate or neural epithelium to a tissue stretching device might be a better approach to assessing strain dependent cell behaviors than relying upon the variable strains produced by the embryo. We circumvented using a such a device by taking advantage of mosaic labeling in *Xenopus* embryos; however mosaic labeling also creates variable patterns of expression. A better experiment might involve overexpressing Vangl2 throughout a neural plate and then taking the entire tissue and stretching it at a known rate and then comparing this to the response of wildtype neural plate cells to exogenous strains. Of course, beyond the mechanics of the experiment, the molecular regulation of PCP based cell shape maintenance should be explored. Likely, this pathway will converge on actomyosin regulation.

6.3.3 What is the function of basal protrusions? Are they necessary and sufficient to drive cell intercalations?

Our analysis of apical and basal cell rearrangement indicates cells initiate rearrangement basally first where they seem to exchange neighbors faster than they do apically. This suggests basal

behaviors drive cell intercalation rather than apical junction remodeling which may be a permissive behavior for rearrangement. Scatter labeling revealed the presence of protrusions that emanate in the basolateral domain and allow cells to interact across neighboring junctions. Do these protrusions drive basal cell rearrangement? What are the molecular regulators of basal protrusion? Recent findings in *C. Elegans* and *Drosophila* demonstrate a role for polarized Rac activity which suggests these structures are similar to lamellipodia (Walck-Shannon, Reiner et al. 2015, Sun, Amourda et al. 2017). Our observations, as well as other's, suggest these protrusions are oriented in the direction of tissue convergence (Williams, Yen et al. 2014, Walck-Shannon, Reiner et al. 2015, Sun, Amourda et al. 2017). Do the polarity mechanisms, such as PCP, guide both apical junction shrinkage and basolateral protrusions? In the *Xenopus* model system, targeted injections of constructs that can overexpress and knockdown PCP components can easily be performed and with our image analysis framework, the effects of PCP on the basal surface rearrangements of cells can be assessed. Do these protrusions generate basal tractions? A technique to measure tractions, traction force microscopy, has been successfully used with *Xenopus* explants before (Zhou, Kim et al. 2010, Jackson, Kim et al. 2017). Theoretically, it may be possible to isolate neuroepithelial grafts and place them on traction force gels to observe traction generation. Ultimately, understanding where forces are generated and how cells respond to altered mechanical and molecular states will reveal the mechanisms regulating neural plate morphogenesis.

APPENDIX A

IMAGE ANALYSIS PROTOCOLS

Included in this appendix are scripts to perform the various image analyses presented in this dissertation.

A.1 EXTRACTING ROIS FROM OUTLINED SEGMENTS

A.1.1 Extracting ROIs from Binary Outline

After segmentation, it is usually useful to quantify morphological data for individual cells. Using the outlines output by SeedWater Segmenter we can generate ROIs for each cell. Briefly, our code turns the outline images into a binary mask. It dilates and inverts the image for use with the Find Particles function in FIJI. It runs find particles on an inverted mask and creates ROIs for the particles which are effectively the shape of the cells. It then saves the detected ROIs for each slice. The following code uses the binary outline produced by SeedWater Segmenter to extract ROIs and cell measurements:

//IMAGEJ REQUIRES YOU TO OPEN UP THE ROI MANAGER BEFORE DOING THE VERTEX ANALYSIS.

```
macro "Cell ROIs [2]"
{

    setBatchMode(true);
    setOption("ExpandableArrays", true);

    /*We first get user input to get the source directory that
    contains folders for each segmented image.
    * It is important to make sure that all images segmented have the
    same scale within that folder
    * It also asks for a midline value in microns (to calculate the
    lateral distance from the midline.) Set to 0 if this value is not
    important
    */
    folder1=getDirectory("Choose a Directory");
    list1=getFileList(folder1);
    scale=getNumber("set scale", 2.239)
    mid=getNumber("where's the midline?", 650);
    //Next line ensures ROIs will track with slice number
    run("Overlay Options...", "stroke=yellow width=0 fill=none set");
    for (q=0; q<list1.length;q++)
    {
        //Declaring Variables
        var major=newArray;
        var minor=newArray;
        var Area=newArray;
        var Angle=newArray;
        var AspectRatio=newArray;
        var CentroidX=newArray;
        var CentroidY=newArray;
        var CellNum=newArray;
        var CellID=newArray;
        var RelX=newArray;
        var SliceNumA=newArray;

        arraycount = 0;
        //This opens the first folder within the source folder. Then
        makes individual directories for CellROIs
        folder0=folder1+list1[q];
        pathname=File.getName(folder0);
        folder=folder0+File.separator+"Outlines";
        File.makeDirectory(folder0 + "CellROIs");
        folderR=folder0+File.separator+"CellROIs";
        list= getFileList(folder);

        //Creating separate stack for
        stack1=folder0+"Segments"+File.separator;
        run("Image Sequence...", "open=&stack1 sort");
        SegID = getImageID();
        selectImage(SegID);
        saveAs("tiff", folder0+"Segments.tif");
        for (n=0;n<list.length;n++)
        {
            var delarray= newArray;
            dcount=0;

```

```

        if (n<10)
        {
open(folder+File.separator+"Outline_0_00"+n+".tif");
        SingleID = getImageID();
        }
        else if ( n< 100)
        {
open(folder+File.separator+"Outline_0_0"+n+".tif");
        SingleID = getImageID();
        }
        else
        {
open(folder+File.separator+"Outline_0_"+n+".tif");
        SingleID = getImageID();
        }

//STARTING HERE IS THE CORE CODE OF TURNING
Binary OUTLINE IMAGE INTO ROIS
        setAutoThreshold("Default dark");
        setOption("BlackBackground", true);
        run("Convert to Mask");
        run("Skeletonize");
        run("Dilate");
        run("Invert");
        run("Analyze Particles...", "size=7-25000
circularity=0.00-1.00 show=Nothing display exclude clear summarize
add");

        selectWindow("Results");
        run("Close");

        selectImage (SegID);
        slicenum=n+1;
        setSlice(slicenum);
        run("Set Measurements...", "area modal centroid fit
redirect=None decimal=2");

        nrois=roiManager("count");

        for (p=0;p<nrois;p++)
        {
                arraycount++;

                CellNum[arraycount]=p+1;
                SliceNumA[arraycount]=n;
                roiManager("Select", p);
                roiManager("Update");
                List.setMeasurements;
                f=scale*scale;
                Area[arraycount]=List.getValue("Area")/f;
                major[arraycount]=List.getValue("Major");
                minor[arraycount]=List.getValue("Minor");
                CellID[arraycount]=List.getValue("Mode");
                CentroidX[arraycount]=List.getValue("X")/scale;
                CentroidY[arraycount]=List.getValue("Y")/scale;
                RelX[arraycount]= abs(CentroidX[arraycount]-
mid);

                AspectRatio[arraycount]=major[arraycount]/minor[arraycount];
                angle1=List.getValue("Angle");
                if (angle1 > 90) {

```

```

        Angle[arraycount]=abs(180-angle1);
    }
    else{
        Angle[arraycount]=angle1;
    }

    //renaming the ROI to its cell ID
    if (CellID[arraycount]==1)
    {
        delarray[dcount]=p;
        dcount++;
    }

    name = d2s(CellID[arraycount],0);
    roiManager("select", p);
    roiManager("Rename", name);
}

    if (delarray.length>0)
    {
        roiManager("select", delarray);
        roiManager("delete");
    }
    roiManager("Select All");
    roiManager("Save",
folderR+File.separator+"cellROIs"+n+".zip");

    roiManager("reset");
    selectImage(SingleID);

    close();

}

    Array.show("Cell Morphology",SliceNumA, CellNum,
CellID ,CentroidX, CentroidY,Area, major, minor,AspectRatio,Angle,RelX);
selectWindow("Cell Morphology");
saveAs("Results",
folder0+"CellMorphology"+"_"+pathname+".txt");
selectWindow("CellMorphology"+"_"+pathname+".txt");
run("Close");
print("Done with folder "+q);

}

    print("Done with all folders");

setBatchMode(false); }

```

A.1.2 Performing Vertex Analysis

The following code extracts individual vertices from the segment output produced by SeedWater Segmenter useful for doing vertex order analyses. Briefly, A circle of a user selected diameter passes over each pixel of the “Segments” output of seedwater. Each unique intensity is detected within the circle as it passes through each pixel using the histogram function in Imagej. The

unique intensities are counted. When 3 or more intensities are detected within the circle, the center pixel of the circle is filled in on a blank image. After the circle has passed over the entire image, the blank image will now contain a cluster of filled in pixels that corresponds each vertex. We run the Find Particles function on this image to extract individual ROIs for each vertex pixel cluster. We then use these ROIs on the “Segments” image to detect the number of unique intensities within each vertex ROI to find the vertex order.

```

var reds, greens, blues;
function generateLUT()
{
    reds=newArray(256);
    greens=newArray(256);
    blues=newArray(256);

    for (i=0; i<256; i++) {

        if (i > 2 && i<= 15)
        {
            reds[i] = 255;
            greens[i] = 255;
            blues[i] = 255;
        }
        else
        {
            reds[i] = 0;
            greens[i] = 0;
            blues[i] = 0;
        }
    }
}

function generateLUT2()
{
    reds=newArray(256);
    greens=newArray(256);
    blues=newArray(256);

    for (i=3; i<256; i++) {

        if (i == 3)
        {
            reds[i] = 86;
            greens[i] = 207;
            blues[i] = 24;
        }
        else if (i ==4)
        {
            reds[i] = 121;
            greens[i] = 0;
            blues[i] = 193;
        }
    }
}

```

```

else if (i >= 5)
{
    reds[i] = 255;
    greens[i] = 103;
    blues[i] = 0;
}
else
{
    reds[i] = 0;
    greens[i] = 0;
    blues[i] = 0;
}
}

}

function histcount(Cellct2)
{
    tempcount=0;
    histMin=0;
    histMax=0;
    getHistogram(values, counts, Cellct2, histMin, histMax);
    for (i=0; i<values.length; i++)
    {
        if (counts[i]>0)
        {
            tempcount++;
        }
    }
    return tempcount;
}

macro "DVRosettes [1]"
{
    setBatchMode(true);
    folder1=getDirectory("Choose a Directory");
    list1=getFileList(folder1);
    S=getNumber("How big of a circle do you want?", 7); // This variable
allows you to adjust the size of the square you are passing over the image
    for(q=0;q<list1.length;q++)
    {
        folder0=folder1+list1[q];
        pathname=File.getName(folder0);
        folder=folder0+File.separator+"Segments";
        File.makeDirectory(folder0+"VertROIs");
        folderR=folder0+File.separator+"VertROIs";
        File.makeDirectory(folder0+"Vertex");
        folderV=folder0+File.separator+"Vertex";
        list= getFileList(folder);

        for (n=0;n<list.length;n++)
        {
            roiManager("Reset"); //opens up ROI Manager
            if(n<10)
            {
                open(folder+File.separator+"Segment_0_00"+n+".tif");
            }
            else if ( n< 100)
            {
                open(folder+File.separator+"Segment_0_0"+n+".tif");
            }
        }
    }
}

```

```

else
    {
        open(folder+File.separator+"Segment_0_"+n+".tif");
    }

SingleID = getImageID();
run("Set Measurements...", "min bounding redirect=None
decimal=3");

List.setMeasurements;

//Declaring + Defining Variables
Cells=List.getValue("Max"); //Finding the number of cells
based on the max intensity in the segments image
Cellct=(Cells-1);
Width=List.getValue("Width");
Height=List.getValue("Height");

j=0;
//Xmax and Ymax set the end points for centroid of last
circle
Xmax=Width-S;
Ymax=Height-S;

//creating new image to create color coded junction squares
newImage("Blank", "8-bit black",Width, Height, 1);
FilledID = getImageID();
start=getTime();
newImage("Blank", "8-bit black",Width, Height, 1);
FilledID2 = getImageID();

print(Cells,Cellct,Xmax,Ymax);

/*This next part causes the circle to traverse through the
image first moving pixel by pixel down the y direction then over one pixel to
the right and down again.
* As it moves down it checks the histogram for the number
of intensities within the cell. It increments a counter each time it finds a
new intensity. */

for (y = 0; y < Ymax; y++)
{
    for (x = 0; x < Xmax; x++)
    {
        selectImage(SingleID);
        makeOval(x-(S/2), y-(S/2), S, S);
        ros=0;

        /*The function histcount Identifies and returns
the number of unique pixel values within the ROI*/
        ros=histcount(Cellct);

        /*This next part checks if the circle has
overlapped more than 2 cells.
If it does it selects the blank image, and sets
the intensity of the centroid pixel of the circle
to the value of "ros" */
        if (ros>2)
        {
            setColor(ros, ros, ros);
            roiManager("Add");
            selectImage(FilledID);

```

```

//drawOval(x, y, S, S);
setPixel(x,y,ros);
    }
}

generateLUT();

//Here we are identifying all of the vertices in the image
selectImage(FilledID);

setLut(reds, greens, blues);
run("8-bit");

run("Make Binary");
roiManager("Deselect");
roiManager("Show All with labels");
roiManager("Show All");
run("Analyze Particles...", "size=0-Infinity
circularity=0.00-1.00 show=Nothing clear add");
roiManager("Select All");
roiManager("Save",
folderR+File.separator+pathname+"vertices"+S+"_"+n+".zip");

selectImage(FilledID);
//saveAs("Tiff", folder0+"/pixrosette"+S+"_"+n+".tif");
run("Close");

//Here we go through and determine how many intensities are in the
vertex ROI
nrois=roiManager("count");
for(i=0; i<nrois;i++)
{
    intensitycount=0;
    selectImage(SingleID);
    roiManager("Select", i);
    intensitycount=histcount(Cellct);

    roiManager("Select",i);
    List.setMeasurements;

    fillv=getResult("Max");
    setForegroundColor(intensitycount,
intensitycount, intensitycount);
    run("Select None");
    selectImage(FilledID2);
    roiManager("Select", i);
    setColor(intensitycount);
    run("Fill", "slice");
    run("Select None");
}

selectImage(SingleID);
run("Close");
roiManager("Reset");

generateLUT2();
selectImage(FilledID2);
setLut(reds, greens, blues);
saveAs("Tiff",
folderV+File.separator+pathname+"_Vertex"+S+"_"+n+".tif");

```

```
        //print("Done with frame "+n);
    }
        print("Done with folder " +q);
    }
    print("ALL FINISHED!!");
    setBatchMode(false);
}
```

BIBLIOGRAPHY

- Aigouy, B., R. Farhadifar, D. B. Staple, A. Sagner, J. C. Roper, F. Julicher and S. Eaton (2010). "Cell flow reorients the axis of planar polarity in the wing epithelium of *Drosophila*." Cell **142**(5): 773-786.
- Alvarez, I. S. and G. C. Schoenwolf (1992). "Expansion of surface epithelium provides the major extrinsic force for bending of the neural plate." Journal of Experimental Zoology **261**(3): 340-348.
- Araya, C., L. C. Ward, G. C. Girdler and M. Miranda (2016). "Coordinating cell and tissue behavior during zebrafish neural tube morphogenesis." Dev Dyn **245**(3): 197-208.
- Arnold, T. R., R. E. Stephenson and A. L. Miller (2017). "Rho GTPases and actomyosin: Partners in regulating epithelial cell-cell junction structure and function." Exp Cell Res **358**(1): 20-30.
- Aw, W. Y., B. W. Heck, B. Joyce and D. Devenport (2016). "Transient Tissue-Scale Deformation Coordinates Alignment of Planar Cell Polarity Junctions in the Mammalian Skin." Curr Biol **26**(16): 2090-2100.
- Baker, P. C. and T. E. Schroeder (1967). "Cytoplasmic filaments and morphogenetic movement in the amphibian neural tube." Developmental Biology **15**(5): 432-450.
- Barbier de Reuille, P., A. L. Routier-Kierzkowska, D. Kierzkowski, G. W. Bassel, T. Schupbach, G. Tauriello, N. Bajpai, S. Strauss, A. Weber, A. Kiss, A. Burian, H. Hofhuis, A. Sapala, M. Lipowczan, M. B. Heimlicher, S. Robinson, E. M. Bayer, K. Basler, P. Koumoutsakos, A. H. Roeder, T. Aegerter-Wilmsen, N. Nakayama, M. Tsiantis, A. Hay, D. Kwiatkowska, I. Xenarios, C. Kuhlemeier and R. S. Smith (2015). "MorphoGraphX: A platform for quantifying morphogenesis in 4D." Elife **4**: 05864.
- Baum, B. and M. Georgiou (2011). "Dynamics of adherens junctions in epithelial establishment, maintenance, and remodeling." J Cell Biol **192**(6): 907-917.

- Belousov, L. V., J. G. Dorfman and V. G. Cherdantzev (1975). "Mechanical stresses and morphological patterns in amphibian embryos." Journal of Embryology and Experimental Morphology **34**(3): 559-574.
- Benko, R. and G. W. Brodland (2007). "Measurement of in vivo stress resultants in neurulation-stage amphibian embryos." Ann Biomed Eng **35**(4): 672-681.
- Bertet, C., L. Sulak and T. Lecuit (2004). "Myosin-dependent junction remodelling controls planar cell intercalation and axis elongation." Nature **429**(6992): 667-671.
- Blanchard, G. B., A. J. Kabla, N. L. Schultz, L. C. Butler, B. Sanson, N. Gorfinkiel, L. Mahadevan and R. J. Adams (2009). "Tissue tectonics: morphogenetic strain rates, cell shape change and intercalation." Nat Methods **6**(6): 458-464.
- Blankenship, J. T., S. T. Backovic, J. S. Sanny, O. Weitz and J. A. Zallen (2006). "Multicellular rosette formation links planar cell polarity to tissue morphogenesis." Dev Cell **11**(4): 459-470.
- Brodland, G. W. and J. H. Veldhuis (2006). "Lamellipodium-driven tissue reshaping: a parametric study." Comput Methods Biomech Biomed Engin **9**(1): 17-23.
- Brown, M. G., V. Hamburger and F. O. Schmitt (1941). "Density studies on amphibian embryos with special reference to the mechanism of organizer action." Journal of Experimental Zoology **88**: 353-372.
- Brun, R. B. and J. A. Garson (1983). "Neurulation in the Mexican salamander (*Ambystoma mexicanum*): a drug study and cell shape analysis of the epidermis and the neural plate." J Embryol Exp Morphol **74**: 275-295.
- Burnside, M. B. and A. G. Jacobson (1968). "Analysis of morphogenetic movements in the neural plate of the newt *Taricha torosa*." Dev Biol **18**(6): 537-552.
- Burnside, M. B. and A. G. Jacobson (1968). "Analysis of morphogenetic movements in the neural plate of the newt *Taricha torosa*." Developmental Biology **18**(6): 537-552.
- Butler, L. C., G. B. Blanchard, A. J. Kabla, N. J. Lawrence, D. P. Welchman, L. Mahadevan, R. J. Adams and B. Sanson (2009). "Cell shape changes indicate a role for extrinsic tensile forces in *Drosophila* germ-band extension." Nat Cell Biol **11**(7): 859-864.
- Butler, M. T. and J. B. Wallingford (2017). "Planar cell polarity in development and disease." Nat Rev Mol Cell Biol **18**(6): 375-388.
- Campinho, P., M. Behrndt, J. Ranft, T. Risler, N. Minc and C. P. Heisenberg (2013). "Tension-oriented cell divisions limit anisotropic tissue tension in epithelial spreading during zebrafish epiboly." Nat Cell Biol **15**(12): 1405-1414.

- Chacon-Heszele, M. F., D. Ren, A. B. Reynolds, F. Chi and P. Chen (2012). "Regulation of cochlear convergent extension by the vertebrate planar cell polarity pathway is dependent on p120-catenin." Development **139**(5): 968-978.
- Chen, X. and G. W. Brodland (2008). "Multi-scale finite element modeling allows the mechanics of amphibian neurulation to be elucidated." Phys Biol **5**(1): 015003.
- Chien, Y. H., R. Keller, C. Kintner and D. R. Shook (2015). "Mechanical strain determines the axis of planar polarity in ciliated epithelia." Curr Biol **25**(21): 2774-2784.
- Christodoulou, N. and P. A. Skourides (2015). "Cell-Autonomous Ca(2+) Flashes Elicit Pulsed Contractions of an Apical Actin Network to Drive Apical Constriction during Neural Tube Closure." Cell Rep **13**(10): 2189-2202.
- Ciruna, B., A. Jenny, D. Lee, M. Mlodzik and A. F. Schier (2006). "Planar cell polarity signalling couples cell division and morphogenesis during neurulation." Nature **439**(7073): 220-224.
- Colas, J. F. and G. C. Schoenwolf (2001). "Towards a cellular and molecular understanding of neurulation." Dev Dyn **221**(2): 117-145.
- Collinet, C., M. Rauzi, P. F. Lenne and T. Lecuit (2015). "Local and tissue-scale forces drive oriented junction growth during tissue extension." Nat Cell Biol **17**(10): 1247-1258.
- Compagnon, J. and C. P. Heisenberg (2013). "Neurulation: coordinating cell polarisation and lumen formation." The EMBO journal **32**(1): 1-3.
- Copp, A. J. and N. D. Greene (2010). "Genetics and development of neural tube defects." J Pathol **220**(2): 217-230.
- Copp, A. J. and N. D. Greene (2013). "Neural tube defects—disorders of neurulation and related embryonic processes." Wiley Interdisciplinary Reviews: Developmental Biology **2**(2): 213-227.
- Costanzo, R., R. L. Watterson and G. C. Schoenwolf (1982). "Evidence that secondary neurulation occurs autonomously in the chick embryo." J Exp Zool **219**(2): 233-240.
- Criley, B. B. (1969). "Analysis of the embryonic sources and mechanisms of development of posterior levels of chick neural tubes." Journal of morphology **128**(4): 465-501.
- Davidson, L. A., S. D. Joshi, H. Y. Kim, M. von Dassow, L. Zhang and J. Zhou (2010). "Emergent morphogenesis: elastic mechanics of a self-deforming tissue." J Biomech **43**(1): 63-70.
- Davidson, L. A. and R. E. Keller (1999). "Neural tube closure in *Xenopus laevis* involves medial migration, directed protrusive activity, cell intercalation and convergent extension." Development **126**(20): 4547-4556.

- Davidson, L. A., M. A. Koehl, R. Keller and G. F. Oster (1995). "How do sea urchins invaginate? Using biomechanics to distinguish between mechanisms of primary invagination." Development **121**(7): 2005-2018.
- Edlund, A. F., L. A. Davidson and R. E. Keller (2013). "Cell segregation, mixing, and tissue pattern in the spinal cord of the *Xenopus laevis* neurula." Dev Dyn **242**(10): 1134-1146.
- Eisenhoffer, G. T., P. D. Loftus, M. Yoshigi, H. Otsuna, C. B. Chien, P. A. Morcos and J. Rosenblatt (2012). "Crowding induces live cell extrusion to maintain homeostatic cell numbers in epithelia." Nature **484**(7395): 546-549.
- Eliceiri, K. W., M. R. Berthold, I. G. Goldberg, L. Ibanez, B. S. Manjunath, M. E. Martone, R. F. Murphy, H. Peng, A. L. Plant, B. Roysam, N. Stuurman, J. R. Swedlow, P. Tomancak and A. E. Carpenter (2012). "Biological imaging software tools." Nat Methods **9**(7): 697-710.
- Elul, T., M. A. Koehl and R. Keller (1997). "Cellular mechanism underlying neural convergent extension in *Xenopus laevis* embryos." Dev Biol **191**(2): 243-258.
- Elul, T., M. A. Koehl and R. E. Keller (1998). "Patterning of morphogenetic cell behaviors in neural ectoderm of *Xenopus laevis*." Ann N Y Acad Sci **857**: 248-251.
- Elul, T. M., M. A. R. Koehl and R. E. Keller (1997). "Cellular mechanism underlying neural convergence and extension in *Xenopus laevis* embryos." Dev Biol **191**: 243-258.
- Eom, D. S., S. Amarnath, J. L. Fogel and S. Agarwala (2012). "Bone morphogenetic proteins regulate hinge point formation during neural tube closure by dynamic modulation of apicobasal polarity." Birth Defects Res A Clin Mol Teratol **94**(10): 804-816.
- Escuin, S., B. Vernay, D. Savery, C. B. Gurniak, W. Witke, N. D. Greene and A. J. Copp (2015). "Rho-kinase-dependent actin turnover and actomyosin disassembly are necessary for mouse spinal neural tube closure." J Cell Sci **128**(14): 2468-2481.
- Etournay, R., M. Merkel, M. Popovic, H. Brandl, N. A. Dye, B. Aigouy, G. Salbreux, S. Eaton and F. Julicher (2016). "TissueMiner: a multiscale analysis toolkit to quantify how cellular processes create tissue dynamics." Elife **5**.
- Etournay, R., M. Popovic, M. Merkel, A. Nandi, C. Blasse, B. Aigouy, H. Brandl, G. Myers, G. Salbreux, F. Julicher and S. Eaton (2015). "Interplay of cell dynamics and epithelial tension during morphogenesis of the *Drosophila* pupal wing." Elife **4**: e07090.
- Ettensohn, C. A. (1985). "Mechanisms of epithelial invagination." Quarterly Review of Biology **60**(3): 289-307.
- Ezin, A. M., P. Skoglund and R. Keller (2003). "The midline (notochord and notoplate) patterns the cell motility underlying convergence and extension of the *Xenopus* neural plate." Dev Biol **256**(1): 100-114.

- Farhadifar, R., J. C. Roper, B. Aigouy, S. Eaton and F. Julicher (2007). "The influence of cell mechanics, cell-cell interactions, and proliferation on epithelial packing." Curr Biol **17**(24): 2095-2104.
- Fernandez-Gonzalez, R., M. Simoes Sde, J. C. Roper, S. Eaton and J. A. Zallen (2009). "Myosin II dynamics are regulated by tension in intercalating cells." Dev Cell **17**(5): 736-743.
- Fernandez-Gonzalez, R. and J. A. Zallen (2011). "Oscillatory behaviors and hierarchical assembly of contractile structures in intercalating cells." Phys Biol **8**(4): 045005.
- Findley, W. N., J. S. Lai and K. Onaran (1989). Creep and relaxation of nonlinear viscoelastic materials. New York, Dover Publications, Inc.
- Fletcher, A. G., M. Osterfield, R. E. Baker and S. Y. Shvartsman (2014). "Vertex models of epithelial morphogenesis." Biophysical journal **106**(11): 2291-2304.
- Gilbert, S. F. (2000). Developmental Biology: 6th Edition. Sunderland, MA, Sinauer Associates.
- Glaser, O. C. (1914). "On the mechanism of morphological differentiation in the nervous system. I. The transformation of a neural plate into a neural tube." The Anatomical Record **8**(12): 525-551.
- Glaser, O. C. (1916). "The theory of autonomous folding in embryogenesis." Science **46**(1136): 505-509.
- Goto, T. and R. Keller (2002). "The planar cell polarity gene *strabismus* regulates convergence and extension and neural fold closure in *Xenopus*." Dev Biol **247**(1): 165-181.
- Grego-Bessa, J., J. Hildebrand and K. V. Anderson (2015). "Morphogenesis of the mouse neural plate depends on distinct roles of cofilin 1 in apical and basal epithelial domains." Development **142**(7): 1305-1314.
- Grosse, S. D., L. Ouyang, J. S. Collins, D. Green, J. H. Dean and R. E. Stevenson (2008). "Economic evaluation of a neural tube defect recurrence-prevention program." Am J Prev Med **35**(6): 572-577.
- Gudipaty, S. A., J. Lindblom, P. D. Loftus, M. J. Redd, K. Edes, C. F. Davey, V. Krishnegowda and J. Rosenblatt (2017). "Mechanical stretch triggers rapid epithelial cell division through Piezo1." Nature **543**(7643): 118-121.
- Habas, R., Y. Kato and X. He (2001). "Wnt/Frizzled activation of Rho regulates vertebrate gastrulation and requires a novel Formin homology protein Daam1." Cell **107**(7): 843-854.
- Haigo, S. L., J. D. Hildebrand, R. M. Harland and J. B. Wallingford (2003). "Shroom induces apical constriction and is required for hinge point formation during neural tube closure." Curr Biol **13**(24): 2125-2137.

- Hardin, J. (1989). "Local shifts in position and polarized motility drive cell rearrangement during sea urchin gastrulation." Dev Biol **136**(2): 430-445.
- Harris, W. A. and V. Hartenstein (1991). "Neuronal determination without cell division in *Xenopus* embryos." Neuron **6**(4): 499-515.
- Hashimoto, H., F. B. Robin, K. M. Sherrard and E. M. Munro (2015). "Sequential contraction and exchange of apical junctions drives zippering and neural tube closure in a simple chordate." Dev Cell **32**(2): 241-255.
- Heid, P. J., W. B. Raich, R. Smith, W. A. Mohler, K. Simokat, S. B. Gendreau, J. H. Rothman and J. Hardin (2001). "The zinc finger protein DIE-1 is required for late events during epithelial cell rearrangement in *C. elegans*." Dev Biol **236**(1): 165-180.
- Heisenberg, C. P. and Y. Bellaïche (2013). "Forces in tissue morphogenesis and patterning." Cell **153**(5): 948-962.
- Heisenberg, C. P., M. Tada, G. J. Rauch, L. Saude, M. L. Concha, R. Geisler, D. L. Stemple, J. C. Smith and S. W. Wilson (2000). "Silberblick/Wnt11 mediates convergent extension movements during zebrafish gastrulation." Nature **405**(6782): 76-81.
- Heller, D., A. Hoppe, S. Restrepo, L. Gatti, A. L. Tournier, N. Tapon, K. Basler and Y. Mao (2016). "EpiTools: An Open-Source Image Analysis Toolkit for Quantifying Epithelial Growth Dynamics." Dev Cell **36**(1): 103-116.
- Heller, E. and E. Fuchs (2015). "Tissue patterning and cellular mechanics." The Journal of cell biology **211**(2): 219-231.
- Higashi, T., T. R. Arnold, R. E. Stephenson, K. M. Dinshaw and A. L. Miller (2016). "Maintenance of the Epithelial Barrier and Remodeling of Cell-Cell Junctions during Cytokinesis." Curr Biol **26**(14): 1829-1842.
- Hildebrand, J. D. and P. Soriano (1999). "Shroom, a PDZ domain-containing actin-binding protein, is required for neural tube morphogenesis in mice." Cell **99**(5): 485-497.
- His, W. (1874). Unsere korperform und das physiologische problem ihrer entstehung. Leipzig, F.C.W. Vogel.
- Irvine, K. D. and E. Wieschaus (1994). "Cell intercalation during *Drosophila* germband extension and its regulation by pair-rule segmentation genes." Development **120**(4): 827-841.
- Itoh, K., O. Ossipova and S. Y. Sokol (2014). "GEF-H1 functions in apical constriction and cell intercalations and is essential for vertebrate neural tube closure." J Cell Sci **127**(Pt 11): 2542-2553.
- Jackson, T. R., H. Y. Kim, U. L. Balakrishnan, C. Stuckenholtz and L. A. Davidson (2017). "Spatiotemporally Controlled Mechanical Cues Drive Progenitor Mesenchymal-to-

- Epithelial Transition Enabling Proper Heart Formation and Function." Curr Biol **27**(9): 1326-1335.
- Jacobson, A. G. (1978). "Some forces that shape the nervous system." Zoon **6**: 13-21.
- Jacobson, A. G. and R. Gordon (1976). "Changes in the shape of the developing vertebrate nervous system analyzed experimentally, mathematically, and by computer simulation." Journal of Experimental Zoology **197**: 191-246.
- Jiang, D., E. M. Munro and W. C. Smith (2005). "Ascidian prickle regulates both mediolateral and anterior-posterior cell polarity of notochord cells." Curr Biol **15**(1): 79-85.
- Karfunkel, P. (1971). "The role of microtubules and microfilaments in neurulation in *Xenopus*." Dev Biol **25**(1): 30-56.
- Karfunkel, P. (1972). "The activity of microtubules and microfilaments in neurulation in the chick." J Exp Zool **181**(3): 289-301.
- Kay, B. K. a. P., H.B. (1991). Xenopus laevis: Practical uses in cell and molecular biology. New York, Academic Press.
- Keller, R. (2002). "Shaping the vertebrate body plan by polarized embryonic cell movements." Science **298**(5600): 1950-1954.
- Keller, R. and S. Jansa (1992). "Xenopus Gastrulation without a blastocoel roof." Dev Dyn **195**(3): 162-176.
- Keller, R., J. Shih and A. Sater (1992). "The cellular basis of the convergence and extension of the *Xenopus* neural plate." Dev Dyn **193**(3): 199-217.
- Kibar, Z., K. J. Vogan, N. Groulx, M. J. Justice, D. A. Underhill and P. Gros (2001). "Ltap, a mammalian homolog of *Drosophila* Strabismus/Van Gogh, is altered in the mouse neural tube mutant Loop-tail." Nat Genet **28**(3): 251-255.
- Kim, H. Y. and L. A. Davidson (2011). "Punctuated actin contractions during convergent extension and their permissive regulation by the non-canonical Wnt-signaling pathway." J Cell Sci **124**(Pt 4): 635-646.
- Kim, Y., M. Hazar, D. S. Vijayraghavan, J. Song, T. R. Jackson, S. D. Joshi, W. C. Messner, L. A. Davidson and P. R. LeDuc (2014). "Mechanochemical actuators of embryonic epithelial contractility." Proc Natl Acad Sci U S A **111**(40): 14366-14371.
- Kinoshita, N., N. Sasai, K. Misaki and S. Yonemura (2008). "Apical accumulation of Rho in the neural plate is important for neural plate cell shape change and neural tube formation." Mol Biol Cell **19**(5): 2289-2299.
- Koehl, M. A. R. (1990). "Biomechanical approaches to morphogenesis." Seminars in Developmental Biology **1**: 367-378.

- Larkin, K. and M. V. Danilchik (1999). "Ventral cell rearrangements contribute to anterior-posterior axis lengthening between neurula and tailbud stages in *Xenopus laevis*." Dev Biol **216**(2): 550-560.
- Lau, K., H. Tao, H. Liu, J. Wen, K. Sturgeon, N. Sorfazlian, S. Lazic, J. T. Burrows, M. D. Wong, D. Li, S. Deimling, B. Ciruna, I. Scott, C. Simmons, R. M. Henkelman, T. Williams, A. K. Hadjantonakis, R. Fernandez-Gonzalez, Y. Sun and S. Hopyan (2015). "Anisotropic stress orients remodelling of mammalian limb bud ectoderm." Nat Cell Biol **17**(5): 569-579.
- Lee, C., H. M. Scherr and J. B. Wallingford (2007). "Shroom family proteins regulate gamma-tubulin distribution and microtubule architecture during epithelial cell shape change." Development **134**(7): 1431-1441.
- Leptin, M. and B. Grunewald (1990). "Cell shape changes during gastrulation in *Drosophila*." Development **110**(1): 73-84.
- Levayer, R., A. Pelissier-Monier and T. Lecuit (2011). "Spatial regulation of Dia and Myosin-II by RhoGEF2 controls initiation of E-cadherin endocytosis during epithelial morphogenesis." Nat Cell Biol **13**(5): 529-540.
- Lewis, W. H. (1947). "Mechanics of Invagination." Anatomical Record **97**(2): 139-156.
- Lienkamp, S. S., K. Liu, C. M. Karner, T. J. Carroll, O. Ronneberger, J. B. Wallingford and G. Walz (2012). "Vertebrate kidney tubules elongate using a planar cell polarity-dependent, rosette-based mechanism of convergent extension." Nat Genet **44**(12): 1382-1387.
- Lofberg, J. (1974). "Apical surface topography of invaginating and noninvaginating cells. A scanning-transmission study of amphibian neurulae." Developmental Biology **36**(2): 311-329.
- Lowery, L. A. and H. Sive (2004). "Strategies of vertebrate neurulation and a re-evaluation of teleost neural tube formation." Mech Dev **121**(10): 1189-1197.
- Ma, X., H. E. Lynch, P. C. Scully and M. S. Hutson (2009). "Probing embryonic tissue mechanics with laser hole drilling." Phys Biol **6**(3): 036004.
- Mahaffey, J. P., J. Grego-Bessa, K. F. Liem, Jr. and K. V. Anderson (2013). "Cofilin and Vangl2 cooperate in the initiation of planar cell polarity in the mouse embryo." Development **140**(6): 1262-1271.
- Martin, A. C. and B. Goldstein (2014). "Apical constriction: themes and variations on a cellular mechanism driving morphogenesis." Development **141**(10): 1987-1998.
- Mashburn, D. N., H. E. Lynch, X. Ma and M. S. Hutson (2012). "Enabling user-guided segmentation and tracking of surface-labeled cells in time-lapse image sets of living tissues." Cytometry A **81**(5): 409-418.

- Massarwa, R. and L. Niswander (2013). "In toto live imaging of mouse morphogenesis and new insights into neural tube closure." Development **140**(1): 226-236.
- McGreevy, E. M., D. Vijayraghavan, L. A. Davidson and J. D. Hildebrand (2015). "Shroom3 functions downstream of planar cell polarity to regulate myosin II distribution and cellular organization during neural tube closure." Biol Open **4**(2): 186-196.
- McShane, S. G., M. A. Mole, D. Savery, N. D. Greene, P. P. Tam and A. J. Copp (2015). "Cellular basis of neuroepithelial bending during mouse spinal neural tube closure." Dev Biol **404**(2): 113-124.
- Messier, P.-E. (1978). "Microtubules, interkinetic nuclear migration and neurulation." Experientia **34**(3): 289-296.
- Miller, C. J. and L. A. Davidson (2013). "The interplay between cell signalling and mechanics in developmental processes." Nature Reviews Genetics **14**(10): 733-744.
- Mitchell, B., R. Jacobs, J. Li, S. Chien and C. Kintner (2007). "A positive feedback mechanism governs the polarity and motion of motile cilia." Nature **447**(7140): 97-101.
- Morita, H., H. Kajiura-Kobayashi, C. Takagi, T. S. Yamamoto, S. Nonaka and N. Ueno (2012). "Cell movements of the deep layer of non-neural ectoderm underlie complete neural tube closure in *Xenopus*." Development **139**(8): 1417-1426.
- Munro, E. M. and G. M. Odell (2002). "Polarized basolateral cell motility underlies invagination and convergent extension of the ascidian notochord." Development **129**(1): 13-24.
- Murisic, N., V. Hakim, I. G. Kevrekidis, S. Y. Shvartsman and B. Audoly (2015). "From discrete to continuum models of three-dimensional deformations in epithelial sheets." Biophysical journal **109**(1): 154-163.
- Nieuwkoop, P. D. and J. Faber (1956). Normal table of *Xenopus laevis* (Daudin). A systematical and chronological survey of the development from the fertilized egg till the end of metamorphosis. Amsterdam, Elsevier North-Holland Biomedical Press.
- Nishimura, T., H. Honda and M. Takeichi (2012). "Planar cell polarity links axes of spatial dynamics in neural-tube closure." Cell **149**(5): 1084-1097.
- Odell, G. M., G. Oster, P. Alberch and B. Burnside (1981). "The mechanical basis of morphogenesis." Developmental Biology **85**: 446-462.
- Ossipova, O., I. Chuykin, C. W. Chu and S. Y. Sokol (2015). "Vangl2 cooperates with Rab11 and Myosin V to regulate apical constriction during vertebrate gastrulation." Development **142**(1): 99-107.
- Ossipova, O., K. Kim and S. Y. Sokol (2015). "Planar polarization of Vangl2 in the vertebrate neural plate is controlled by Wnt and Myosin II signaling." Biol Open **4**(6): 722-730.

- Palm, M. M. and R. M. Merks (2015). "Large-scale parameter studies of cell-based models of tissue morphogenesis using CompuCell3D or VirtualLeaf." Tissue Morphogenesis: Methods and Protocols: 301-322.
- Pyrgaki, C., P. Trainor, A. K. Hadjantonakis and L. Niswander (2010). "Dynamic imaging of mammalian neural tube closure." Dev Biol **344**(2): 941-947.
- Rauzi, M., P. Verant, T. Lecuit and P. F. Lenne (2008). "Nature and anisotropy of cortical forces orienting Drosophila tissue morphogenesis." Nat Cell Biol **10**(12): 1401-1410.
- Rhumbler, L. (1902). "Zur mechanik des gastrulationsvorganges insbesondere der invagination." Archiv Fur Entwicklungsmechanik **14**: 401-476.
- Roffers-Agarwal, J., J. B. Xanthos, K. A. Kragtorp and J. R. Miller (2008). "Enabled (Xena) regulates neural plate morphogenesis, apical constriction, and cellular adhesion required for neural tube closure in Xenopus." Dev Biol **314**(2): 393-403.
- Rolo, A., D. Savery, S. Escuin, S. C. de Castro, H. E. Armer, P. M. Munro, M. A. Molè, N. D. Greene and A. J. Copp (2016). "Regulation of cell protrusions by small GTPases during fusion of the neural folds." eLife **5**: e13273.
- Rolo, A., P. Skoglund and R. Keller (2009). "Morphogenetic movements driving neural tube closure in Xenopus require myosin IIB." Dev Biol **327**(2): 327-338.
- Roszko, I., S. S. D., J. R. Jessen, A. Chandrasekhar and L. Solnica-Krezel (2015). "A dynamic intracellular distribution of Vangl2 accompanies cell polarization during zebrafish gastrulation." Development **142**(14): 2508-2520.
- Roux, W. (1885). "Beitrage zur Morphologie der funktionellen Anpassung." Arch Anat Physiol Anat Abt **9**: 120-158.
- Sandersius, S. A., C. J. Weijer and T. J. Newman (2011). "Emergent cell and tissue dynamics from subcellular modeling of active biomechanical processes." Phys Biol **8**(4): 045007.
- Sasai, Y. (2013). "Cytosystems dynamics in self-organization of tissue architecture." Nature **493**(7432): 318-326.
- Sater, A. K., R. A. Steinhardt and R. Keller (1993). "Induction of neuronal differentiation by planar signals in Xenopus embryos." Dev Dyn **197**(4): 268-280.
- Sausedo, R. A., J. L. Smith and G. C. Schoenwolf (1997). "Role of nonrandomly oriented cell division in shaping and bending of the neural plate." J Comp Neurol **381**(4): 473-488.
- Savin, T., N. A. Kurpios, A. E. Shyer, P. Florescu, H. Liang, L. Mahadevan and C. J. Tabin (2011). "On the growth and form of the gut." Nature **476**(7358): 57-62.

- Sawyer, J. M., J. R. Harrell, G. Shemer, J. Sullivan-Brown, M. Roh-Johnson and B. Goldstein (2010). "Apical constriction: a cell shape change that can drive morphogenesis." Dev Biol **341**(1): 5-19.
- Schechtman, A. M. (1942). "The mechanics of amphibian gastrulation I. Gastrulation-producing interactions between various regions of an anuran egg (*Ityla regila*)." University of California Publications in Zoology **51**: 1-39.
- Schneider, C. A., W. S. Rasband and K. W. Eliceiri (2012). "NIH Image to ImageJ: 25 years of image analysis." Nat Methods **9**(7): 671-675.
- Schoenwolf, G. C. (1984). "Histological and ultrastructural studies of secondary neurulation in mouse embryos." Am J Anat **169**(4): 361-376.
- Schoenwolf, G. C. and M. V. Franks (1984). "Quantitative analyses of changes in cell shapes during bending of the avian neural plate." Dev Biol **105**(2): 257-272.
- Schoenwolf, G. C. and M. L. Powers (1987). "Shaping of the chick neuroepithelium during primary and secondary neurulation: role of cell elongation." Anat Rec **218**(2): 182-195.
- Schoenwolf, G. C. and J. L. Smith (1990). "Mechanisms of neurulation: traditional viewpoint and recent advances." Development **109**(2): 243-270.
- Schroeder, T. E. (1970). "Neurulation in *Xenopus laevis*. An analysis and model based upon light and electron microscopy." Journal of Embryology and Experimental Morphology **23**(2): 427-462.
- Selman, G. G. (1955). "Studies on the forces producing neural closure in amphibia." Proceedings of the Royal Physical Society of Edinburgh **24**: 24-27.
- Selman, G. G. (1958). "The forces producing neural closure in amphibia." Journal of Embryology and Experimental Morphology **6**: 448-465.
- Shawky, J. H. and L. A. Davidson (2015). "Tissue mechanics and adhesion during embryo development." Dev Biol **401**(1): 152-164.
- Shih, J. and R. Keller (1992). "Cell motility driving mediolateral intercalation in explants of *Xenopus laevis*." Development **116**(4): 901-914.
- Sive, H. L., Grainger, R.M, Harland, R.M. (2000). Early development of *Xenopus laevis*: a laboratory manual. Cold Spring Harbor, New York, Cold Spring Harbor Laboratory Press.
- Sokol, S. Y. (2016). "Mechanotransduction During Vertebrate Neurulation." Current Topics in Developmental Biology **117**: 359-376.

- Song, J., J. H. Shawky, Y. Kim, M. Hazar, P. R. LeDuc, M. Sitti and L. A. Davidson (2015). "Controlled surface topography regulates collective 3D migration by epithelial-mesenchymal composite embryonic tissues." Biomaterials **58**: 1-9.
- Stooke-Vaughan, G. A., L. A. Davidson and S. Woolner (2017). "Xenopus as a model for studies in mechanical stress and cell division." Genesis **55**(1-2).
- Strutt, D. I., U. Weber and M. Mlodzik (1997). "The role of RhoA in tissue polarity and Frizzled signalling." Nature **387**(6630): 292-295.
- Sun, Z., C. Amourda, M. Shagirov, Y. Hara, T. E. Saunders and Y. Toyama (2017). "Basolateral protrusion and apical contraction cooperatively drive Drosophila germ-band extension." Nat Cell Biol **19**(4): 375-383.
- Suzuki, M., Y. Hara, C. Takagi, T. S. Yamamoto and N. Ueno (2010). "MID1 and MID2 are required for Xenopus neural tube closure through the regulation of microtubule organization." Development **137**(14): 2329-2339.
- Suzuki, M., H. Morita and N. Ueno (2012). "Molecular mechanisms of cell shape changes that contribute to vertebrate neural tube closure." Dev Growth Differ **54**(3): 266-276.
- Taber, L. A. (1995). "Biomechanics of growth, remodeling, and morphogenesis." Appl Mech Rev **48**(8): 487-545.
- Tada, M. and J. C. Smith (2000). "Xwnt11 is a target of Xenopus Brachyury: regulation of gastrulation movements via Dishevelled, but not through the canonical Wnt pathway." Development **127**(10): 2227-2238.
- Townes, P. L. and J. Holtfreter (1955). "Directed movements and selective adhesion of embryonic amphibian cells." Journal of Experimental Zoology **128**: 53-120.
- Usui, T., Y. Shima, Y. Shimada, S. Hirano, R. W. Burgess, T. L. Schwarz, M. Takeichi and T. Uemura (1999). "Flamingo, a seven-pass transmembrane cadherin, regulates planar cell polarity under the control of Frizzled." Cell **98**(5): 585-595.
- Van Straaten, H. W., H. C. Janssen, M. C. Peeters, A. J. Copp and J. W. Hekking (1996). "Neural tube closure in the chick embryo is multiphasic." Dev Dyn **207**(3): 309-318.
- Varner, V. D., J. P. Gleghorn, E. Miller, D. C. Radisky and C. M. Nelson (2015). "Mechanically patterning the embryonic airway epithelium." Proc Natl Acad Sci U S A **112**(30): 9230-9235.
- Vogel, S. (2003). Comparative biomechanics: life's physical world. Princeton, Princeton University Press.
- von Dassow, M. and L. A. Davidson (2011). "Physics and the canalization of morphogenesis: a grand challenge in organismal biology." Phys Biol **8**(4): 045002.

- von Dassow, M., J. A. Strother and L. A. Davidson (2010). "Surprisingly simple mechanical behavior of a complex embryonic tissue." PLoS One **5**(12): e15359.
- Wainwright, S. A., W. D. Biggs, J. D. Currey and J. M. Gosline (1976). Mechanical Design in Organisms. New York, John Wiley and Sons.
- Walck-Shannon, E., D. Reiner and J. Hardin (2015). "Polarized Rac-dependent protrusions drive epithelial intercalation in the embryonic epidermis of *C. elegans*." Development **142**(20): 3549-3560.
- Wallingford, J. B. and R. M. Harland (2002). "Neural tube closure requires Dishevelled-dependent convergent extension of the midline." Development **129**(24): 5815-5825.
- Wallingford, J. B., L. A. Niswander, G. M. Shaw and R. H. Finnell (2013). "The continuing challenge of understanding, preventing, and treating neural tube defects." Science **339**(6123): 1222002.
- Weber, G. F., M. A. Bjerke and D. W. DeSimone (2012). "A mechanoresponsive cadherin-keratin complex directs polarized protrusive behavior and collective cell migration." Dev Cell **22**(1): 104-115.
- Weliky, M., S. Minsuk, R. Keller and G. Oster (1991). "Notochord morphogenesis in *Xenopus laevis*: simulation of cell behavior underlying tissue convergence and extension." Development **113**(4): 1231-1244.
- Wiebe, C. and G. W. Brodland (2005). "Tensile properties of embryonic epithelia measured using a novel instrument." J Biomech **38**(10): 2087-2094.
- Williams, J., C. T. Mai, J. Mulinare, J. Isenburg, T. J. Flood, M. Ethen, B. Frohnert and R. S. Kirby (2015) "Updated Estimates of Neural Tube Defects Prevented by Mandatory Folic Acid Fortification — United States, 1995–2011." CDC: Morbidity and Mortality Weekly Report (MMWR) **64**, 1-5.
- Williams, M., W. Yen, X. Lu and A. Sutherland (2014). "Distinct apical and basolateral mechanisms drive planar cell polarity-dependent convergent extension of the mouse neural plate." Developmental cell **29**(1): 34-46.
- Williams, M., W. Yen, X. Lu and A. Sutherland (2014). "Distinct apical and basolateral mechanisms drive planar cell polarity-dependent convergent extension of the mouse neural plate." Dev Cell **29**(1): 34-46.
- Williams-Masson, E. M., P. J. Heid, C. A. Lavin and J. Hardin (1998). "The cellular mechanism of epithelial rearrangement during morphogenesis of the *Caenorhabditis elegans* dorsal hypodermis." Dev Biol **204**(1): 263-276.
- Winter, C. G., B. Wang, A. Ballew, A. Royou, R. Karess, J. D. Axelrod and L. Luo (2001). "Drosophila Rho-associated kinase (Drok) links Frizzled-mediated planar cell polarity signaling to the actin cytoskeleton." Cell **105**(1): 81-91.

- Yamashita, S., T. Tsuboi, N. Ishinabe, T. Kitaguchi and T. Michiue (2016). "Wide and high resolution tension measurement using FRET in embryo." Sci Rep **6**: 28535.
- Yin, C., M. Kiskowski, P. A. Pouille, E. Farge and L. Solnica-Krezel (2008). "Cooperation of polarized cell intercalations drives convergence and extension of presomitic mesoderm during zebrafish gastrulation." J Cell Biol **180**(1): 221-232.
- Yu, J. C. and R. Fernandez-Gonzalez (2016). "Local mechanical forces promote polarized junctional assembly and axis elongation in *Drosophila*." Elife **5**.
- Zajac, M., G. L. Jones and J. A. Glazier (2003). "Simulating convergent extension by way of anisotropic differential adhesion." J Theor Biol **222**(2): 247-259.
- Zhou, J., H. Y. Kim and L. A. Davidson (2009). "Actomyosin stiffens the vertebrate embryo during critical stages of elongation and neural tube closure." Development **136**: 677-688.
- Zhou, J., H. Y. Kim, J. H.-C. Wang and L. A. Davidson (2010). "Macroscopic stiffening of embryonic tissues via microtubules, Rho-GEF, and assembly of contractile bundles of actomyosin." Development **137**(16): 2785-2794.
- Zhou, J., S. Pal, S. Maiti and L. A. Davidson (2015). "Force production and mechanical accommodation during convergent extension." Development **142**(4): 692-701.
- Zhou, J., S. Pal, S. Maiti and L. A. Davidson (2015). "Force production and mechanical adaptation during convergent extension." Development **142**: 692-701.
- Zulueta-Coarasa, T., M. Tamada, E. J. Lee and R. Fernandez-Gonzalez (2014). "Automated multidimensional image analysis reveals a role for Abl in embryonic wound repair." Development **141**(14): 2901-2911.